Development of Extinction Imagers for the Determination of Atmospheric Optical Extinction

Final Report for JTO/ONR Grant N00014-07-1-1060

UNIVERSITY OF CALIFORNIA SAN DIEGO

SCRIPPS INSTITUTION OF OCEANOGRAPHY

Janet E. Shields
Monette E. Karr
Vincent W. Mikuls
Paul J. Berger
Paul A. Frederickson
Richard J. Lind
William S. Hodgkiss

MARINE PHYSICAL LAB San Diego, CA 92152-6400

REPORT DOCUMENTATION PAGE

Form Approved
OMB No. 0704-0188

PLEASE DO NOT RETURN YOUR FORM TO THE ABOVE ADDRESS.

1. REPORT DATE *(DD-MM-YYYY)*	2. REPORT TYPE	3. DATES COVERED *(From - To)*
26/09/2014	Final Report	07/01/2007 - 12/31/2013

4. TITLE AND SUBTITLE

Development of Extinction Imagers for the Determination of Atmospheric Optical Extinction

5a. CONTRACT NUMBER

5b. GRANT NUMBER

N00014-07-1-1060

5c. PROGRAM ELEMENT NUMBER

6. AUTHOR(S)

Janet E. Shields
Monette E. Karr
Vincent W. Mikuls
Paul J. Berger
Paul A. Frederickson
Richard J. Lind
William S. Hodgkiss

5d. PROJECT NUMBER

5e. TASK NUMBER

5f. WORK UNIT NUMBER

7. PERFORMING ORGANIZATION NAME(S) AND ADDRESS(ES)

Marine Physical Laboratory of the Scripps Institution of Oceanography
University of California, San Diego
291 Rosecrans Street
San Diego, California 92106

8. PERFORMING ORGANIZATION REPORT NUMBER

9. SPONSORING/MONITORING AGENCY NAME(S) AND ADDRESS(ES)

Office of Naval Research
875 N. Randolph Street, ONR
Arlington, VA 22203-1995
Sarwat Chappell

10. SPONSOR/MONITOR'S ACRONYM(S)

11. SPONSOR/MONITOR'S REPORT NUMBER(S)

12. DISTRIBUTION/AVAILABILITY STATEMENT

Approved for public release; distribution is unlimited

13. SUPPLEMENTARY NOTES

14. ABSTRACT

The primary goals of this project for JTO and ONR (Grant N00014-07-1-1060) were to further develop Extinction Imagers for use in the ocean environment, and to extend the capabilities into the Short Wave IR (SWIR). Extinction Imaging is a method for determining the effective extinction coefficient over an extended path using a sensor at one end of the path. It uses calibrated imagers to acquire the relative radiance of a dark target near the other the end of the path and the horizon sky in the direction of the dark target. It is completely passive and thus covert, and the hardware is robust and relatively inexpensive. It uses rigorous equations, which determine the extinction coefficient from the measured apparent contrast of the radiance of the dark target with respect to the horizon sky.

The project was very successful. We found that the ocean surface could readily be used as a dark target in red and SWIR wavelengths. Both the red and the SWIR measurement results were excellent for daytime. Comparisons with standard instruments

15. SUBJECT TERMS

Extinction imager, extinction coefficient, beam transmittance, atmospheric extinction, and atmosphere

16. SECURITY CLASSIFICATION OF:			17. LIMITATION OF ABSTRACT	18. NUMBER OF PAGES	19a. NAME OF RESPONSIBLE PERSON
a. REPORT	b. ABSTRACT	c. THIS PAGE			Anne J. Footer
Unclassified	Unclassified	Unclassified	None	151	19b. TELEPHONE NUMBER *(Include area code)* 858-534-1802

Reset

Standard Form 298 (Rev. 8/98)
Prescribed by ANSI Std. Z39.18

Abstract

The primary goals of this project for JTO and ONR (Grant N00014-07-1-1060) were to further develop Extinction Imagers for use in the ocean environment, and to extend the capabilities into the Short Wave IR (SWIR). Extinction Imaging is a method for determining the effective extinction coefficient over an extended path using a sensor at one end of the path. It uses calibrated imagers to acquire the relative radiance of a dark target near the other the end of the path and the horizon sky in the direction of the dark target. It is completely passive and thus covert, and the hardware is robust and relatively inexpensive. It uses rigorous equations, which determine the extinction coefficient from the measured apparent contrast of the radiance of the dark target with respect to the horizon sky.

The project was very successful. We found that the ocean surface could readily be used as a dark target in red and SWIR wavelengths. Both the red and the SWIR measurement results were excellent for daytime. Comparisons with standard instruments, as well as uncertainty analysis, indicated that extinction imagers provide better measurements of the atmospheric extinction losses over extended paths than other methods of which we are aware.

Our secondary goals were to address the night regime, and to address slanted paths above the horizontal. Regarding night, we found that the visible sensor acquired excellent data, but the ocean surface was not a good dark target in our wavelengths. Recommendations on the handling of night are given in the report. Regarding the lines of sight above the horizon, we developed a slant path algorithm that determines beam transmittance. It performed very well. Recommendations are made regarding integration of these techniques for military applications.

Table of Contents

List of Figures

List of Tables

Table Page

Development of Extinction Imagers For the Determination of Atmospheric Optical Extinction

Janet E. Shields[1], Monette E. Karr[1], Vincent W. Mikuls[2], Paul J. Berger[3], Paul A. Frederickson[4], Richard J. Lind[4] and William S. Hodgkiss[1]

1. Marine Physical Laboratory, Scripps Institution of Oceanography, University of California San Diego, La Jolla, CA
2. Previously with Marine Physical Laboratory, currently at Ametek Programmable Power, San Diego, CA
3. MIT Lincoln Laboratory, Lexington, MA
4. Naval Postgraduate School, Monterey, CA

1. SUMMARY OF THE PROJECT

This is the final report for Grant N00014-07-1-1060 with the Office of Naval Research (ONR). The source of the funding was the High Energy Laser – Joint Technology Office (JTO), and both ONR and JTO were active in providing help and guidance. The purpose of the project was to develop concepts and methods for using imagers to measure atmospheric extinction at sea. We will refer to these instruments and their associated algorithms in the generic sense as Extinction Imagers (EI). The atmospheric extinction and the related path beam transmittance affect numerous applications involving imaging through the atmosphere, the use of high energy laser weapons, and detection of optical targets.

This work is collaboration between the University of California San Diego (UCSD), the Lincoln Laboratory at the Massachusetts Institute of Technology (MIT), and the Naval Postgraduate School (NPS). The Marine Physical Lab (MPL) at Scripps Institution of Oceanography (SIO) is part of UCSD. The authors from MPL were part of the Atmospheric Optics Group (AOG), and were responsible for developing the EI hardware and concepts. The author at MIT Lincoln Laboratory provided supporting instrumentation, as well as guidance. The authors at NPS provided instrumentation to document weather conditions, and monitored and installed the weather instruments.

The AOG first developed the EI concept in the late 1980's under Air Force funding. More recently, the EI concept was further developed for the Navy, using an extinction imager to image a dark target and the horizon sky. The imagers measure the effective extinction for the full path between the imager and the target. This extinction is derived from the measured contrast between the radiance of the dark target and the horizon sky. The equations for this derivation are rigorous in the absence of measurement uncertainties. Under this earlier contract with the Navy, the method was shown to work very well for fixed dark targets in visible wavelengths. For the current grant, our goal was to determine whether the ocean surface was sufficiently well behaved optically to be used as a dark target, and to further develop this capability both in the visible and in the

Short Wave Infrared (SWIR). The ultimate goal is to develop the technique sufficiently so that it can be used in the field, either on land or on the sea, for test scenarios as well as shipboard operational use.

This development is of interest because the system is single-ended, yet it measures an extended path in any direction. It can be adapted for different wavelengths. It is covert (due to having no active beam), and expected to be robust and cost-effective. Other standard approaches include transmissometers which require a transmitter at one end and a sensor at the other end of the path making use over extended paths in any direction impractical. Point Scatter Meters and Nephelometers both use a very limited path (typically a few inches or less), and do not provide the extinction over an extended range. Some lidars can provide relative aerosol amount and/or detect the presence of clouds, but it is difficult to determine the absolute value of the extinction coefficient with lidars. Lidars also can be much more costly and less robust than an extinction imager. In addition, lidars put out an active signal that can potentially be detected by others. In comparison, extinction imagers are completely passive, and thus more covert. Extinction imagers are single-ended systems that can be used to determine the effective extinction over an extended path. They can be modified to use any wavelength in the visible through short-wave infrared, and they can quickly be pointed in any direction, to document the full surround.

During the project, we built and fielded a visible extinction imager entitled the Multispectral Scattering Imager (MSI), and a SWIR band imager entitled the Shortwave Infrared (IR) Extinction Imager (SRI). (The MSI actually measures extinction, but it was named when the work was being done only in the visible, where scattering and extinction are nearly equivalent). These instruments were fielded along with several support instruments at a site looking over the ocean from the west side of Point Loma in the San Diego area. This site provided a full 180º view over the ocean, including islands to the south that were very useful in image assessment. The support instruments included a weather station, a weather buoy, two transmissometers, a ceilometer, and a Point Scatter Meter (PSM). The imagers and their control software were provided by the MPL team. The weather station and buoy were provided and supported by the NPS team, and the transmissometers were provided by the MIT Lincoln Laboratory team. The PSM was purchased and supported by the MPL team. Data collection software was developed by each of the support teams for their respective instruments.

Following extensive data collection and analysis, the MPL team optimized the data processing algorithms, developed under the previous contract, to adapt them for the current experiment and the ocean environment. These data processing algorithms are designed to determine the extinction coefficients for the line of sight from the raw data, and are referred to as Extinction Algorithms in this report. We found that the extinction results were excellent under most conditions, and that the ocean surface worked quite well as a well-behaved dark target in the red and SWIR wavelengths. The correlation between the visible and the SWIR results was excellent. The extinction coefficients often, but not always, were consistent with the scattering coefficients from the PSM and the extinction coefficients from the transmissometers. However, the PSM scattering

coefficients were much more consistent with the MSI and SRI extinction coefficients than with the transmissometer extinction coefficients, even though the PSM and transmissometers are considered standard instruments. Differences between the PSM and MSI or SRI appeared generally to be due to the difference between the limited path and the extended path. The only exception (i.e., when the MSI and SRI did not do well) was under high gloss sea conditions, which will be discussed in the body of this report.

In the optional Phase II of the project, we were asked to evaluate nighttime scenarios, and to also evaluate the possibility of extending the algorithm to address slant paths, i.e. paths looking at angles above the horizontal. We were able to acquire good night-time data in the visible, but unfortunately the ocean surface did not appear to be an adequate dark target at night. We could find no reason that the extinction imager technique should not work well at night with a dark target despite the ocean not appearing to be an adequate dark target. We were more successful with the slant path task. We developed a Slant Path Algorithm that should provide good transmittance results for paths looking above the horizontal. This algorithm uses the MSI or SRI extinctions as an input, and also can use ceilometer data if available.

The grant research was successful in developing both a visible and a SWIR extinction imager, along with the methods and algorithms to provide excellent determinations of transmittance over extended horizontal or slant paths under most conditions.[1] The pros and cons of using the visible vs. the SWIR will be discussed in the body of the report. The two remaining weaknesses of this approach are that the system may not yet work in high sea gloss conditions such as may occur under very low wind, and on those nights when the ocean surface fails to work well as a dark target`. The strengths of the instrument concepts are that they are relatively inexpensive, robust, and covert, and as single-end systems, can provide beam transmittance over an extended path. They can easily be modified with different spectral filters, and can be expected to work for any site, in any direction. Although developed for land tests using a dark target or using the ocean surface as a target of opportunity, they also hold promise for other applications using other targets of opportunity.

[1] Particularly significant findings and recommendations will be noted in the text with the words "Finding" or "Recommendation" in blue after the paragraph discussing the result, and will be listed in the Conclusions Section.

2. INTRODUCTION AND GOALS

This is the final report for Grant N00014-07-1-1060 with the Office of Naval Research (ONR). The source of the funding was the High Energy Laser – Joint Technology Office (JTO). Both ONR and JTO were active in providing help and guidance. The project is entitled "Passive Imaging System for Measuring Atmospheric Scattering and CFLOS". Only the development of the imaging systems was funded. The CFLOS (Cloud Free Line of Sight) effort was not of as much direct interest, and was not funded. This work is collaboration between the University of California San Diego (UCSD), the Lincoln Laboratory at the Massachusetts Institute of Technology (MIT), and the Naval Postgraduate School (NPS). The Marine Physical Lab (MPL) at Scripps Institution of Oceanography (SIO) is part of UCSD.

The purpose of the project was to develop the concepts and methods for using imagers to determine atmospheric extinction coefficients and optical beam transmittance in operational or test environments at sea. Atmospheric extinction and the related path beam transmittance affect numerous applications involving light propagation through the atmosphere, including the use of high energy laser weapons, and detection of optical targets. The ultimate goal this project is to make more practical the measurement of optical extinction at sea and in other environments.

As discussed in Sections 1 and 2.3, we had previously developed Extinction Imagers (EI) using black targets at visible wavelengths. For this project, we further developed EI systems to use the ocean surface in place of a black target. We extended the measurement capability to the Short Wave Infrared (SWIR) wavelengths, and developed methods to extend the capability from horizontal to slanted lines of sight. As part of the project, we improved a visible/Near Infrared (NIR) EI system called the Multispectral Scattering Imager (MSI)[2], and developed a SWIR version called a SWIR band imager entitled the Shortwave Infrared (IR) Extinction Imager (SRI). The project was very successful in further developing these extinction imager capabilities.

2.1. Overview of the Method

The Extinction Imager method requires an imaging sensor that can measure either the absolute radiance of objects in a scene or the relative radiance of the elements within the scene. The method depends on having a dark optical target and measuring the contrast between the dark target and the horizon sky (i.e. sky just above the horizon). Once the contrast for a very clear day has been characterized, the effective extinction of the line of sight to the target can be derived from the measured contrast. As will be described Section 3, the theory behind this method is rigorous, and based on standard atmospheric extinction theory.

In a previous project, funded by the Navy [1] from 2005 to 2007, the AOG developed this technique using an imager viewing a passive black target across the San Diego Bay [2,

[2] The MSI actually measures extinction, but it was named when the work was being done only in the visible, where scattering and extinction are nearly equivalent.

3]. As discussed in Section 4, the results were excellent, and compared well with transmissometer measurements. For this project, we wished to extend the development to determine the feasibility of using targets of opportunity such as portions of the ocean surface in place of the black target. We also wished to extend the capability from the visible into the Short Wave IR, and compare the use of visible sensors and SWIR sensors. Goals added later in the program included evaluation of the possibility of extending the methods to night-time and extending the results from horizontal lines of sight to slanted lines of sight.

Extinction coefficient will be defined in Section 3. Extinction includes both scattering of light out of a beam, and absorption of light (changing it to another form of energy). When we first began our work with extinction imagers, we were working only in visible bands, where the absorption is negligible. In these bands, scattering coefficient and extinction coefficient are essentially equal. When we extended the capability to the SWIR, we determined that imagers actually determine extinction coefficient, which was the preferred parameter. Although we have tried to be consistent in using the term "Extinction", particularly in the SWIR bands, some of our earlier usage, including the original title of the project, includes the term "Scattering".

2.2. Applications

The intent of this development is that Extinction Imagers should determine the beam transmittance for horizontal or slant-paths of known length and direction. EIs directly determine the effective extinction coefficient over a horizontal line of sight of extended length in essentially any direction for essentially all conditions. From this value, beam transmittance for horizontal path lengths can be determined directly, and beam transmittance for slant-paths can be determined with reasonable accuracy. Such a system could be used for several applications.

Extinction imagers can be used in the test of lasers and laser weapons, or other tests impacted by atmospheric conditions, either at sea or on the land. As laser weapons are in development, it is important to understand the losses due to the atmosphere and their impact, so that test results may be properly analyzed and understood.

With the developments funded under this grant, EIs can be modified for operational use on ships or aircraft carriers. For example, if there is a moving target, an extinction imager could be part of a ship-board system to provide updated optical beam transmittance from the ship to the target. The ship's systems could continually update range and direction to the target, and in real time, the extinction imager could determine the beam transmittance to the target. For laser weapons, this transmittance could be used as input to the algorithms that determine required laser dwell time on a target. We would anticipate that the EI systems would routinely monitor the beam transmittance over extended paths in essentially all directions, but in a test or operational situation, the instrument would look only in the direction of interest.

The beam transmittance affects not only the energy reaching a target, but also the ability to detect a target. Thus the EI systems should be applicable to a variety of optical test scenarios in the real world environment. Extinction imagers could also be used over the long term for developing statistical data bases of extinction coefficient measurements over various parts of the globe.

As a result of the work on this project, the EI systems can be used either with black target or with the ocean surface as a target. We feel that future systems could also be developed to use other targets of opportunity such as drones or natural terrain features.

2.3. Overview of Historic Developments in Extinction Imagers

The theory of radiative transfer and extinction in the atmosphere has been developed over many years and documented in many texts. Some of the early developers include Koschmeider [4] and Duntley [5]. More recent discussions are included in Boy [6], McCluney [7], McCartney [8], and Liou [9]. The theory as it applies to Extinction Imagers will be discussed in Section 3 and in Appendix A. Appendix A discusses the MSI system from the report for a previous contract [1]. Whereas that full report has limited distribution, the MSI chapter has been approved for general distribution.

Many researchers have been involved in measurements of extinction coefficients and other related atmospheric parameters over the years. For example, our Atmospheric Optics Group (AOG) has for many years been part of MPL, which in turn is part of SIO at the University of California, San Diego. The AOG was originally part of the Visibility Laboratory at SIO. Our early work included many projects to measure atmospheric parameters including scattering coefficient in several wavelengths in the visible, using airborne systems. Simultaneous measurements included temperature and dewpoint temperature, as well as upwelling and downwelling irradiance and the radiance distribution in the upper and lower hemisphere. [References 10-12 are examples of the resulting reports]. As part of these projects, the AOG developed high precision Nephelometers, which measured the total volume scattering coefficient as well as the directional scattering functions at 30º and 150º scattering angle for an incremental volume of air as the aircraft transited the path [13].

Early developments of the concepts used in the EI systems include Curio and Durbin [14] and Hood [15]. Radiometers were used with black targets by Malm [16, 17] for determining extinction over extended paths. In the late 1980's, the AOG began development of imagers for determination of extinction over extended paths [18 - 20]. This instrument was designated the Horizon Scanning Imager (HSI) and is shown in Fig. 2-1. This is the first example of using the Extinction Imager concept with digital imagers that we are aware of.

The HSI worked reasonably well. Using an imaging sensor as opposed to a radiometer meant that multiple dark targets could be used. Also, the darkest part of each target could be automatically selected to preclude alignment issues. Although the digital cameras available to us at the time were somewhat primitive, the project was a major step forward

and also yielded experience in understanding the types of uncertainties inherent in the methods [21].

Fig. 2-1. Horizon Scanning Imager developed in late 1980's for determining Visibility

During 2005 – 2007, the EI concept was further developed by the AOG under funding from the Navy, using a modern 16 bit Charge-coupled Device (CCD) camera pointing across the San Diego Bay at a known dark target [1 - 3]. This instrument was the first generation that was entitled the MSI. Although this development was based in part on the earlier HSI system, it was a huge step forward, because the imager was much better, and we had a better understanding of the camera calibrations. This work is discussed in Section 4 and in more detail in Appendix A.

Janeiro et al. have recently developed systems using two dark targets [22]. Their primary goal was the development of an inexpensive and cost-effective system. In addition, during the current AOG project, we collaborated with a team at Pennsylvania State University's Electro-Optics Center (EOC)[3] in order to transfer the technology to them. They have modified these concepts and the AOG extinction algorithms for their setup, and successfully applied the technique in field tests [23].

We also mention related developments that provided the AOG with useful experience in this project. Over many years, the AOG developed Day/Night Whole Sky Imagers using 16 bit digital cameras [24 - 26], which gave us extensive experience with high quality CCD cameras and atmospheric optics. The AOG developed a SWIR optical system for use in airborne measurements of upwelling and downwelling radiance distributions [27], which provided experience with SWIR cameras. In addition to this experimental work, we carried out analysis of the measured relationships between ground-based visible and infrared extinction coefficients measured in Europe [28, 29].

[3] EOC is also referred to as PSU in some of the memos

2.4. Alternative Approaches to Measuring Extinction

Several other approaches to measuring extinction have been used. Transmissometers [30] have been a standard instrument for many years. By using a source and a receiver, they provide a direct measurement of the total beam transmittance along a fixed path. Their primary disadvantage for our applications is that they are not single-ended systems, and are thus difficult to deploy from a ship for measurements of extended paths beyond the ship. In addition, the path for a given transmissometer is fixed in length and direction. A second type of system measures the scattering in an incremental volume of air. Both Nephelometers [13] and Point Scatter Meters [31] are of this type. Unlike transmissometers, they are single ended and only measure the air in one location. On a ship, this air may not be representative of the general surround, due to unequal heating around the ship. These instruments do not measure an extended path in different directions.

Most lidars can measure over extended paths in different directions, and at least one has been developed to determine extinction coefficients [32]. However, as discussed in Technical Memorandum AV10-005t[4], it is quite difficult for lidars to provide the absolute magnitude of extinction coefficients. Extinction Imagers have the advantage that they are completely passive, i.e. they do not require an active beam, and are thus more covert. In general, EI systems are expected to be smaller, less costly, and more robust than lidars that may provide extinction coefficients.

As a result of the analysis of the current and previous projects, we feel that EI systems not only have the advantages discussed above, but also provide for more accurate determinations of beam transmittance than the alternative methods.

2.5. Specific Goals of the Project

Our AOG group has developed two generations of Extinction Imagers: the HSI discussed in Section 2.3, and the first generation MSI mentioned in Section 2.3 and further discussed in Section 4. The first generation MSI was not fully single ended, because it used a black target at the end of the path. One of the specific goals of this current project was to determine whether the ocean surface or other targets of opportunity could act as a well behaved dark target, so that the system could be single ended. Additionally, we could compare results in the visible and the SWIR, and determine which might be better for future operational use. All of these goals were met. Originally, the proposal included a Phase II option to build and test prototype systems optimized for the operational scenario (as opposed to the test and development scenario) but this task was not funded. However, other higher priority tasks were funded under the Phase II option.

Another task was to develop a method to extend the results from the horizontal to slant paths through the atmosphere. This goal was successfully completed. We were also

[4] All technical memoranda referenced in this report should be available to the reader. The memoranda are listed in Section 16.1, along with additional information on their availability. Throughout the remainder of this report, we will use the more informal term "Memo(s)".

asked to evaluate whether it would be possible to use the extinction imager technique at night using the ocean surface as a target. We completed the test and evaluation, and found that although the system acquired excellent images at night, the ocean surface did not appear to be a good target. The technique should work at night with a dark target. An additional goal was to evaluate what would be needed to transition the capability into use on military programs. This goal was also completed, and the technology was successfully transitioned to the EOC research group for laser tests [23].

The theory is discussed in following Section 3, and previous results are discussed later in Section 4. The goals discussed here and the associated work are discussed in Sections 5 through 13.

3. THEORY

A simple derivation of the equations used in the MSI and SRI is given in earlier documents [2, 3] and based on the work of Duntley [5, 10, 11, and 12]. Because there is often confusion between the definitions of radiance, irradiance, illuminance, and similar terms, as well as confusion regarding which parameters decrease with distance squared and which do not, we would like to go back to a more basic discussion in this section. If the reader is familiar with terms such as "radiance", skip to Section 3.3, which discusses how the equations are used in the extinction imagers. Much of this discussion is also included in Appendix A. However, in Appendix A, we have used terminology more familiar to some of the other authors unchanged from the report of which it was a part [1].

3.1. Basic Terms and Equations

As discussed in Boyd [6], McCluney [7] and others, a source radiating energy or flux dφ into a solid angle dΩ has a radiant intensity I in a given direction defined by I = dφ/ dΩ. Boyd shows that if the source has an area given by dA, then the irradiance of this source, as seen from a distance r and angle θ is given by

$$E = \frac{d\phi}{dA} = \frac{I \cos\theta}{r^2} \qquad 3.1$$

Boyd also shows that the inverse-square law, i.e. the $1/r^2$ term, in general is valid only for the irradiance of point sources, where the source is much smaller than the sensor field of view. The term irradiance may be taken as the energy per unit area emitted by a radiant source. It can also be taken as the energy per unit area received by a surface. Also spectral irradiance refers to the irradiance per wavelength, integrated over a source and sensor effective waveband. Illuminance is a similar term integrated over the waveband corresponding to the responsivity of the human eye, as discussed in Boyd and McCluney.

Boyd also defines the related term radiance as the energy per unit area per unit solid angle emitted by a radiant source, and shows that it can be defined by the equation

$$L = \frac{d^2\phi}{dA \cos\theta d\Omega} \qquad 3.2$$

In this equation the cosθ term comes from the fact that we are talking about a source of area dA, but when viewed from an angle θ, its effective area is cosθ dA. It is generally used to indicate the energy in a given direction, i.e. with a somewhat limited solid angle. More generally, if a sensor such as a radiometer views any extended source that fills the field of view of the radiometer, we define the radiance as the energy per unit area per solid angle received by the radiometer. That is, the term radiance can be used to describe either the energy leaving the source or the energy measured by a sensor.

The spectral radiance refers to the radiance per wavelength. Luminance is a similar term when the waveband corresponds to the responsivity of the human eye. The path along

which the radiance travels will be referred to as either the line of sight or the path of sight.

An imaging system such as a camera with lens measures radiance, if no diffuser is present in the system and the extended source is large enough to fill a pixel. That is, each pixel acts like a radiometer, and measures radiance, not irradiance. Few sensors are perfect though. Often the response of the sensor to the radiant field varies slightly as a function of pixel (due to chip non-uniformity) or of angle through the lens (due to Fresnel losses). And often the response is not quite linear (a doubling of the radiance may not cause an exact doubling of the signal). As a result, calibration is typically required to rigorously relate the signal to the radiance of the elements in the scene. The calibration is discussed in Section 8.3.

One of the basic laws of radiometry is that in the absence of atmospheric losses, and with uniform index of refraction, radiance is conserved. The radiance of an extended source as viewed from distance r_1 is the same as the radiance as viewed from distance r_2, where by definition the extended source must fill the field of view of the radiometer or pixel at both distances. This law that radiance is conserved is also derived in Boyd. From an intuitive point of view, one can think of a simple radiometer or Gershun tube, i.e. a tube with a sensitive area dA and solid angle dΩ. As the distance r of this tube to an extended source is increased, the amount of flux received from any point on the source decreases by $1/r^2$; however the total area seen by the sensor increases by r^2, so that the radiance seen by the sensor remains constant in the absence of atmospheric attenuation or extinction (the terms are equivalent, and include both absorption and scattering). The irradiance of a point source does decrease as a function of r^2, but in a totally clear atmosphere radiance does not.

In the presence of a real atmosphere of other attenuating medium, the signal is attenuated as the range increases. Attenuation is sometimes defined as the loss of irradiance in an incremental path if and only if the light is collimated [e.g. McCartney 8]. Since we are working with radiances, we prefer to define attenuation as the loss of radiance in an incremental path as in Duntley [5] and Liou [9], as illustrated in Fig. 3-1. In this case, the extinction or attenuation coefficient is defined by Eq. 3.3.

$$dL/L = \alpha dr = \alpha dz \sec\theta \qquad 3.3$$

In this equation, L is radiance, α is attenuation or extinction coefficient, dr is incremental distance along the path, dz is incremental altitude, and θ is the zenith angle (angle from the vertical, also sometimes called "zenith distance").

The beam transmittance for an extended path is defined as the fractional loss of this radiance over the whole path, and is given by Eq. 3.4.

$$T_r(z,\theta) = \int_{r_1}^{r_2} e^{-\alpha r}\, dr \qquad 3.4$$

where r is the length of the path, z is the altitude of the observer or sensor, θ is the zenith angle (from 0° overhead to 90° at the horizon), and α is the extinction coefficient. The θ term enters into the equation when the incremental path dr is computed for the path.

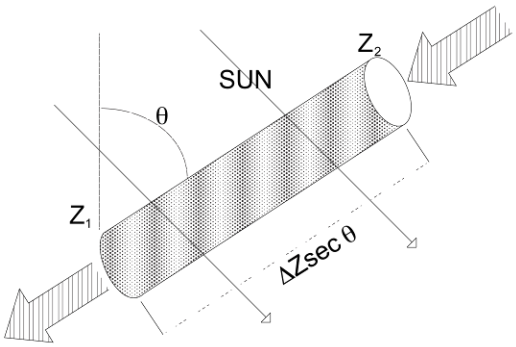

Fig. 3-1. Light attenuation and scattering in the incremental path

Note that if the extinction is uniform along the path, this simplifies to

$$T_r(z,\theta) = e^{-\alpha r} \qquad 3.5$$

Our goal is to determine the effective extinction coefficient and the beam transmittance for extended paths, using the measured radiance (or relative radiance) of a target and the horizon sky.

The radiance of an optical target is affected not only by extinction along the path, but also by stray light from the surround. In the atmosphere, light is scattered into the incremental path from the surround, and the total incremental radiance change is given by Eq. 3.6.

$$dL/dr = L_*(z,\theta,\phi) - L(z,\theta,\phi)\alpha \qquad 3.6$$

In this equation L_* is the path function, which is the light scattered from the sun, sky, and terrain into the direction of the path of sight by the atmosphere in the incremental volume. We next define the radiance of a target at range 0 as inherent radiance, designated as ${}_tL_0(z_t,\theta,\phi)$ where z_t is the altitude of the target. Similarly, the radiance of a target at range r is called the apparent radiance and designated as ${}_tL_r(z,\theta,\phi)$ where z is the altitude from which the target is observed.

Integrating the equation of transfer 3.6, we can derive that these terms are related by Eq. 3.7.

$${}_tL_r(z,\theta,\phi) = {}_tL_0(z_t,\theta,\phi) * T_r(z,\theta) + {}_pL_r^*(z,\theta,\phi) \qquad 3.7$$

In this equation, T_r is the beam transmittance of the path, defined by Eq. 3.4. Typically the ϕ term is not included in Eq. 3.4, because in a reasonably uniform atmosphere, the

beam transmittance is not dependent on the azimuth angle; however the EI theory does not require it to be independent of azimuth angle. In the Eq. 3.9, the ${}_pL_r^*(\theta,\phi)$ term is called the path radiance, and is defined as

$${}_pL_r^*(\theta,\phi) \equiv \int_0^r L_*(\theta,\phi)T_{ri}(\theta)dr \qquad 3.8$$

In this equation, $T_{ri}(\theta)$ is the transmittance from the observer to the path increment. That is, we integrate the path function over the whole path, taking into account that light scattered into any incremental path will be further attenuated by the path between the observer and the incremental path position.

Thus our integrated form of the equation of transfer Eq. 3.7 shows that the apparent radiance of a target is equal to the inherent radiance of the target times the transmittance from the observer to the target, plus the light scattered into the path from the surround for the whole path. The former term is the light with information about the target which has been attenuated by the atmosphere, and the latter term can be thought of as an additive noise term, as it has no information about the target.

All of these equations apply both to radiance at a single wavelength and to near-monochromatic spectral radiance (i.e. radiance per wavelength). If we are dealing with spectral radiance, then typically the spectral radiance is in the units of watt/ster m^2 μm, z and r can be given in m or km, and α has the units of m^{-1} or km^{-1}. In the visible system, we use reasonably narrow pass bands such that the theory also applies to the spectral radiance averaged over our pass bands. The SWIR system uses a broader pass band that includes absorption windows where absorption is low as well as regions where the absorption is higher. The impact of this pass band on the SWIR system results will be discussed later in this section.

3.2. Derivation of Extinction Coefficients from the Measurements

This section shows how these equations can be applied for extinction imaging, and provides the specific equations used in the MSI and SRI extinction algorithms. As shown in Eq. 3.7, the apparent radiance ${}_tL_r$ of a visual target t, as observed from range r, is a function of the inherent radiance of the target measured from range 0, the beam transmittance T_r of the path, and the path radiance ${}_pL_r^*$ of the path. The beam transmittance is a loss term, and represents the loss in radiant energy due to both scattering and absorption (which together comprise extinction or attenuation). The path radiance is a gain term; however, it contains no information about the target. It consists of the radiance scattered into the line of sight by the molecular, aerosol and other scattering components along the path. However, it is also affected by absorption, because the light scattered into an incremental path length is then attenuated by both scattering and absorption as it approaches the sensor, as shown in Eq. 3.8.

All of these components are directionally dependent, as shown in Section 3.1. However for notational convenience we will express Eq. 3.7 as shown in Eq. 3.9.

$$ {}_t L_r = {}_t L_0 * T_r + {}_p L_r^* \qquad 3.9 $$

For the EI method, we introduce the universal contrast which is defined as the contrast between the target and its background as shown in Eq. 3.10. The two terms in Eq. 3.10 are the inherent contrast, measured from range 0 and apparent contrast measured from with range r.

$$ C_0 = \frac{{}_t L_0 - {}_b L_0}{{}_b L_0} \quad \text{and} \quad C_r = \frac{{}_t L_r - {}_b L_r}{{}_b L_r} \qquad 3.10 $$

Substituting Eq. 3.9 into Eq. 3.10, we have

$$ C_r = \frac{{}_t L_r - {}_b L_r}{{}_b L_r} = \frac{({}_t L_0 * T_r + {}_p L_r^*) - ({}_b L_0 * T_r + {}_p L_r^*)}{{}_b L_r} \qquad 3.11 $$

For this application, we define the inherent background radiance to be the radiance of the background as measured from the target location. In this case, the path radiance over range r from the viewer to the target is the same as the path radiance over range r from the viewer to the defined location for the inherent background, and the path radiance terms cancel as in Eq. 3.12.

$$ C_r = \frac{{}_t L_0 * T_r - {}_b L_0 * T_r}{{}_b L_r} \qquad 3.12 $$

In practice, we can use a background that is close enough to being adjacent so that the path radiances are the same. (The impact of using the horizon for the background will be discussed later.) Now we can rearrange this equation as in Eq. 3.13, and substitute Eq. 3.10 for the inherent contrast to yield Eq. 3.14.

$$ C_r = \frac{T_r * ({}_t L_0 - {}_b L_0)}{{}_b L_r} = \frac{T_r * ({}_t L_0 - {}_b L_0)}{{}_b L_0} \frac{{}_b L_0}{{}_b L_r} \qquad 3.13 $$

$$ C_r = T_r * C_0 * \frac{{}_b L_0}{{}_b L_r} \qquad 3.14 $$

So far no approximations have been made as long as inherent background radiance is defined as stated above. Next consider the case where the background is in fact the horizon sky. In this case, ${}_b L_r$ is the horizon as seen from a distance r from the target, and ${}_b L_0$ is the horizon as seen from the position of the target. Duntley [5] discusses the concept of equilibrium radiance. Equilibrium radiance is defined as the radiance for which the transmission losses over an incrementally small path are equal to the path radiance increases over an incrementally small path, so that there is no difference between the radiance when it enters the increment and leaves the increment. If a target is very bright, the radiance of a target will asymptotically decrease and approach equilibrium radiance as r increases. If the target is very dark, the radiance of a target will asymptotically increase and approach equilibrium radiance as r increases. All targets will asymptotically approach the equilibrium radiance along a uniform path such as a

horizontal path in a uniform atmosphere. For this horizontal path, the equilibrium radiance will be a function of atmospheric conditions and will also vary as a function of azimuth angle around the horizon.

Duntley shows that the clear horizon radiance in each direction along the horizon is equal to the equilibrium radiance in that direction. That is, in a uniform atmosphere, for a horizontal line of sight, the horizon radiance in a given direction will reach the equilibrium for that direction, assuming it is not so clear that the earth curvature effects become significant. There will be times when there are scattered clouds on the horizon. We have introduced features into the extinction algorithm to deal with this situation. It turns out that because the background radiance appears in both the numerator and denominator of Eq. 3.10, the impact of non-ideal horizons on the derived extinction is quite small for dark targets. This will be discussed in later sections. For now, we assume uniform conditions.

As a result, if we use the horizon as our background, then ${}_bL_r$, i.e. the horizon as seen from a distance r from the target, is equal to ${}_bL_0$, the horizon as seen from the position of the target. These terms cancel in Eq. 3.14, yielding Eq. 3.15

.

$$C_r = T_r * C_0 \qquad 3.15$$

By definition, we also have the equation for transmittance of a horizontal path in uniform conditions given in Eq. 3.5, $T_r(z,\theta) = e^{-\alpha r}$. Inserting Eq. 3.5 into 3.15 and rearranging, we have the results shown in Eq. 3.16 and 3.17.

$$C_r = e^{-\alpha r} * C_0 \qquad 3.16$$

$$\alpha = -\frac{1}{r}\ln(C_r / C_0) \qquad 3.17$$

Likewise, the beam transmittance for the horizontal line of sight to the target is derived by substituting the results of Eq. 3.17 into Eq. 3.5. In the visible, the scattering coefficient s is, for all practical purposes, equivalent to the extinction coefficient α, and may be substituted in the above equations.

The MSI and SRI extinction algorithms use Eq. 3.17 to derive the extinction coefficient from the measured apparent contrast, using the known range to the target and the estimated inherent contrast. The assumptions that have gone into this equation for the MSI and SRI are:

a) The target background is the horizon sky. The MSI and SRI are set up such that this is true.

b) The angle to the horizon is close enough to the angle to the target that the path radiance will be the same for the target and background, within measurement error. The MSI and SRI are set up such that this is true.

c) The horizontal line of sight is reasonably uniform in a given direction. In practice, we need not assume this, because the MSI and SRI provide the effective extinction coefficient and the total beam transmittance for the path from the sensor to the dark target. If derived transmittance for other path lengths in the same direction (using Eq.

3.5), then we are assuming reasonable uniformity, but for the range to the dark target this assumption is not needed.
d) The horizon is close to the equilibrium radiance. In practice, we find this assumption has little impact as mentioned above and further discussed in Section 8.5.

Although the extinction algorithm derives beam transmittance using measurements of contrast transmittance, we are in fact deriving beam transmittance, and not contrast transmittance which is also defined by Duntley [5]. As discussed in Duntley [5], contrast transmittance is defined by Eq. 3.18.

$$\tau_r = C_r \Big/ C_0 = T_r \frac{{}_b L_0}{{}_b L_r} \qquad 3.18$$

Unlike beam transmittance, contrast transmittance is not the same for a path and its reciprocal. The AOG participated in extensive programs designed to determine contrast transmittance [10, 11], but it is not the desired parameter for this application. The MSI extinction algorithm uses Eqs. 3.17 and 3.5, so that the result is beam transmittance and not contrast transmittance.

For the MSI, the extinction algorithm also derives visibility. Visibility is typically defined as the range r at which a large black target is just at threshold for a human viewer [33]. Although the human contrast threshold depends on a number of parameters such as light adaptation and target shape, Duntley used ε = -.05 as a good rule of thumb when the human is looking at a large black target when visually adapted for the horizon radiance. Some researchers prefer a human threshold value of -.02, and our understanding is that this is why meteorological range is defined with a contrast of -.02. If the target is completely black, it has a radiance given by ${}_t L_o = 0$, and the inherent contrast, from Eq. 3.12, is

$$C_0 = \frac{(0 - {}_b L_0)}{{}_b L_0} = -1 \qquad 3.19$$

To derive the equation for visibility, we substitute V for r and s for α in Eq. 3.16. Also, the apparent contrast is at threshold when the range equals visibility, so we substitute a value of -.05 or ε for C_r. And since the visibility equation is only applied to black targets we substitute a value of -1 for C_0. The result is shown in Eq. 3.20

$$\varepsilon = e^{-sV} * (-1) \qquad 3.20$$

When rearranged, this becomes

$$V \equiv -\ln(-\varepsilon)/s = 3/s \qquad 3.21$$

This very simple equation V = 3/s is in common usage, but it assumes that the human is viewing a large object that is truly black, that it is seen against a clear horizon, and that it is at such a range that its apparent contrast is really at the human threshold. These are a lot of assumptions, and this is one reason why visibility determined by human estimation is often considered a rough estimate.

With the MSI and SRI, however, these same assumptions are unnecessary. The target does not have to be at the threshold value, because its apparent contrast can be measured. The target does not have to be exactly adjacent to the horizon, because the horizon can be measured separately (as long as it's at the same approximate angle). A completely black target is not necessary, because most targets can be measured from close range or on clear days, and their inherent contrast estimated. The definition of visibility remains the same, but by measuring the actual apparent and inherent contrast, visibility can be determined much more accurately than estimated by a human.

In the MSI extinction algorithm, Eq. 3.17 determines the extinction coefficient. Since in the visible, extinction coefficient is nearly equal to scattering coefficient, by using Eq. 3.21, which is the definition of visibility, the visibility can be derived. Equivalently, by substituting the definition of visibility, Eq. 3.21, into Eq. 3.17 and rearranging, the equation for determining visibility from MSI measurements becomes

$$V = \frac{r * \ln(-\varepsilon)}{\ln(C_r / C_0)} \qquad 3.22$$

Although the concept of visibility in the other wavelengths, and especially the SWIR, is perhaps a bit odd, we also found it useful in our analysis to evaluate the spectral Visibility V', which is derived with the same equations discussed above. This was useful in evaluating the derived extinctions in comparison with the visual appearance of the islands in the acquired imagery.

3.3. Application of the Equations with the MSI and SRI

This section provides an outline of how these equations are used with an imager to determine extinction. The details are given in Section 8. The extinction algorithm uses Eqs. 3.10 and 3.17 from Section 3.2. To use these equations with an extinction imager, the following steps are taken:

a) Prior to fielding, linearity and uniformity calibrations are acquired for the camera.

b) An image of the scene is acquired at an appropriate exposure[5]. Also, dark images (an image with no input light, acquired at the same exposure) are acquired hourly or daily depending on the system. The image of the scene includes a dark target at range r, and the horizon (or more accurately, the sky just above the horizon). The target and horizon need not be physically adjacent, as long as they are at essentially the same elevation and azimuth angles.

c) The dark calibration is applied by subtracting it from the scene image. The linearity calibration and uniformity calibration are applied to the image as discussed in later

[5] In our developmental systems, a single exposure was chosen in advance, such that it minimizes the number of pixels that will be offscale bright or dark. More automated systems would include a flux control algorithm to identify the optimal exposure as a function of solar position.

sections. At this point, the corrected (calibrated) signals at each pixel are proportional to radiance of the portion of the scene imaged by that pixel.

d) These calibrated signals are then used in Eq. 3.10 repeated below to directly determine the apparent contrast.

$$C_r = \frac{{}_t L_r - {}_b L_r}{{}_b L_r} \qquad 3.23$$

e) Prior to final processing, the inherent contrast is determined based on data analysis including analysis of clear day data and close targets[6]. During the current project, we used only the red and SWIR filters. We found that the inherent contrast of the ocean surface with respect to the horizon sky, as viewed from near the ground, was approximately -.85 in the red and -.73 in the SWIR. These values were based on measurements. They perform well for all the data we processed and appear to be reasonably universal, in the sense that their uncertainties cause small uncertainties in extinction. It is also necessary to determine the range to the targets, as discussed in Section 8.

f) The extinction coefficient is then derived from Eq. 3.17, repeated below.

$$\alpha = -\frac{1}{r}\ln(C_r / C_0) \qquad 3.24$$

3.4. Additional Comments and Modified Approaches

This approach and the equations were originally developed for visible wavelengths. During the project, we carefully evaluated what happens in the SWIR, where absorption is significant, and scattering and extinction are no longer equal. As discussed in Memo AV12-017t, we showed that the above equations apply directly to extinction, and the instruments are in fact measuring extinction. In addition, we were concerned that we were measuring with a semi-broadband response in the SWIR. As discussed in Memo AV13-007t, the SRI measures the effective extinction in the absorption windows, as opposed to the average extinction in the whole passband. That is, the extinction as measured includes the absorption that is present in the least absorbing part of the pass band, which is near 1.6 μm.

While working to transition the technology to other users, we were asked whether this approach is compatible with Dr. Duntley's equations. The approaches are indeed consistent, as shown in Memo AV12-007t. The AOG was originally part of the Visibility Laboratory before it closed, and Dr. Duntley was the director of the Visibility Lab, as well as the professor who taught many of the courses the first author of this report took in graduate school.

[6] For the black target used in the prior project the inherent contrast with respect to the horizon sky was measured to be -.99 in all the spectral filters used in that project, as discussed in Section 4.

We have been asked by others whether it is feasible to use a white target such as a cloud in place of the black target. As discussed in Memo AV12-008t, there are no theoretical errors with the use of a white target for the target. However, the uncertainties in resulting extinction become very large if a white target is used. This is due in part to the difficulty in estimating inherent contrast for a white target. The inherent contrast of a black target is constrained between values of 0 and -1, whereas for a white target inherent contrast can range from 0 to + ∞. From Eq. 3.10 it can be seen that the blacker the target is, the less the resulting uncertainty in inherent contrast if the horizon radiance is not at equilibrium.

We have also been asked whether it is feasible to use a white or grey plaque in place of the horizon sky. As discussed in Memo AV12-008t, there are theoretical errors if one uses a white target for the background. However, Lehecka et al. [23] tested the use of grey and white plaques in place of the horizon, and we were surprised and pleased that these two plaques yielded almost identical and very reasonable results. We believe that this is because when the active target is nearly black, the background radiance nearly cancels in Eq. 3.10.

Other researchers [15, 22, and 23] have also modified the equation to use an apparent contrast measured at two different ranges, as in Eq. 3.25 [23].

$$C_{r1} \Big/ C_{r2} = e^{-\alpha(r1-r2)} \qquad 3.25$$

Although this approach alleviates the need to estimate an inherent contrast, the resulting extinctions are impacted by the measurement error for both ranges. As a result, we would expect this method to work well, except in very clear cases with targets at close ranges or in very foggy cases with targets at farther ranges. Lehecka et al [23] found that indeed the method worked well for them except in clear conditions. Depending on the test conditions, this can be a very useful approach to take.

Although the theory presented in this section has been established for quite some time, we feel that the use of accurate sensors, combined with accurate calibrations and extinction algorithm features designed to detect abnormal conditions have made the technique much more accurate than previously. In addition, in this grant, we were able to show that in the red and SWIR wavelengths, the ocean surface can be used as a reliable target under most conditions. This extends the capability of Extinction Imagers considerably, as it enables the system to become truly single-ended, and to be able to point in any direction and evaluate the effective extinction over ranges of practical interest (as opposed to short ranges to artificial targets).

4. PREVIOUS RESULTS USING A FIXED TARGET

The AOG's initial work with extinction imagers began in the late 1980's with development of the HSI, briefly discussed in Section 2.3 [18 - 21]. The HSI performed well, but was limited by the capability of solid state imagers available to us at that time. During 2005 – 2007, we were funded to develop an extinction imager using a modern CCD camera system [2, 3]. This work was done in conjunction with the Navy's Zuniga Shoals project [1]. During this project, P. Berger (one of the authors of this report) acquired measurements along the same line of sight using transmissometers. This enabled very useful comparisons of the data.

The MSI was slightly modified from a Whole Sky Imager developed originally for other programs [18 - 20, 24 - 27]. The sensor included a 16 bit Photometrics Series 300 slow scan CCD imager, and a filter changer built by AOG. The filter changer included filters in the visible and NIR. The camera was pointed across the entrance to the San Diego Bay, looking at a black target. This target was an open wooden box that was 8' x 8' at the opening, and 12' deep, and painted with a black paint. This project is documented in Appendix A and in somewhat more detail in Memo AV10-18t. In this section, we provide a brief overview, as the end of this project represented the starting point of the grant discussed in this report.

The MSI sensor used in the Zuniga Shoals project is shown in Fig. 4-1, and imagery for a very clear day is shown in Fig. 4-2. Additional images from days with lower visibility are shown in Appendix A, Figs. A-5 through A-7.

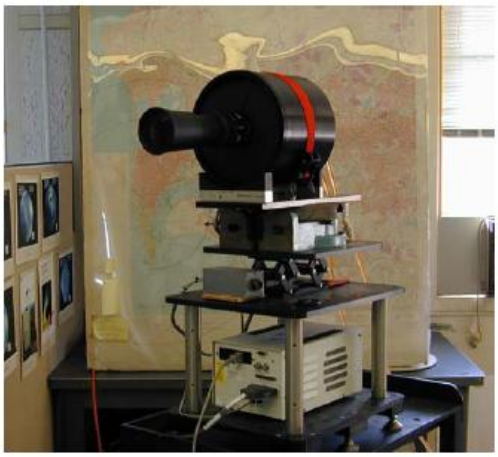

Fig. 4-1. MSI sensor head, Zuniga Shoals Project, with zoom lens and 16-bit CCD camera

During this project, we measured the inherent contrast of the target from a distance of a few feet, and found it to be nearly invariant with sun position. This target had a contrast of -.99 ± .01. During the project, we programmed the extinction algorithm, and added some features to account for abnormal conditions. Most importantly, we added a feature to find the target in the image. In some conditions, the refraction along the path moved the position of the target in the image by a few pixels. Since the target was fairly small in angular size, it was important to select the proper Region of Interest (ROI) within the

target. Special target logic within the extinction algorithm looked for the darkest 3 x 3 pixel ROI in a region that was within ± 10 pixels of the anticipated position.

Fig. 4-2(a). Image on 4 Dec 2005
V = 74 km, S = 0.04 km^{-1}

Fig. 4-2(b). Zoomed image showing black target at 7.07-km range

Other extinction algorithm features included a check for clouds on the horizon, similar to the current cloud feature discussed in Section 8.5. We also included calibration corrections similar to those discussed in Section 8.3 in this earlier system. The extinction algorithm and data processing are discussed in more detail in Memos AV07-014t, AV07-015t, and AV07-016t.

With this excellent black target and a fixed position, the results were excellent. They corresponded well with the visual assessment of the images, and corresponded well with the transmissometer results. There were two test periods that were analyzed: August 2005 and a period in Nov – Dec 2006. The results for August 2005 are shown in Fig. 4-3, which shows a plot of the MSI photopic (green) scattering coefficient as a function of the transmissometer photopic scattering coefficient. The slope is not quite 1, but my understanding is that it turned out later that this was due to calibration issues with the transmissometer. The R^2 correlation coefficient was 0.92. By comparison, the comparison between the two standard instruments, i.e. the nephelometer and the transmissometer shown in Fig. 4-4 was not nearly as good, with a correlation constant of .73.

The initial results for the 2006 period were not quite as good, due to a few cases with a ground fog that affected the target but not the sky radiance, because the sky radiance was acquired above the mountains. However, even for that data set the correlation constant was .87 for the full data set and .91 if the cases affected by the high horizon are removed. These results are shown in Fig. 4-5. Once the transmissometer data were further calibrated and processed, the results were excellent, as shown in Figs. 4-6 and 4-7.

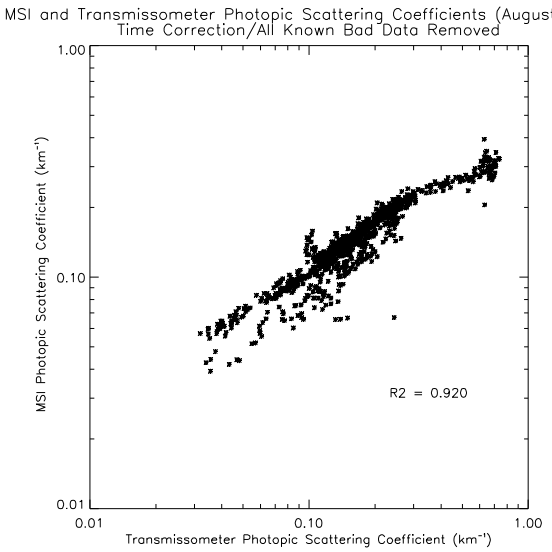

Fig. 4-3. MSI Scattering vs. Transmissometer Scattering for August 2005 period

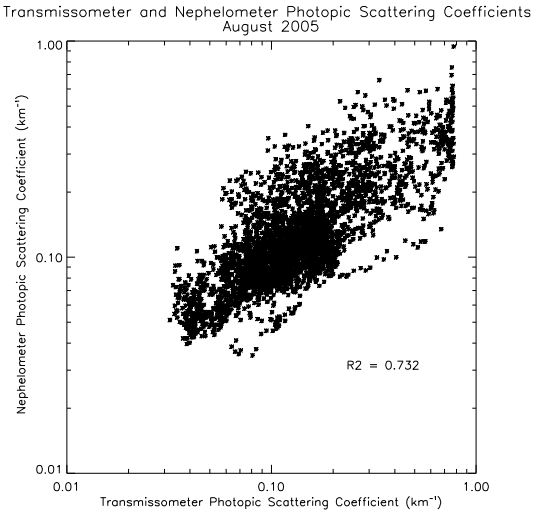

Fig. 4-4. Nephelometer Scattering Coeff. vs. Transmissometer Scattering for August 2005

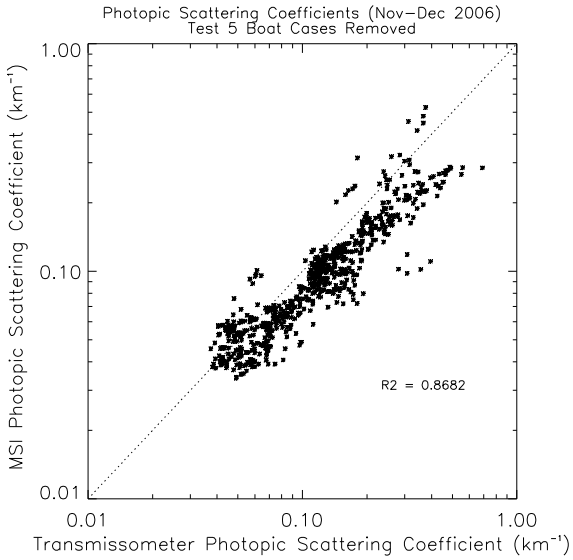

Fig. 4-5. MSI Extinction vs. Transmissometer Extinction for Nov – Dec 2006 period

This experiment convinced us that extinction imagers can provide excellent measurements of extinction over extended paths when a black target is used. This also required that reasonable care is used in selecting a good camera, calibrating the camera, and developing the extinction algorithm to detect and mitigate unusual conditions such as refraction moving the position of the target in the image. Our next goal was to determine whether it is possible to use the ocean surface as a reasonably dark target, and to extend and evaluate the capabilities into the SWIR. This goal was the primary goal of the JTO-ONR project that is the subject of this report.

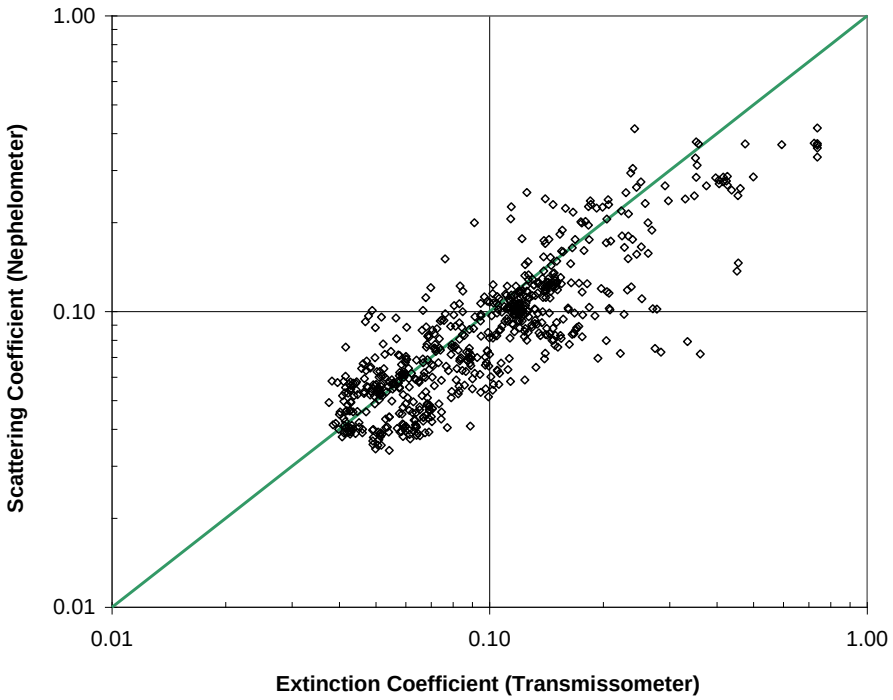

Fig. 4-6. MSI Scattering Coefficient vs. transmissometer for Nov – Dec 2006 period after final calibration and sorting of transmissometer data (y axis should be labeled MSI)

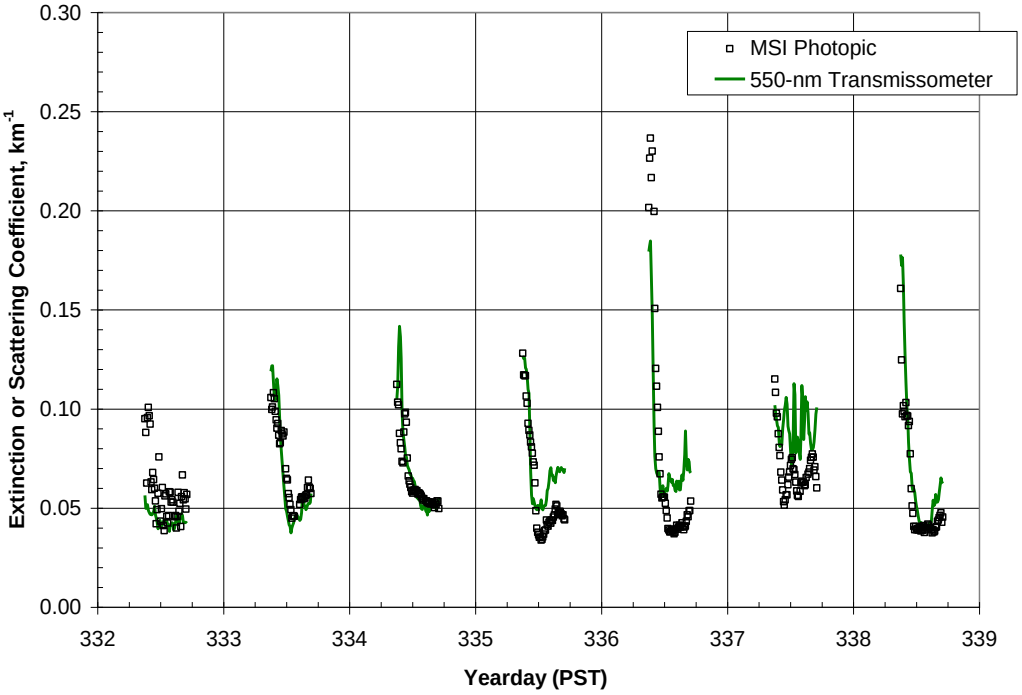

Fig. 4-7. Time series of MSI Scattering Coefficient and Transmissometer Scattering Coefficients for 28 November 2006 – 4 December 2006

5. SUPPORTING MODELING STUDIES

One of the goals of this project was to extend the extinction imager concept into the Short Wave Infrared (SWIR) band. To have a better understanding of how the SWIR extinction should relate to the visible extinctions we were more familiar with, we did some modeling studies using the US Air Force's MODTRAN© atmospheric model [34]. These results, and other modeling studies needed in the project analysis, are presented in this section.

The initial modeling studies are documented in Memo AV09-038t. We derived the extinctions (including both scattering and absorption) modeled for visibility conditions of 1 km, 5 km, and 23 km visibility, for Maritime, Urban, Rural, and Desert air masses. The results for Maritime and Urban air masses are shown as a function of wavelength in Fig. 5-1. The results for Rural and Desert are reasonably similar to the Urban results. In Fig. 5-2, we show the same data as in Fig. 5-1, but have superimposed the wave bands of the instruments being used in the experiment.

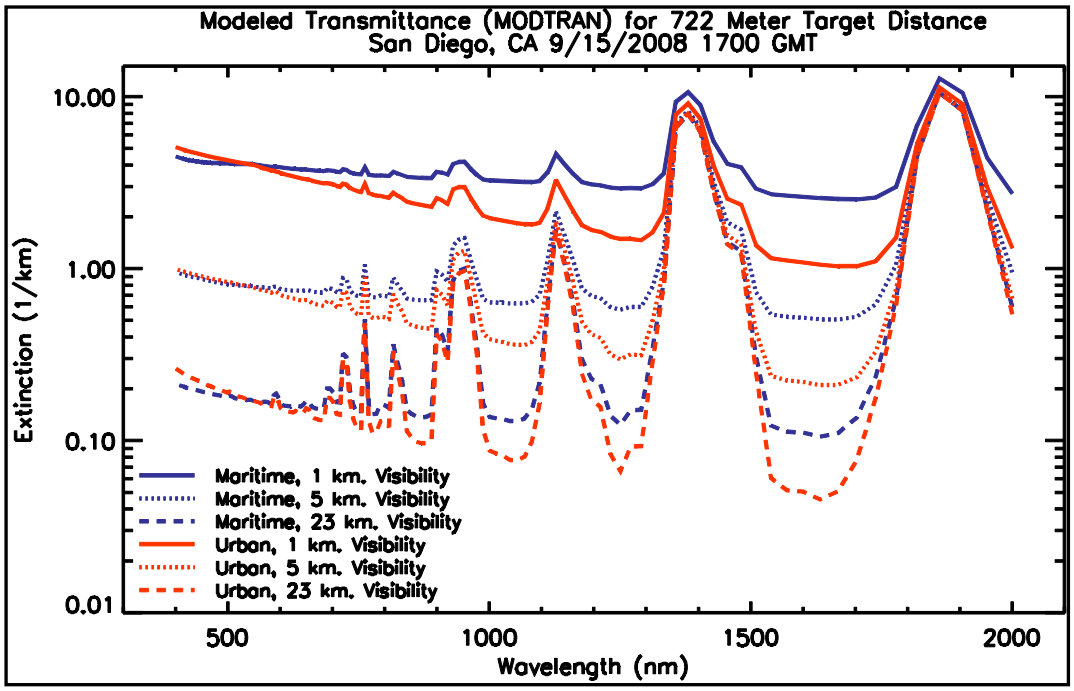

Fig. 5-1. Extinction Coefficients from MODTRAN©, for Maritime and Urban Aerosols, computed with a passband of 50 nm

From Figs. 5-1 and 5-2, it appears that under most conditions, we should expect the SWIR extinction coefficients in the absorption windows near 1.06 µm and 1.6 µm to be slightly lower than the visible extinction.

As documented in Memo AV12-017t, we carefully evaluated the equations to verify that the extinction imagers do in fact measure extinction, and not just scattering. Initially we had expected that because our SRI instrument was not filtered for these specific wavelength windows, we should expect our measured extinction to be the average

absorption over the semi-broadband response of the system. Memo AV10-004t compares this average extinction (computed with MODTRAN©) with the extinction at 1.06 and 1.6 µm. Upon later additional evaluation, we discovered that with the extinction imager method, we were effectively measuring the extinction within the absorption windows. This is documented in Memo AV13-007t.

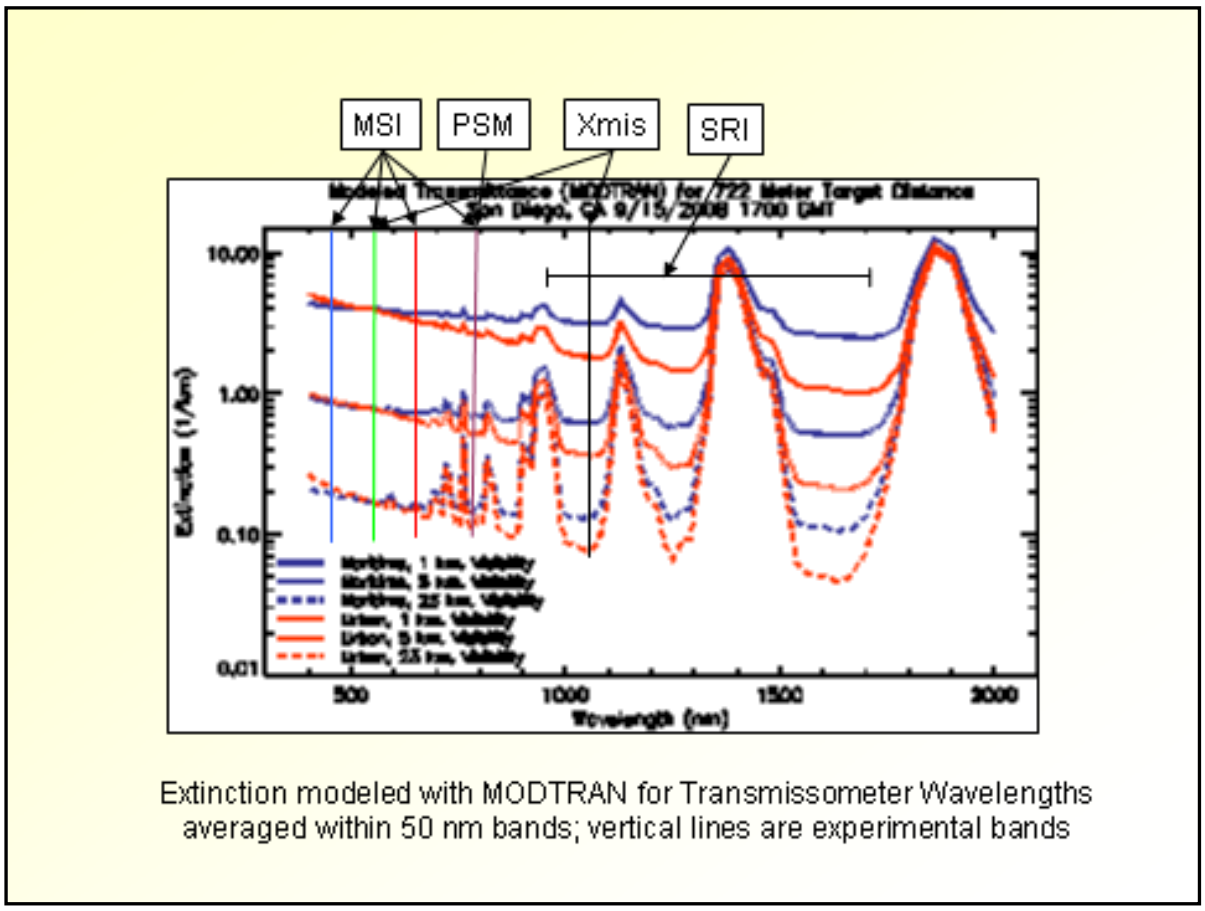

Fig. 5-2. Extinction Coefficients with the passbands of the instruments superimposed

Using modeling, we also addressed whether it is reasonable to measure the extinction with an MSI-like instrument using visible and NIR bands, and then use modeling to estimate the SWIR extinction. This question was important, because we were aware that the CCD-based camera in the MSI has a number of features that should enable it to determine extinction coefficient more accurately than the "Complementary Metal Oxide Semiconductor" (CMOS)-based camera in the SRI. (CCD refers to Charge Coupled Device chips used in most visible imagers; CMOS technology is used in many applications, including infrared camera sensor chips.) In particular, the SRI camera is less linear, has higher noise, and less uniformity across the image. As a result, we were concerned whether the SRI would provide data of adequate quality, and understood that it might be necessary to use a CCD-based sensor and extrapolate to the SWIR wavelengths of interest.

As presented in Memo AV09-038t, we made several MODTRAN©[7] runs to help evaluate how well the SWIR extinctions might be predicted on the basis of visible or NIR extinctions measured by the MSI. In Figs. 5-3, we show the model results for the extinction at 1.06 μm as a function of the extinction at 800 nm. Based on the analysis in Memo AV09-038t, the extinctions at 1.06 μm can be predicted with about ±11% accuracy as air mass and visibility change. On the other hand, if a MSI with two filters at 800 nm and 550 nm were used, the accuracy of the SWIR precision improves to approximately ±1% under maritime conditions, and ±3% under other conditions. Of course, we recognize that the real world is never as simple as models, so these estimated uncertainties are surely under-estimates. However, this does give a feel for the penalty if one uses the visible or NIR to estimate the SWIR. [Finding]

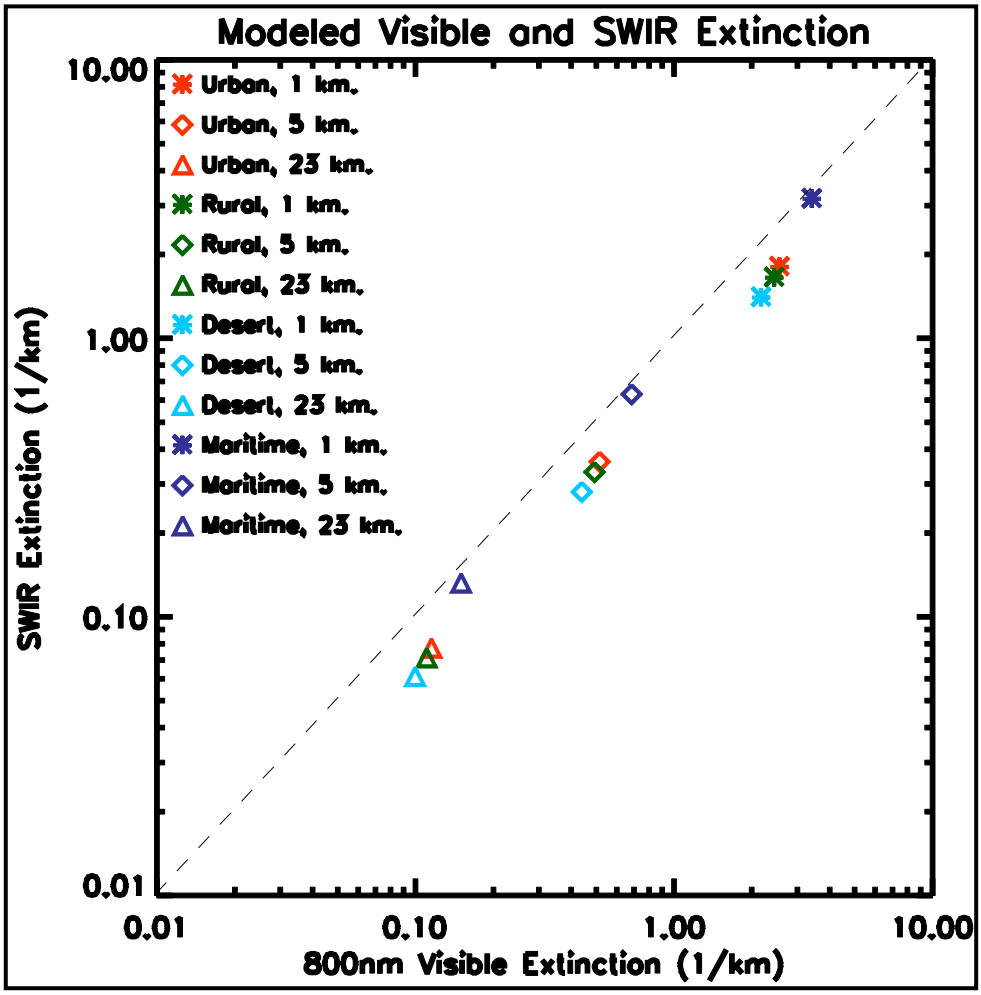

Fig. 5-3. Plot of MODTRAN© results showing SWIR modeled extinction at 1.064 μm as a function of modeled extinction at 800 nm

We also used an independent data set of strictly empirical data to further evaluate the relationships shown in Fig. 5-3. Our report co-author P. Berger explored the relationship between the visible and SWIR wavelength extinctions based on measured data, as

[7] MODTRAN refers to "Moderate resolution atmospheric transmission model".

discussed in (ref 20). He found the relationship to be reasonably well defined, and as a result modeled the relationship. The best fit results are shown in Fig. 5-4. Like Fig 5-3, these plots show that for atmospheres dominated by oceanic aerosols, we should expect the SWIR extinctions to be slightly lower than the visible extinctions. Also like Fig. 5-3, they show that for other aerosols, the SWIR extinctions should be even lower in relation to the visible extinctions. Thus these empirical results support the modeled results discussed above.

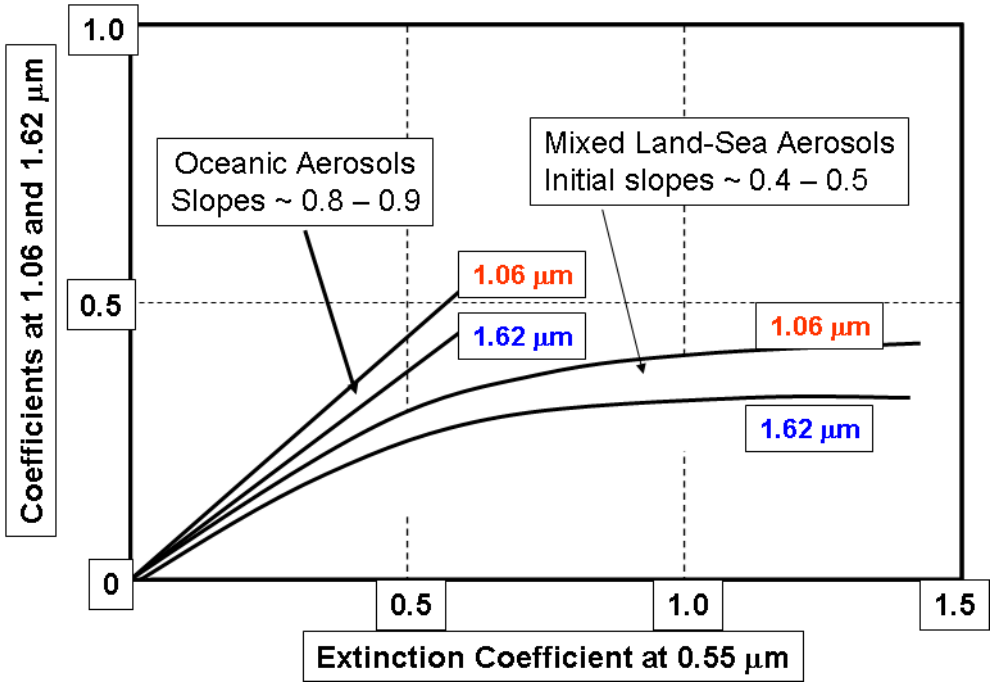

Fig. 5-4. Relationships between Measured Extinctions in the visible and SWIR

As we began approaching the subject of slant path transmittance, which is presented in Section 11, we also ran a series of MODTRAN© tests to determine how much the transmittance over a 5 km path at a 10° elevation slant path might be expected to differ from the transmittance over a 5 km horizontal path, for a 1.6 µm laser. We ran the calculations for Urban, Rural, Desert, and Maritime air masses, and for visibilities of 1 km, 5 km, and 25 km. These results are shown in Fig. 5-5, extracted from Memo AV10-006t.

As expected, the beam transmittance for the slant path is slightly higher, as it traverses through slightly clearer air. The difference is relatively independent of the visibility, since this difference is only affected by the shape of the vertical profile of the extinction coefficient. Note that a 5 km long slant path at 10° elevation only reaches an altitude of about 1 km, so the height of the top of the haze layer is not important for this scenario. We expect that for most scenarios it is the lowest part of the atmosphere that is most critical.

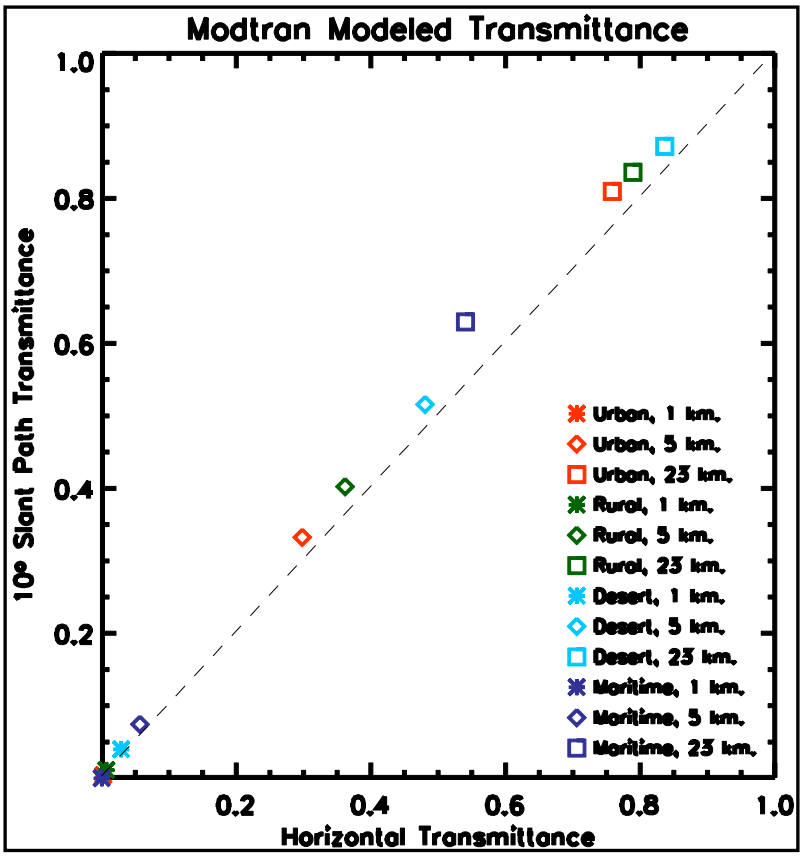

Fig. 5-5. MODTRAN Slant Path Transmittance vs. Horizontal Transmittance for a 5 km path and a wavelength of 1.6 μm

6. EXPERIMENTAL SETUP

As discussed in earlier sections, the primary purpose of the experimental setup was to:
a) Determine whether the ocean surface could be used in place of a black target, so that we could easily use the extinction imager approach at sea.
b) Determine whether it is better to use a visible system, with extrapolation to yield an estimate of the SWIR extinction, or better to use a SWIR imager.

In order to address item "a", it was important to determine how the inherent contrast of the ocean surface radiance with respect to the horizon behaved, especially with respect to solar position. This required developing an instrument that could scan the horizon and would be environmentally protected. It also required choosing a site where we could automatically acquire imagery over the ocean under a wide range of lighting and weather conditions, and over a wide range of look (azimuth) angles.

Requirement "b" dictated the development of two systems, a visible/NIR and a SWIR system, so that we could run experiments in both wavelength regimes and evaluate the results. It was also necessary to include supporting instrumentation, so that we could monitor the atmospheric conditions and compare results with known and trusted instruments. Finally, an important criterion was that we needed to leverage the project heavily with equipment available from past projects, in order to keep the costs within the budget. Since this was a developmental project and we were not required to provide the final optimal configuration, this was not a problem. In general, the equipment we used was much more sophisticated and physically larger than would be desirable for an extinction imaging system. For example the environmental housing was quite large for the application.

For this project, we only needed to acquire sufficient test data to evaluate our goals described above. Although there was not a requirement to run the systems continuously, we did so to the extent that we could without interfering with other priorities, in order to maximize the data base we could choose to analyze. The dates the systems were in the field are discussed in the section for each system. Memo AV10-007t shows when each system was running through March of 2010. Soon after that, our priorities changed as we entered Phase 2 of the grant, as documented in Memo AV10-019t. Soon after that, we concentrated on night tests. We also kept detailed site logs throughout the experimental period. Most of the instruments ran from 2008 to 2013, although operation was intermittent at times, due to site power failures and occasional hardware issues. We also had some data gaps when we bought instruments in-house for modification or calibration.

6.1. Site Properties

Our offices are on the Navy's Space and Naval Warfare Systems Command (SPAWAR) Systems Center (SSC) base on Pt. Loma in San Diego California. An ideal experimental site was available on the West side of Point Loma. This location was under the management of the Atmospheric Propagation Branch of SSC, and they were kind enough to let us use this site. The location of the site is illustrated in Fig. 6-1. One of the

advantages of this site is that it has a full 180º view of the ocean, and the scene includes a view to islands at 40 km range, which is very useful in the data evaluations.

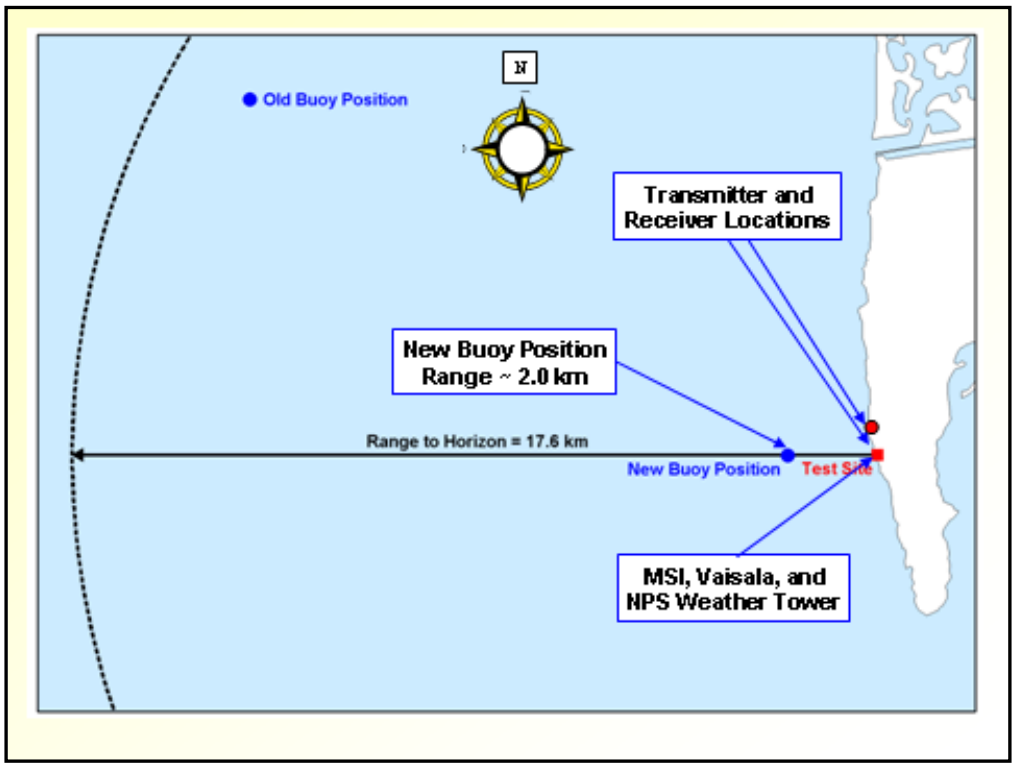

Fig. 6-1. Illustration of Site Location relative to Point Loma

At this site, a dock extended out over the cliff, and it was at a height of approximately 20 – 21 m above the surface of the ocean. Our sponsors indicated that this height conveniently matches the height of an aircraft carrier deck, and thus the horizon was at roughly the same range as would be encountered on a carrier. Finally, a building was conveniently close by and provided electrical power, and our site hosts were willing to let us use this power. The site is shown from above and below in Figs. 6-2 and 6-3.

Fig. 6-2. Experimental Site seen from above

Fig. 6-3. Site seen from the shore

The details of the site and its impact on the experiment are discussed in more detail in Memos AV07-046t and AV08-016t. In Memo AV07-046t we evaluate the range to the horizon, we show two "cartoons" illustrating the experimental options, and show some derivations of the impact of noise and target range on the determined extinction uncertainty. Memo AV08-016t further comments on the experiment and the hardware and software priorities. Initially we thought that the site would provide good answers for atmospheric visibilities between 10 and 50 km, but once we realized that we could use the ocean surface at a variety of ranges, this extended the useful visibility range to near-zero to 50 km. The transmissometer had a fixed path, and we derived that it should provide 10% accuracy or better over a range of visibility conditions from about .8 to 9 km visibility.

In November 2010, the Navy decided that the platform was unsafe. We were required to move the instruments onto the asphalt next to the building shown in Fig. 6-2, and continued the experimental data acquisition from that site until the end of the project.

6.2. MSI Hardware

The MSI we developed for the Zuniga Shoals experiment [1] was based on the knowledge and hardware we gained developing Day/Night Whole Sky Imagers (WSI) [24]. One of the WSI systems was modified to use a zoom lens for the MSI. For the current project, the MSI used in the Zuniga Shoals experiment was further modified to include a rotary table and environmental housing, so that it could scan the horizon and be weather-proof.

From Eq. 3.23, we can see that it is important that the measurement of relative flux within an image is accurate, in order to measure apparent contrast accurately. Also the noise level is important, as this impacts the accuracy of the apparent contrast measurement. Absolute radiance is not important, because apparent contrast only depends on relative radiance. The optical systems developed for the MSI met these needs nicely.

The MSI system, as shown in Figs. 6-4 and 6-5, includes a 512 × 512 16-bit digital CCD camera, a filter changer, and a Sigma 170 – 500 mm zoom lens with a doubler. The filter changer has two filter wheels. One wheel contains four spectral filters: blue (450 nm), green (550 nm), red (650 nm), and NIR (800 nm). Each of the filters has a Full Width at Half Maximum (FWHM) bandwidth of approximately 40 nm, although 70 nm filters were used in the initial experiments. The spectral response of the green filter is similar to the photopic band and we may at times refer to data acquired with the green filter as the photopic band data. A second filter wheel contains neutral density filters that may be used to adjust the flux levels over a range of approximately 3 logs (10^3). The spectral response of the MSI is defined in Memo AV12-004t. Unlike the more common 24-bit color camera with 8-bit resolution in each color, this system has 16-bit (65,536 grey levels) in each spectral filter, as well as additional neutral density filters and exposure control for a useful dynamic range of over 10 logs or 10^{10}. The daytime experiments

reported in this document were taken at f# 350 with a doubler, and the resulting image has a 2.25° field of view.

Fig. 6-4. MSI System on Pier

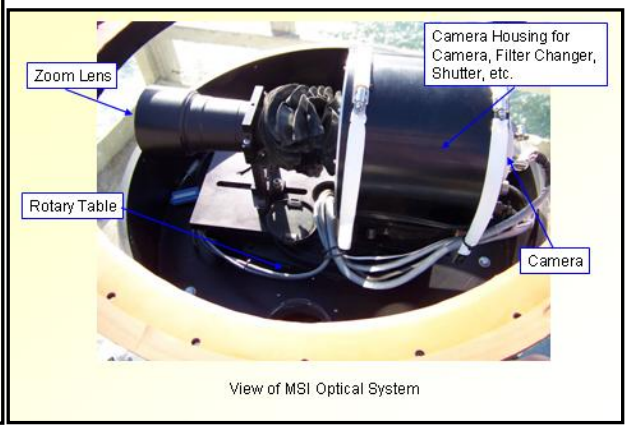

Fig. 6-5. MSI Optical System

For this project, we modified the MSI system to use the environmental housing from the WSI, and we also added a rotary table and controls for the rotary table. The environmental housing provides protection for the camera electronics unit, the camera cooling elements, and other components that provide real time readout of system conditions such as camera chip temperature. System electronics called the Accessory Control Panels enable both manual and computer control of the filter changer, as well as system condition readouts.

A control computer and a separate processing computer were housed in the nearby building, and connected to the system hardware with 100' cables. These computers provided automated control of the filters, exposure, and rotary table, and also monitored system parameters to ensure safety of the hardware. The software and data collection will be discussed in Section 7.

The system was first deployed in March 2008. It was taken out of the field in July 2011, in order to modify it for night tests. It was redeployed in January 2012. The MSI was shut down in August 2013, because we had completed data acquisition. More details regarding the MSI hardware and field work, including lists of components, are included in the following memos: AV08-003t, AV08-015t, AV09-031t, AV10-007t, AV10-008t, AV10-010t, AV11-010t, AV10-032t, AV11-010t, AV11-012t, AV12-001t, AV12-002t, and AV13-016 t. Several of these memos also include information on the SRI and the environmental support hardware.

6.3. SRI Hardware

As discussed in Section 4, it was necessary to develop a SWIR version of the MSI operating near wavelengths of 1.06 and 1.6 μm. The SRI instrument was designed and built in 2009, and deployed on July 22, 2009. We did not have a SWIR camera available from previous projects that could be used in the SRI; however we did have an additional

WSI environmental housing and computers that we could modify for use with the SRI. As with the MSI, this housing is much bulkier than would be used in a system for operational purposes, but for developmental purposes it met the needs well.

The most important component selection for the SRI was the camera. We chose an Alpha NIR camera, for reasons documented in Memo AV09-003t. This camera is a 12 bit camera, with 320 x 256 pixel format. The FWHM passband of the camera is from 950 nm to 1700 nm. This is an excellent SWIR camera, but in general SWIR cameras are not expected to be as good as the MSI camera in terms of dynamic range, low noise, and image uniformity.

The design and development of the SRI are discussed in Memo AV10-002t. We did not modify the system to include a filter changer, as we felt it was not needed for this development. We evaluated the pros and cons of installing a single filter, as documented in Memo AV10-004t, and determined that it was better to set up the system without a filter. The spectral response of the SRI system is documented in Memo AV12-005t. The lens was a 150 mm fixed zoom lens we had on hand.

The resulting system and its rotary table are shown in the environmental housing in Fig. 6-6, and placed on top of the housing in Fig. 6-7. For this system, we were able to place the control computer inside the environmental housing, so no extended cables were required. The system was designed and developed during the second year of the contract, and deployed in July 2009. It was shut down in May 2013, because we had completed data acquisition.

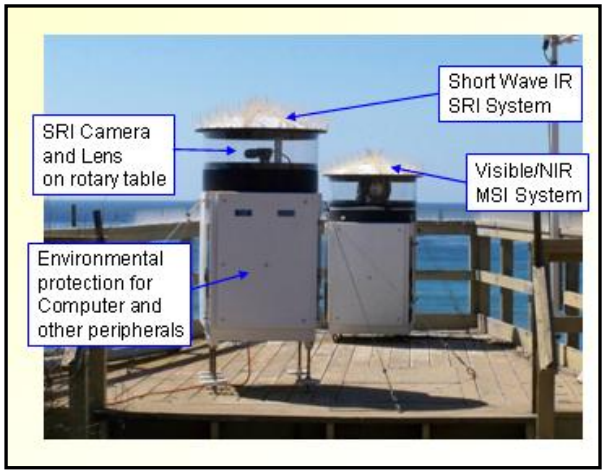

Fig. 6-6. Image of SRI, showing environmental housing and placement relative to the MSI

Fig. 6-7. SRI placed on top of MSI dome

More details regarding the SRI hardware and field work, including lists of components, are included in some of the Memos referenced in Section 6.2, and in Memos AV11-011t, AV11-013t, AV11-014t, and AV12-009t.

6.4. Supporting Instrumentation

A vital part of this project was measurement of meteorological and optical parameters at the site. Our colleagues at Naval Postgraduate School installed a meteorological buoy (called the Flux Buoy) and a shore meteorological station. Two transmissometers [30] were provided by our colleagues at MIT Lincoln Laboratory. A Vaisala Present Weather Detector (PSM) [31] was purchased under the grant. In this report, we usually refer to this instrument using the more generic term Point Scatter Meter (PSM). Later this instrument was supplemented by a Vaisala Ceilometer [35] purchased by NPS under the grant. The primary function of the Present Weather Detector was the determination of scattering, and throughout this report we have designated this instrument using the more generic (but more descriptive) term Point Scatter Meter (PSM)

6.4.1. Flux Buoy

The flux buoy was originally designed primarily to provide scintillation measurements and a broad range of other parameters in support of experiments involving turbulence effects (Ref 20.) These include wind speed and direction, temperature and relative humidity at three levels, atmospheric pressure, sea temperature, turbulent wind and virtual temperature from a sonic anemometer, waves (one-dimensional and directional spectra), and shortwave irradiance. For this experiment, the most important parameters were the wind speed, irradiance, and temperature. The buoy is shown and these sensors are indicated in Fig. 6-8 and 6-9.

Fig. 6-8. NPS Flux Buoy

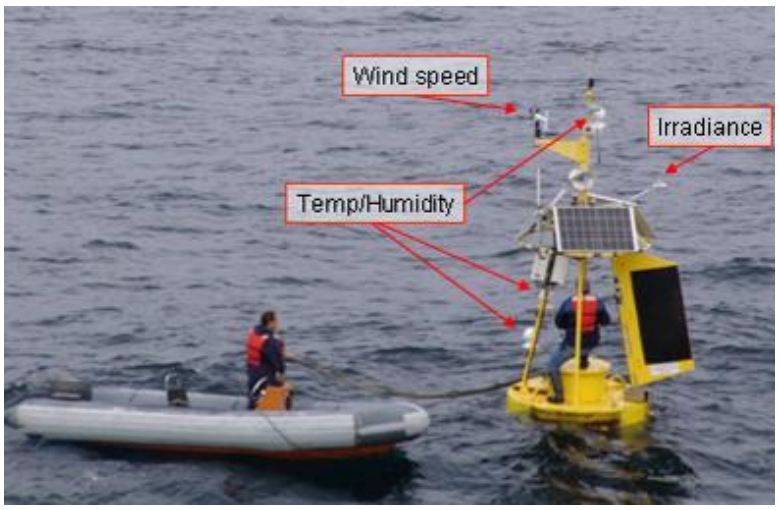

Fig. 6-9. Deployment of Flux Buoy

The buoy was deployed along a path looking to the North-West or West of the shore site, as shown in Fig. 6-1. The buoy was originally deployed prior to the start of our work under funding from another contract. Initially it was deployed to the North-West at a range of approximately 20 km. Following a "hit and run" accident in May 2008, it was repaired and redeployed to the same location in October 2008. It was then retrieved in January 2009, refurbished, and installed in a more optimal location in June 2009. At that time it was deployed to the West at a range of 2.29 km. It broke loose from its mooring

in August 2010. Following receipt of supplemental funding, the mooring was replaced and the buoy was redeployed in February 2011 at a range of 2.36 km. It was removed in August 2012, because we had the data we needed, and NPS had far exceeded their project requirements.

6.4.2. Shore station Meteorological Tower

The shore station meteorological tower was provided to anchor the meteorological conditions at the shore end of each path. This station and its instruments are shown in Fig. 6-10. We made most use of the wind speed, radiation, and rain indicators. The meteorological tower was deployed February 2008. It was removed in May 2012, because we had all the data we needed, and NPS had far exceeded the project requirements. This system was extremely reliable, and had only a few data gaps, which were mostly caused by site power outages.

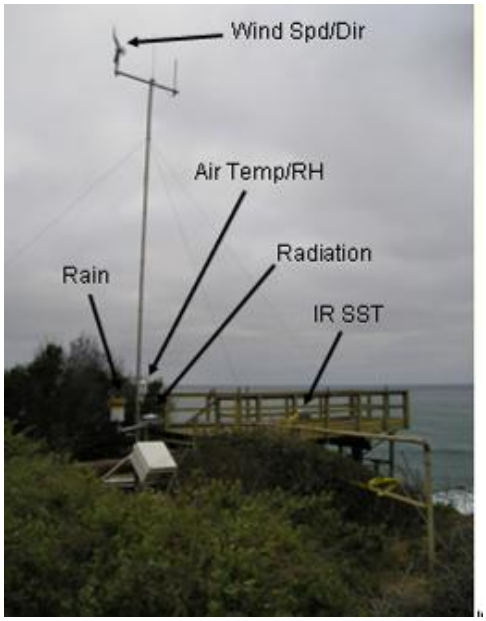

Fig. 6-10. Shore Meteorology Station provided by NPS, with location of sensors

6.4.3. Transmissometers

Two Optec LPV-3 long-path transmissometers, from Optec Inc. of Lowell Michigan [30] were provided by our colleagues at MIT Lincoln Laboratory. One acquired measurements in the visible (near our green filter) at 0.55 μm, and the other acquired measurements in the SWIR at 1.06 μm (Ref 20). The line of sight extended from near the dock to a location 0.72 km to the north along the shore. This location is shown in Fig. 6-1. The instruments are shown in Figs. 6-11 and 6-12. The two transmissometers were deployed in May 2008. They were taken down in June 2010, initially because our site hosts needed the space where they were mounted. We received permission from the sponsors to retire them soon after this date, because maintenance of the transmissometers is fairly time-intensive, and we felt that the PSM data were meeting our needs.

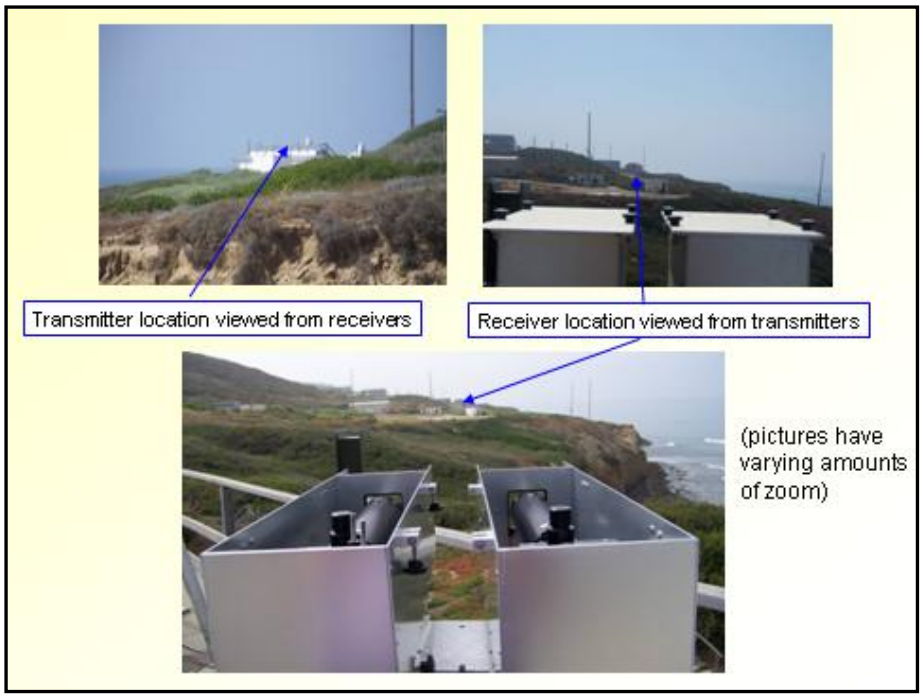

Fig. 6-11. Path of Sight for the two Transmissometers

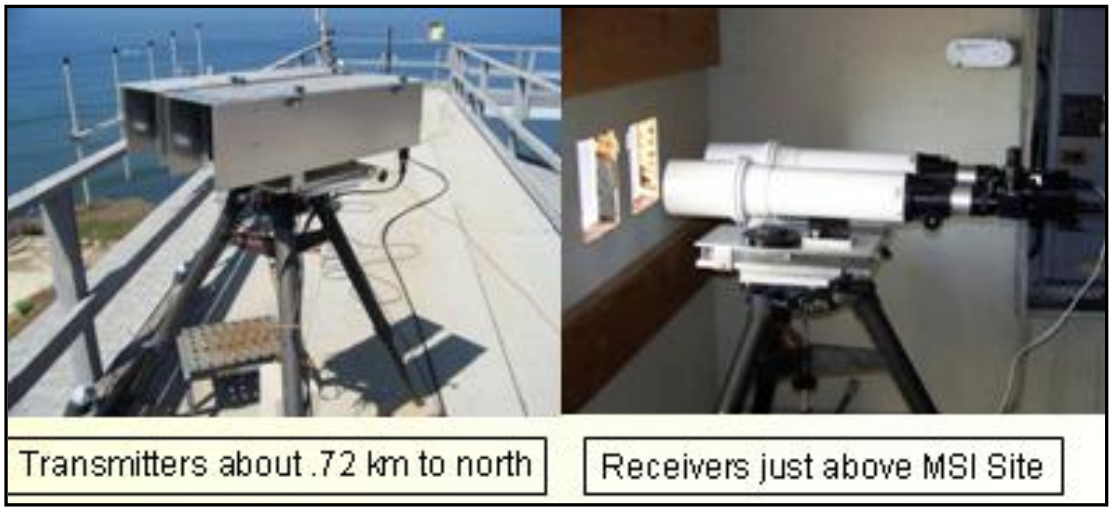

Fig. 6-12. Transmissometer Transmitters and Receivers

6.4.4. Vaisala Present Weather Detector and Ceilometer

The Vaisala Present Weather Detector PWD22 (which we have referred to more generically as a Point Scatter Meter) [31] is a commercial device that measures the scattering coefficient at .875 μm in a small sample volume of about 0.1 liters. The results are automatically truncated under clear conditions with extinctions less than .15 km^{-1} (visibilities greater than 20 km). We primarily used the scattering coefficient measurements, but also occasionally used the precipitation measurements that it acquired. The PSM system was deployed in March 2008. It was shut down in November 2013, because we had completed data acquisition.

In addition, a Vaisala ceilometer CL31 [34] was purchased by NPS later in the program. We used this instrument most importantly for cloud height and cloud amount, as well as an estimated aerosol backscatter profile. The cloud amount is based on a 30-minute weighted average of measurements at the zenith, and is thus only an estimate of instantaneous cloud amount, but is still very useful in distinguishing clear, scattered to broken, and overcast conditions. The ceilometer was deployed in April 2010. It was removed in May 2012, because it was needed by NPS for another project, and they had far exceeded project requirements. However, they were able to reinstall it in August 2012 for our continued use. It was shut down in April 2013 and returned to NPS, because we had completed data acquisition.

We would have liked to include a lidar in the experimental setup. Although the ceilometer is in principal a lidar, it was not designed to acquire accurate aerosol data over long ranges. We did an evaluation of more sensitive lidars that were available and could be modified to detect aerosols at slant ranges. However systems with these capabilities were far beyond the budget of this project. This is discussed in Memo AV10-005t.

7. DATA ACQUISITION FOR DAYTIME

This section discusses the data collection methods and software used for daytime, and presents samples of the raw data. The methods used at night were quite similar, but with longer exposures. These methods and the night data are discussed in Section 10.

Data acquisition for the program began in with the first system deployment in February 2008. The MSI was deployed in March 2008. The SRI had to be designed and built under the program, so it was not deployed until July 2009. Most of the instruments ran most of the time until April 2013, when we began turning off systems, with the final instrument turned off in November 2013. Our goal was only to acquire useful sample data sets in the most efficient manner, and the data acquisition was interrupted many times to do tests such as the night tests. As a result, the data acquisition was quite intermittent, but several fairly extensive test sets were successfully acquired.

7.1. Data Acquisition Methods and Software

Both the MSI and the SRI camera systems were mounted on rotary tables, and fully enclosed in environmental housings. They could be run automatically without frequent human intervention. Similarly, the meteorological systems were designed for outdoor use. The instruments were inspected and cleaned as necessary approximately weekly during the initial few years of the grant (and less often later in the grant, as our priorities shifted). They ran automatically 24 hours a day, but generally were specifically setup to acquire either good daytime data or good night data, since different lenses were required for these two modes.

For this program, we did not develop an automated flux control algorithm, which would enable optimal data for the full 24-hour cycle, because this was not our priority. As a result we analyzed data for the 4 hours before and after approximate noon, to be sure the data were reasonably onscale. Although we acquired MSI data in all four spectral filters, we generally only analyzed the data in the most optimal filter. For the daytime, this was the red filter, because the upwelling light off the ocean is very low in the red waveband. For the night-time, we analyzed the red and the open hole data, which gave us more flux and hence lower noise.

The MSI was controlled by Program RunMSI, discussed in Memo AV09-020t. The SRI was controlled by Program RunSRI, documented in Memo AV11-006t. Programs RunMSI and RunSRI are quite similar. The final versions of these programs are documented in Memo AV12-011t. The general logical flow of these programs is listed below:

a) On startup, initialize the camera system. The MSI checks for normal camera startup and cooling of the camera CCD chip. The MSI also includes several sensors to test the state of the system, including the temperatures of the camera housing and environmental housing. These readouts are checked for normal values. The SRI does not include any sensors of this sort, but the program does check for normal camera startup.

b) Initialize the rotary table, and set it to the home position, which is true north.
c) Move the rotary table to its first position for data acquisition. The rotary table moves counter-clockwise. Early in the program, the initial data acquisition position was 330° relative to true north, which we will designate 330° (T).[8]
d) For the MSI, if this is either the first acquisition after starting the program or the first acquisition of the hour, acquire dark images in each filter position. These images are acquired with the shutter closed, but with the normal integration times used in normal data acquisition for each filter. The SRI cannot acquire dark images, because it has an electronic shutter rather than a mechanical one, so it is difficult to acquire an image at the right exposure with no input light. As a result, images acquired at night were used instead for the dark images in the processing.
e) Acquire raw images. For the MSI, these are acquired in the blue at exposure 25 msec, green at exposure 25 msec, red at exposure 50 msec, and NIR at exposure 1500 msec. The SRI data are acquired at exposure 32,000 μsec in the daytime (the SRI camera requires its input exposures in μsec, so we have followed this convention in the text). The MSI raw images are 512 x 512 16 bits, and the SRI raw images are 320 x 256 12 bits. Special care was taken in the program to acquire and save the SRI data at 12 bits. (The software provided with the camera would normally store images at 8 bits, but as part of this process, they are modified to look nice, and relative radiances are no longer valid in the 8-bit mode. Hence we use alternative software that saves and stores raw undistorted 12 bit images.)
f) Add headers to the raw images. The MSI headers are documented in Memo AV09-020t, and the SRI headers are documented in Memo AV11-006t.
g) Save the resulting images to the data archival system. The MSI had an external 500 MB or 1 TB drive that was changed occasionally. The SRI system saved the data to the local hard disk. We periodically copied the SRI data to the archive disk used by the MSI. The SRI wasn't networked to the MSI so we couldn't automatically archive the SRI images to the MSI external disk.
h) Steps b – g are repeated at each rotary table position. Initially, the rotary table positions were 30°, 60°, 90°, another position near 95° that pointed at the buoy, 120°, 150°, and 180° or near 180° such that the image included the "Los Coronados" Islands 40 km to the south in Mexico. The number of data acquisition angular positions was decreased later in the project.
i) When all positions have been acquired, the system returns to the home position to re-zero the rotary table.
j) Steps c through i are repeated every 10 minutes continuously until the program is turned off.

Data were downloaded manually to external drives when needed, because the Navy's concern for security precluded the use of other data transfer methods from the data site to our offices. The format of the data drives are documented in Memo AV10-011t.

[8] The rotary table moves counter-clockwise starting at True North, and the readout is the relative angle. For example, the rotary table position 30° is 360°-30°=330° relative to True North. Look angles in this report will always be given relative to True North, with the designation (T), except as noted on some plots.

The MSI control computer used a Windows NT environment, for compatibility with the camera. Both the MSI processing computer and the SRI control computer used a Windows XP environment. All of the control and processing software, including the processing software used to analyze the archival data, were written in C using the Microsoft Visual Studio Development environment.

In addition, the buoy data, weather station data, and ceilometer data were acquired on computers provided by the Naval Postgraduate School (NPS), and pre-processed by NPS software. These data were automatically transferred to the MSI computer and saved on the MSI hard drives. The PSM data were automatically recorded on the MSI computer drive. The transmissometer data were recorded on separate computers, and downloaded to external drives as needed.

The programs RunMSI and RunSRI will be placed on a CD delivered to the sponsor, as well as on the web site listed in Section 16. It should be remembered that these were designed for experimental purposes, and not intended to be polished deliverables. Early versions of the extinction algorithms were included in the RunMSI code, but were not updated, because we did all the analysis in archival mode.

7.2. Sample Raw Data

A sample raw MSI image is shown in Fig. 7-1.[9] The initial analysis of the MSI data is discussed in Memo AV09-035t. The data quality was excellent, with data well onscale, and in good focus. The analysis is discussed in some detail in Section 9.

Sample raw and calibrated SRI images are shown in Fig. 7-2. The non-uniformity is more significant with the SRI camera than in the MSI camera, so we have shown both a raw image and a corrected image in Fig. 7-2. The initial SRI data were documented in Memos AV09-038t and AV10-013t. Although initially there was some abnormal noise as discussed in Memo AV10-013t, this did not recur after the first few days. The initial noise is discussed in Memo AV10-017t. The vertical lines in the Fig. 7-2 raw image occur during readout, and are corrected using the uniformity calibration, as shown in the calibrated image and discussed in Section 8.

[9] All of the MSI or SRI images in this report have been "windowed". The MSI raw data are 16 bit data, covering a grey scale range from 0 to 65,535 bits. Similarly the SRI raw data are 12 bit, with a grey scale range of 0 to 4035. To show the images in the report, they must be converted first to 8 bit displays, with grey levels from 0 to 255 bits. In order to display an image so it can be interpreted by the human eye, it is necessary to select the range of grey levels which will be mapped into the 8 bit display. If the maximum pixel value is near 10,000, for example, we may choose to map the values from 0 to 10,000 into the 8 bits. However, if we wish to show the details near a signal level of 5000, for example, we may choose to map the values from 4000 to 6000 into the 8 bit display. The algorithm always retains access to the full radiometric resolution data, and can thus make use of features that are inherent in the raw imagery that may not be seen in the displays. For this report, we have generally windowed from a value near the brightest pixel to a value near the darkest, except as noted. As a result, relative brightness changes in the appearance of the windowed image are not significant.

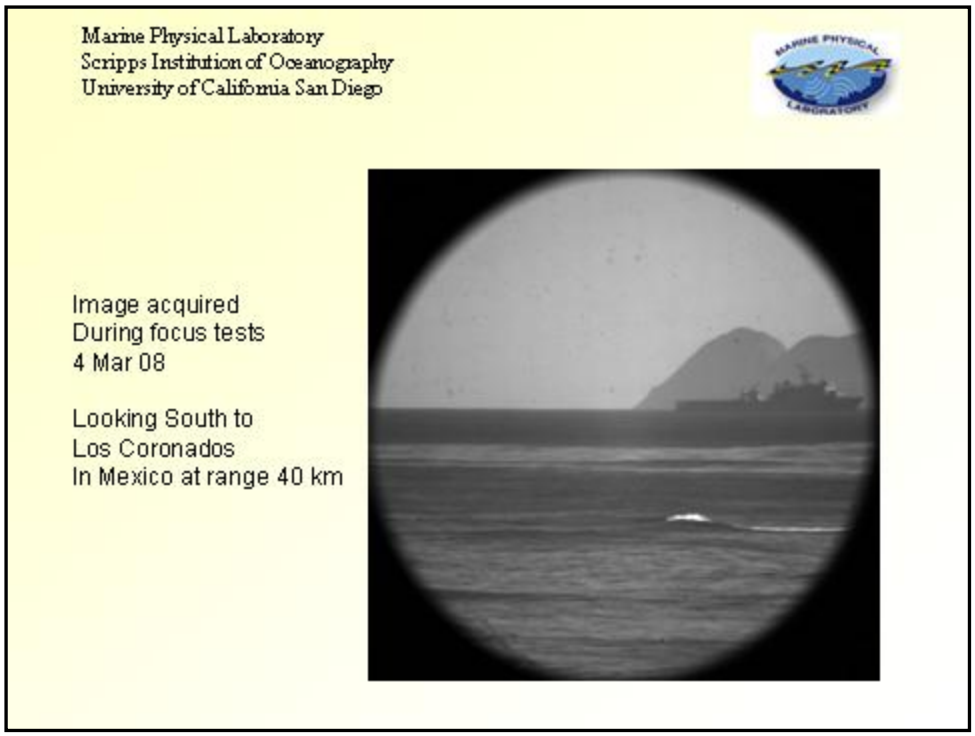

Fig. 7-1. MSI Image acquired on a clear day looking due south at 180° (T)

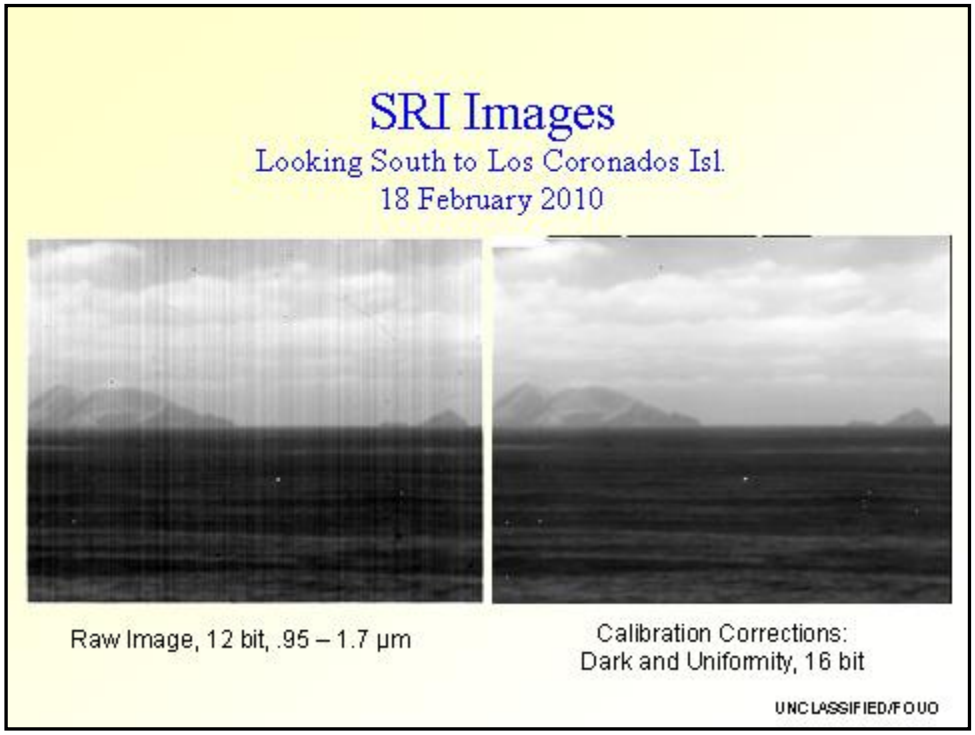

Fig. 7-2. SRI Image acquired looking due south at 180° (T)

Sample data from the buoy are shown in Fig. 7-3. These data include radiance, pressure, relative humidity, sea and air temperature, and wind speed and direction. Similar data were acquired at the shore meteorological station, located beside the MSI and SRI.

Displays similar to that shown in Fig. 7-3 were available to us online for both the shore station and the buoy, and in addition the data were saved digitally. Fig. 7-4 shows a comparison between the shore and buoy data. Although this report concentrates primarily on the extinction data and its analysis, these meteorological data were very useful to us in the evaluation of the raw extinction data.

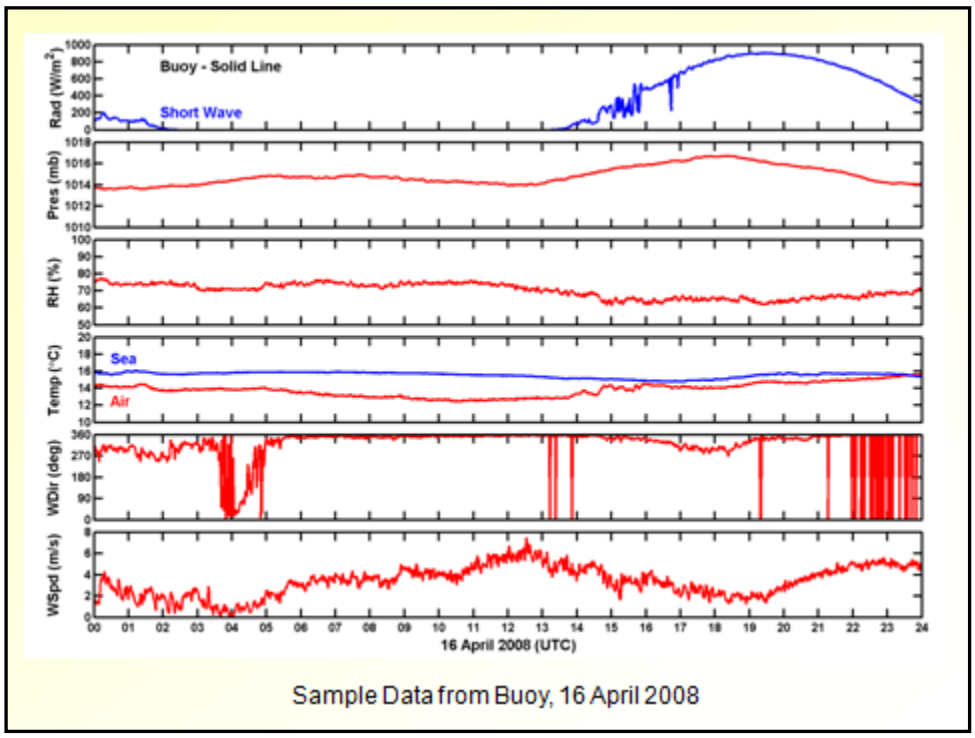

Fig. 7-3. Sample Meteorological Data from Buoy, 16 April 2008

The raw data from the transmissometers and PSM are documented in Memos AV09-033t, AV09-034t, and AV09-036t. Sample transmissometer and PSM results are shown in Fig. 7-5.

The data in Fig. 7-5 show similar trends and peaks, with highest extinctions typically near dawn. During this period, sunrise and sunset were at about 1340 GMT and 0150 GMT respectively, or .56 and .06 in decimal days. Note in Fig. 7-5 that often the reported extinction from the transmissometers was higher in the SWIR than in the visible, which is not an expected result. As a result we did some tests and further evaluation. We found that some internal components in the transmissometer had degraded. These were replaced by the manufacturer in January 2010. The transmissometer tests, as well as later repair of the transmissometers, are documented in Memos AV09-047t and AV10-003t. Most of the analysis is documented in Section 9.

In addition, after we moved the instruments off the dock, the PSM was mounted above the SRI on a pole. We were concerned that this might result in distortions of the data due to the light reflecting off the SRI housing. However, as documented in Memo AV11-001t, we saw no resulting distortions.

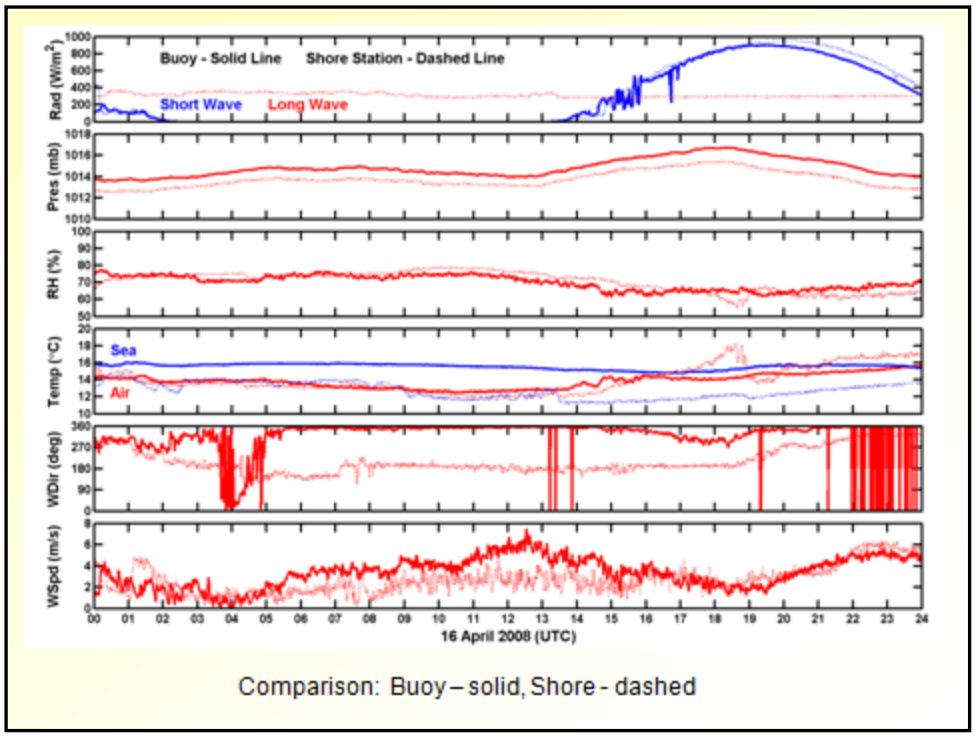

Fig. 7-4. Plot showing a comparison of the shore station and the buoy meteorological data

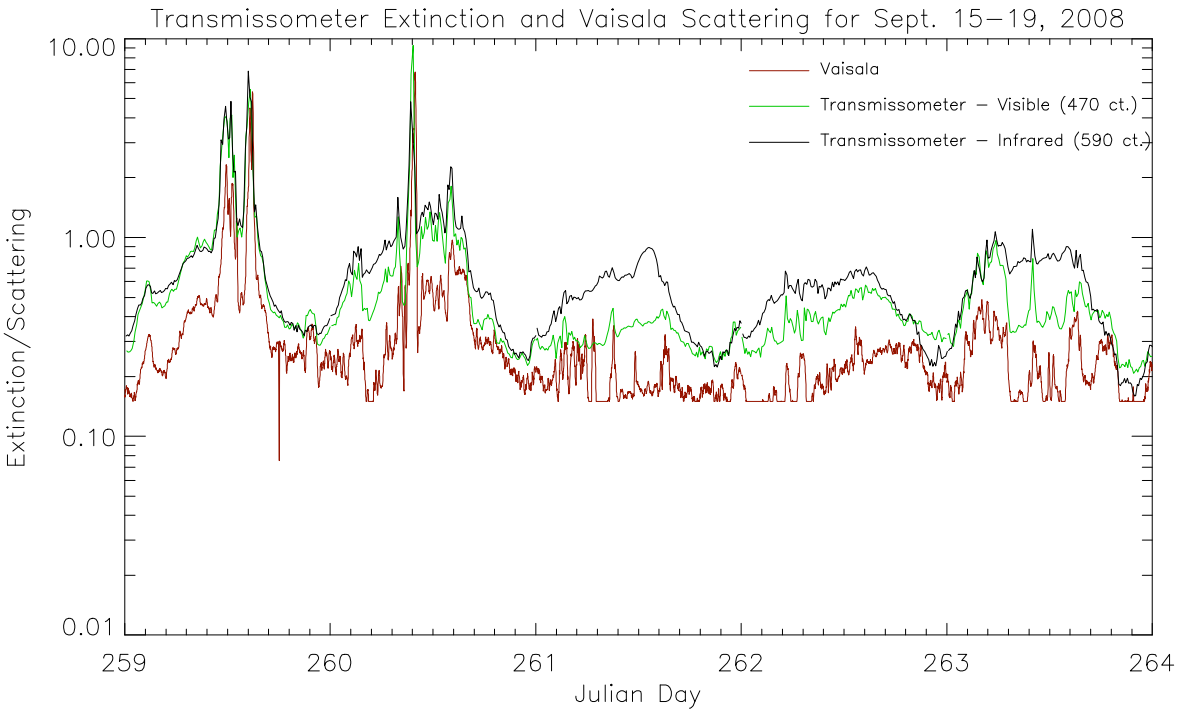

Fig. 7-5. Transmissometer extinction with the Vaisala scattering coefficient at 875 nm for the first five days of the study period

The data processing algorithms that estimate extinction from the raw data are discussed in Section 8. The resulting data and its analysis and interpretation are discussed in Section 9.

8. PROCESSING ALGORITHM FOR DAYTIME EXTINCTION

The adaptation of the daytime extinction algorithm for the ocean environment was one of the most important developments during this project. In this section, we will provide an overview of the extinction algorithm requirements, discuss the analysis that went into addressing these requirements, and then summarize the resulting extinction algorithm. Section 9 will present some of the final extinction results.

8.1. Overview of the Extinction Algorithm

The extinction algorithm is based on the theory presented in Section 3. An earlier version of the MSI data processing program was developed for the staring system looking across San Diego Bay, as discussed in Section 4. This earlier version of the extinction algorithm is discussed in Memo AV07-014t. It used the same equations from Section 3 - however it was optimized for the staring setup used in the earlier contract. In that experiment, the MSI was looking in only one direction at a black box. Because this was angularly a small target as seen from the camera, we included a feature to find the target, even if the scene was distorted by refraction. This is discussed in Section 4.

For the current project, we adapted the MSI extinction algorithm software for the current setup, and wrote a very similar program to analyze the data from the SRI. The logic in these two programs is very similar, but because the cameras are different, the details of image handling are different. For both instruments, the primary differences in comparison with the version discussed in Section 4 are as follows: 1)We added the ability to handle data at a variety of look angles, and adapted the programs to use ocean water as the dark targets; 2) We removed the feature to hunt for the target, as it was not needed for our current targets (although it would be useful if the extinction imagers are used with distant black targets in the future); 3) As the project developed, we added many features to handle situations such as boats in the field of view and other scene abnormalities.

The programs are called AutoProcMSI and AutoProcSRI. As noted in Section 7, the extinction algorithm was initially included in the RunMSI program, but it was never updated. The stand-alone versions of the extinction algorithm designed for evaluation of the archived data were developed to maturity, and are the versions that should be used. The basic logic in both of these programs is as follows:

a) On startup, handle housekeeping, including reading in the inputs such as the target ROI.
b) Read in the archived raw imagery, and read the headers from these images to determine the parameters of interest such as filter and exposure selection.
c) Apply calibration corrections to the images, including dark corrections.
d) Extract the data from the ROI's, and determine averages and standard deviations.
e) Apply special logic to detect and handle special situations, such as looking up-sun.
f) Derive extinction results using equations from Section 3.

g) Apply headers to the processed images, and save these images and the extinction results.

The following memos document the extinction algorithm software: AV10-020t, AV10-021t, AV10-022t, AV10-028t, AV13-003t, AV13-004t, AV13-005t, AV13-006t, AV13-020t, and AV14-001t.

Samples of the most significant input files for AutoProcMSI are listed in Appendix B, and may be useful to reference in the remaining discussion.

8.2. Selected Targets and Range to Targets

The targets used for our analysis of the Feb 2010 data are fairly typical, and are shown in Fig. 8-1.

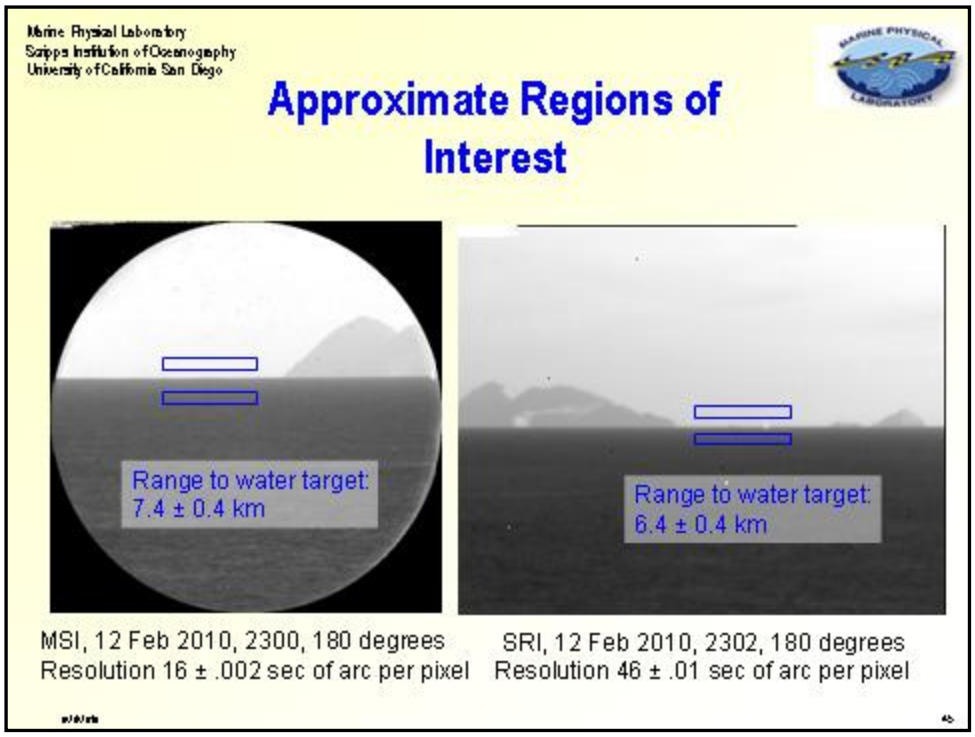

Fig. 8-1. Typical Target Areas for MSI and SRI, looking due south at 180º (T)

In selecting the ocean ROI's, we chose ROI's which are narrow in a vertical direction on the image, so that the uncertainty in range is minimized. They are wide in the horizontal direction on the image, so that we have a large number of pixels, and can determine representative averages and standard deviations.

We evaluated how much the position of the horizon in the imagery varied as a function of time and rotary table orientation, because we wanted each ROI to be close to the horizon yet not impinge on the horizon interface. As documented in Memo AV09-032t, for the MSI we found that the vertical position of the horizon interface in the images varied as a function of azimuth, because the camera mount was not quite level. However, the

variation from day to day or during a day was less than 2 pixels. We chose ROI's at least 4 pixels from the horizon interface. Thus the ROI's were the same number of pixels from the horizon at each rotary table position, and this distance from the horizon was sufficient to handle the uncertainty in the horizon position.

The position of the horizon in the SRI imagery also varied as a function of azimuth. Initially, the position was quite stable. However toward the end of the deployment the SRI hardware was less stable. For this later period, which occurred after some changes to the hardware, we found that the position of the horizon interface in the imagery varied by a few pixels from day to day, but did not vary significantly during each given day. (It may have been that we didn't get it back in its mount as tightly as optimal.) We added a feature to the extinction algorithm to allow for a correction in the daily horizon interface position, as documented in Memos AV13-005t and AV13-009t. This type of correction should not be needed in an operational system with better mounting and leveling.

To determine the range to the targets, we measured the angular resolution of each system, from which we could determine the angle in degrees below the horizon for each ROI. Range was computed from this angle. Our initial method is documented in Memo AV10-015t, and the updated version is documented in Memos AV12-022t and AV12-023t. There was some residual uncertainty in the range due to the difficulty in measuring the resolution, particularly in the SRI. The impact of uncertainties in range is discussed in Section 9.

8.3. Calibrations to Correct for Sensor Characteristics

To use the equations in Section 3 accurately, we must have measurements that are reasonably accurate. As seen in Eq. 3.23 and 3.24, the method uses the apparent contrast of the ocean target with respect to the horizon target. This contrast is a ratio, and, as a result, it is only necessary to know the relative (and not absolute) radiance of each pixel. The purpose of the calibrations is to determine how to adjust the measured signals so that they are proportional to the scene radiances.

Several calibration steps were used. The calibrations and their impact are documented in the following memos: AV09-067t, AV09-073t, AV09-102t, AV11-002t, AV11-003t, AV11-004t, AV11-007t, AV11-008t, AV11-009t, and AV12-021t.

Dark images are acquired in the field, and measure the electronic bias and the thermally-generated dark current. The dark calibration is measured in the field at least daily, and subtracted from the raw images acquired at the same integration time. The MSI dark image can be measured by closing the mechanical shutter, and exposing the sensor chip for the necessary integration time. This is done hourly. The SRI does not have a mechanical shutter, so we used an image acquired in the middle of the night.

Linearity calibrations are acquired in the lab, and used to correct any non-linearities in the signal as a function of input radiance and exposure time. The linearity calibrations are applied as a correction that depends on exposure and signal. The camera we

happened to have available for the MSI was a costly camera, with excellent characteristics. Its signal was linear to within 1% for signals between 3 and 23,000, increasing to a non-linearity of about 3.5% for signals at full scale at 65,535. The results were linear both as a function of exposure setting and radiance on the camera at a fixed exposure.

The SRI camera however is less well behaved. The behavior is not linear as a function of exposure. The manufacturer was able to duplicate our results, and recommended that we only use a few fixed exposures, and to calibrate at those exposures. At a fixed exposure, the response as a function of radiance is smooth, but not very linear. The calibration as a function of relative input flux is shown in Fig. 8-2, which shows the signal, and Fig. 8-3, which shows the percent non-linearity with respect to a signal of 1000. These non-linearities are corrected in the extinction algorithm. The impact of uncertainties in linearity calibrations are discussed in Section 9.4.

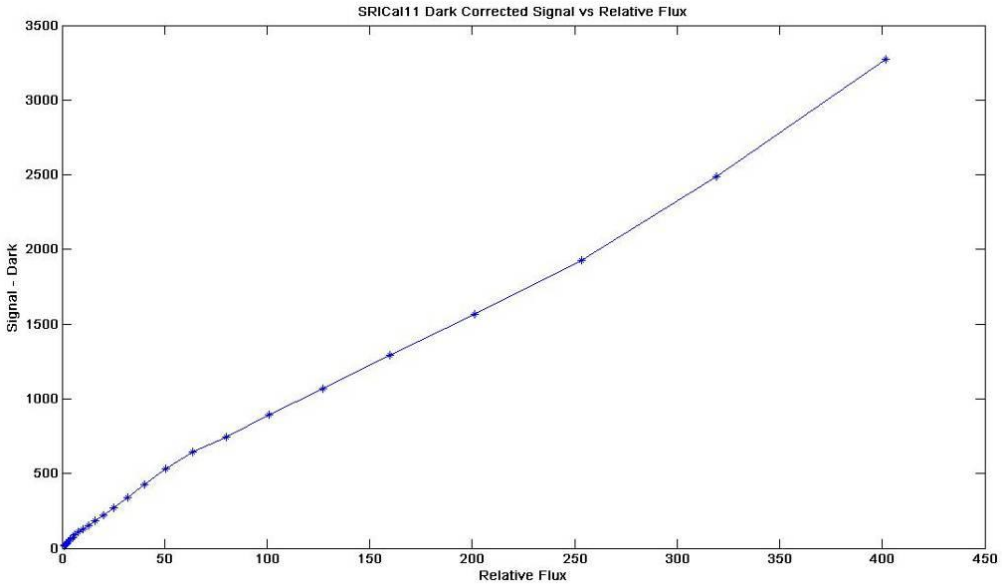

Fig. 8-2. Linearity calibration vs. radiance for Exposure 32,000 μsec, plot of dark-corrected signal vs. relative flux

Finally, a uniformity correction measures variance in system response as a function of pixel. The uniformity calibration is designed to characterize pixel-to-pixel differences in responsivity of the system resulting from the effects of both the optics and the camera system (including the electronics). The MSI sensor includes a fiber optic taper bonded to the chip, which also impacts the uniformity calibration. The SRI uniformity is strongly influenced by the readout electronics.

The uniformity can be measured in the calibration room, and measured almost as accurately in the field (using a white diffuse reflector or transmitting diffuser). A sample MSI uniformity image is shown in Fig. 8-4, where it has been windowed (displayed) over

a narrow signal range of signal values to exaggerate the non-uniformities (see footnote in Section 7.2).

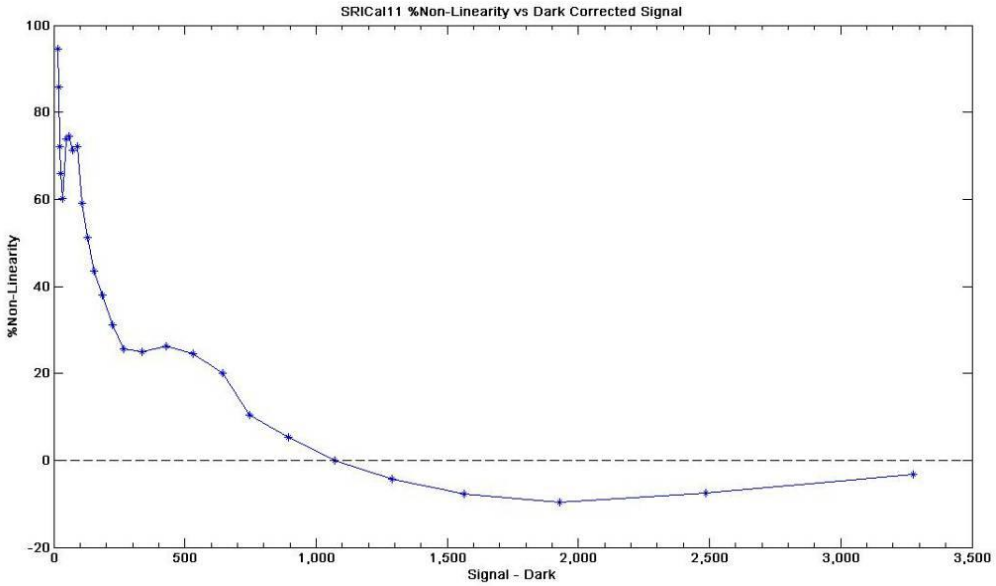

Fig. 8-3. Linearity calibration vs. radiance for Exposure 32,000 μsec, plot of % non-linearity vs. dark-corrected signal

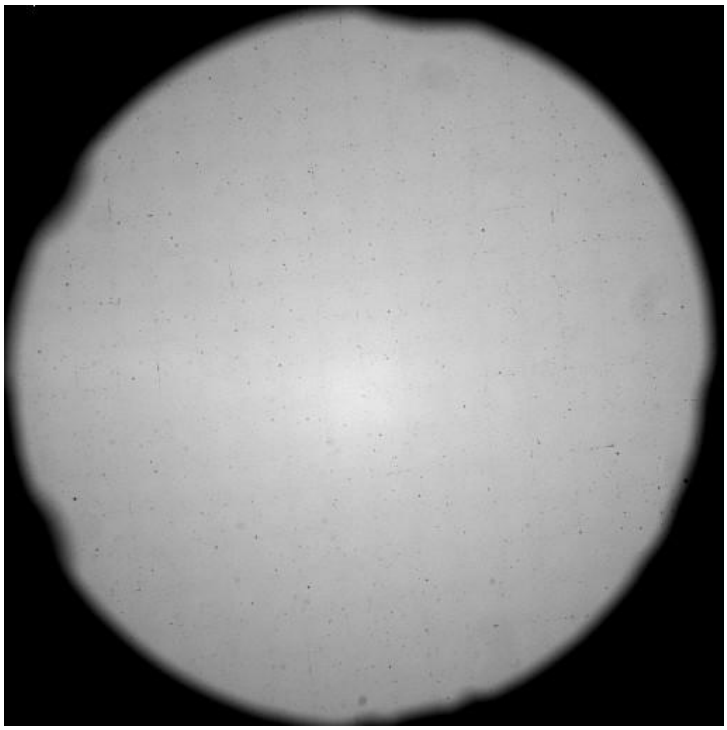

Fig. 8-4. Uniformity calibration image for MSI Red Filter, windowed over a very narrow range to bring out the non-uniformity features

The impact of the MSI non-uniformity on the field data is quite small even before the calibration correction, and can be seen in Section 7, Fig. 7-1. The rectilinear features and most of the small dots in Fig. 7-1 are due to the fiber optic taper in the system. The brighter region near the center is due to the lens optics. To apply the correction, the raw image, which has been dark and linearity-corrected, is divided by the dark-corrected uniformity image. This correction nicely corrects the raw images, as shown in Memo AV09-102t.

The SRI non-uniformity is much more significant, as may be seen from a comparison of the two images in Section 7, Fig. 7-2. A SRI uniformity image is shown in Fig. 8-5. Our understanding is that these vertical lines are associated with the readout process of the CMOS chip used in the SRI. The uniformity correction is quite effective in cleaning up the SRI imagery, as can be seen in Fig. 7-2 and the remainder of the SRI imagery in this report.

In the future, other systems may be developed based on the MSI methods using other cameras. In that case, the calibration corrections will differ from those presented here. For most of the cameras we have dealt with, dark calibration and uniformity calibration can be especially important, and linearity calibration may be important. However, the important point is that depending on the accuracy required for the application, it may be very important that the data be calibrated and processed in such a way that the signal is proportional to the radiances. Our belief is that careful calibration is one of the key factors in getting good results with this method. We would expect that it would suffice to measure a few cameras of a given make and model, so that each camera going into the field would not need to be characterized. This is discussed more in Section 9. [Recommendation]

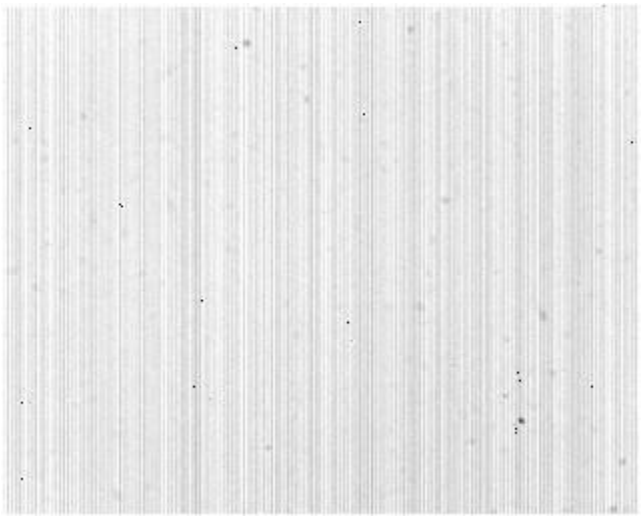

Fig. 8-5. Uniformity calibration image for SRI, without minor windowing

8.4. Evaluation of Inherent Contrast

One of the major goals of this project was to determine whether a region of the ocean surface could be used as a dark target for determining extinction. In the previous contract

discussed in Section 4, we used a black target which was a hollow black box. Clearly it would be a major advantage if we could use "targets of opportunity" from a ship, and in particular use the ocean surface as a target rather than using a hard target. From Eq. 3.24, it is clear that the target need not be black, but it does need to have a known inherent contrast.

We measured the inherent contrast of our black target used in the previous contract, and it was -0.988 ± .01, where the variation is as a function of solar angle and spectral wavelength. For the ocean, we found that the inherent contrast was essentially constant, with a value of about -0.85 in the red, and about -0.73 in the SWIR, as will be discussed in this section. That is, the ocean is not as dark relative to the horizon sky as a black box, but it is reasonably dark.[10]

Equally important is the question of how much the inherent contrast of the ocean ROI (with respect to the horizon ROI) changes as a function of solar position and other factors. In our initial processing, we used a constant for the inherent contrast, and were surprised to find that the resulting extinctions looked quite reasonable, and did not appear to have significant azimuthal offsets. Following more detailed analysis, we were able to confirm that in both the red and the SWIR, the inherent contrast appears to be independent of the solar position. This was a surprise, but certainly a convenient one, and it will be discussed below.

The most complete memos discussing the inherent contrast analysis are AV11-005t and AV13-011t. To determine the absolute value of the optimal inherent contrast, we first evaluated the apparent (measured) contrast and its variance as a function of time and date. The inherent contrast should be closer to 1 than the highest measured contrast, in the absence of measurement error. (In this discussion, we are always referring to absolute value.)

Fig. 8-6 shows a time series of the measured apparent contrast C_r for the red filter, for a period of 6 days. In this plot, four targets are shown, of which Target 4 is the closest to the observer and thus should have the highest apparent contrast. On the y axis, the highest values should correspond with the lowest extinction values or clearest air (for a given target), because the absolute value of the apparent contrast is highest under clear conditions. We carefully evaluated the data by comparing the values in Fig. 8-6 with the images. In the imagery, the islands to the south are easily seen under low extinction or clear conditions, and the horizon generally appears sharper under low extinction conditions. We verified that the measured C_r values vary in accordance with the clarity of the scene, as expected.

[10] Keep in mind that when we look at the ocean with our eyes, we are using a photopic band which peaks near 550 nm. In that wavelength, the upwelling radiance of the ocean is significant, but it drops off quickly in the red. Thus even though our visual experience leads us to expect that the ocean is not dark, it is much darker in the red and SWIR.

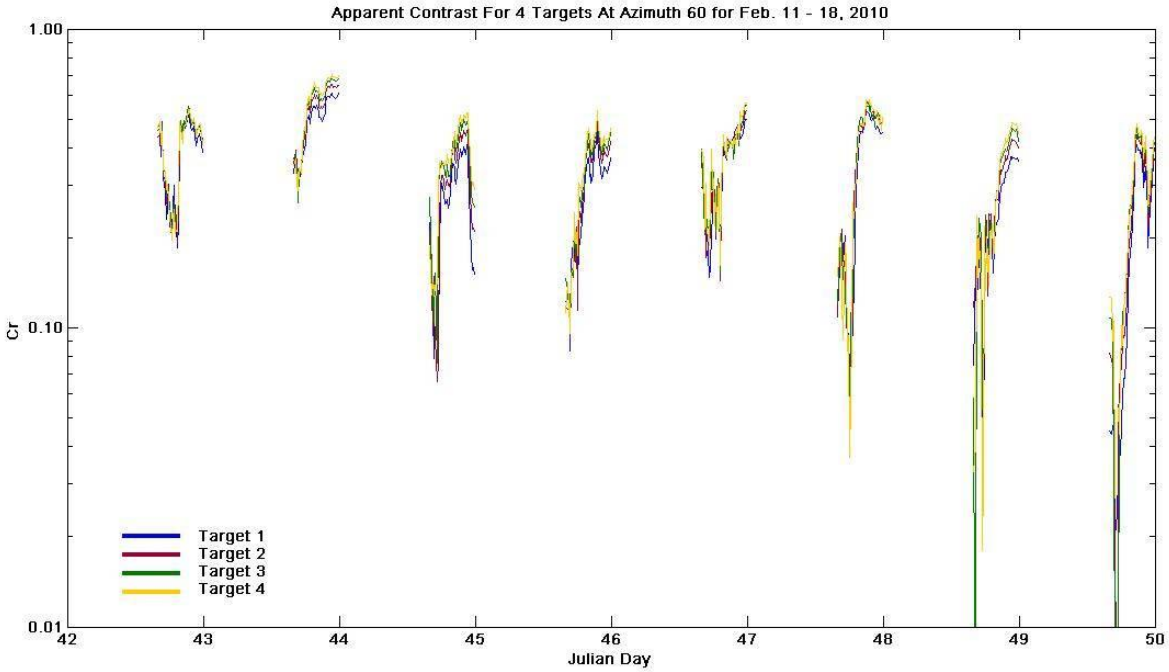

Fig.8-6. MSI Measured Apparent Contrast looking WNW at 300° (T), Targets 1-4, Feb 11 – 18 2010 (Azimuth listing at top of plot refers to the rotary table readout value)

During the data period shown in this plot, the measured apparent contrast C_r was always less than 0.7. During the remainder of the test period, the maximum measured C_r value was approximately 0.77. By extracting the images associated with these cases of high measured C_r, we were able to verify that they occurred on very clear days. Since we know that the C_r value should never exceed the inherent contrast C_0 (in the absence of measurement error), this indicates that the inherent contrast C_0 is probably greater than 0.77. This approach gives us a first ballpark value for the inherent contrast. This approach is essentially the same as basing the inherent contrast estimates on very clear days.

To further refine the inherent contrast estimate, we next evaluated the resulting extinction for a range of inherent contrast values. These results are shown in Fig. 8-7. In this plot, the low extinction or clear cases are on the low end of the y axis. Note that the plot values of .01, .1, 1, and 10 km^{-1} correspond to red visibility values of 300, 30, 3, and .3 km. Fig. 8-7 illustrates that when the extinction is reasonably high (i.e. conditions are hazy), the inherent contrast makes little difference in the resulting extinction. Under very clear conditions, as we would expect, the selected value of inherent contrast becomes more important. The value of the inherent contrast makes little difference for extinctions greater than about .1 km^{-1}, i.e. red visibilities less than about 30 km. Our understanding is that knowing exactly how clear it is under clear conditions is not a priority to our Navy sponsors. Using additional analysis discussed in Memo AV11-005t, we determined that a C_0 value near .85 was optimal for the red. As we continued to process additional data sets, we found this value to yield good results (see, for example, AV13-017t). Using

similar evaluation, we determined that an optimal C_0 value for the SWIR is 0.73, as discussed in Memo AV13-011t.

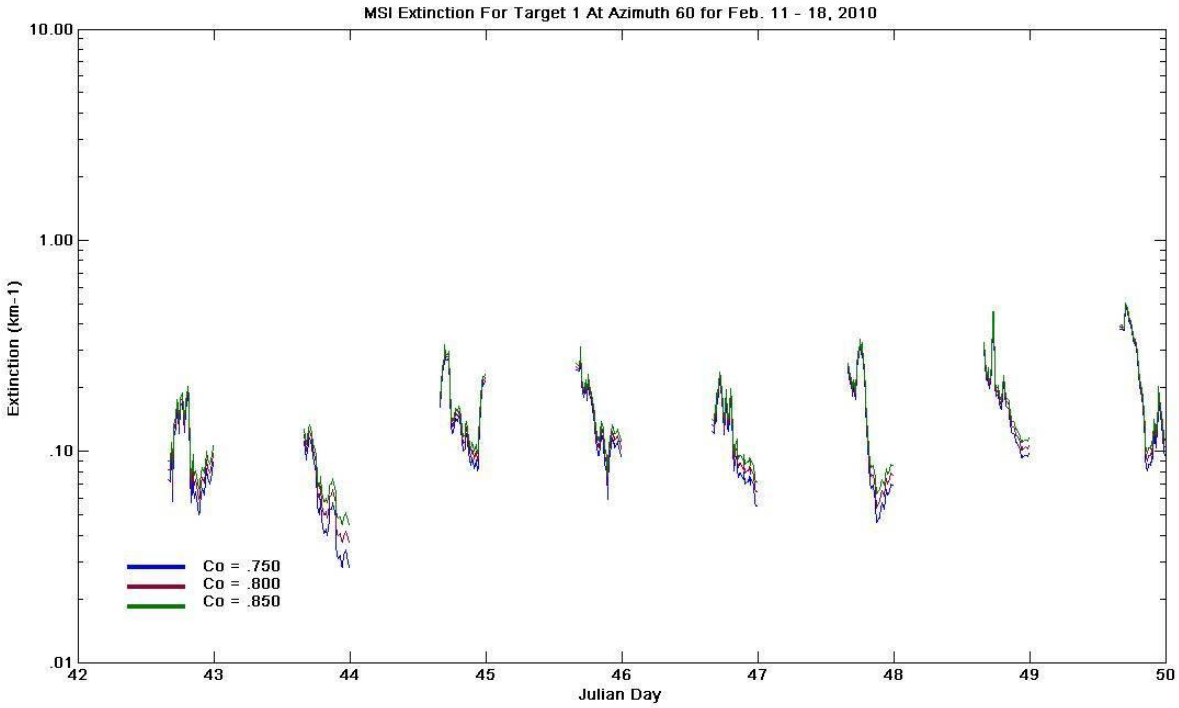

Fig. 8-7. MSI Extinction at 300° (T), Target 1, for inherent contrast values .75, .80, and .85, Feb 11 – 18 2010 (Azimuth listing at top of plot refers to the rotary table readout value)

Regarding the question of variation in the inherent contrast as a function of solar position, when we processed extinctions at a variety of azimuths and times, we found that there does not appear to be any systematic variance as a function of azimuth relative to the sun. For example, Fig. 8-8 shows the extinctions at all azimuth angles for the Feb 2010 data set. If there were systematic azimuthal effects, we would expect there to be a strong peak or other abnormality at 180° (T) rotary table position (south) near noon (lavender curve).

Each of the time plots in Fig. 8-8 includes data for a period from 1600Z to 2400Z for each day. Noon is near 2000Z, at the center of each day's data. We do not see any systematic difference in most cases. Similarly, we would have expected a systematic difference near 210^0 (T) (southwest – turquoise curve) and 270^o (T) (west – green curve) later in the day, but we do not see any systematic differences.

This result is very convenient, but somewhat unexpected, because clearly the horizon radiance is higher at look angles near the sun. However, additional plots shown in Memo AV11-005t show that the ocean radiance is also higher at look angles near the sun and that these factors cancel to yield inherent contrasts and thus extinctions that do not vary systematically with azimuth relative to the sun.

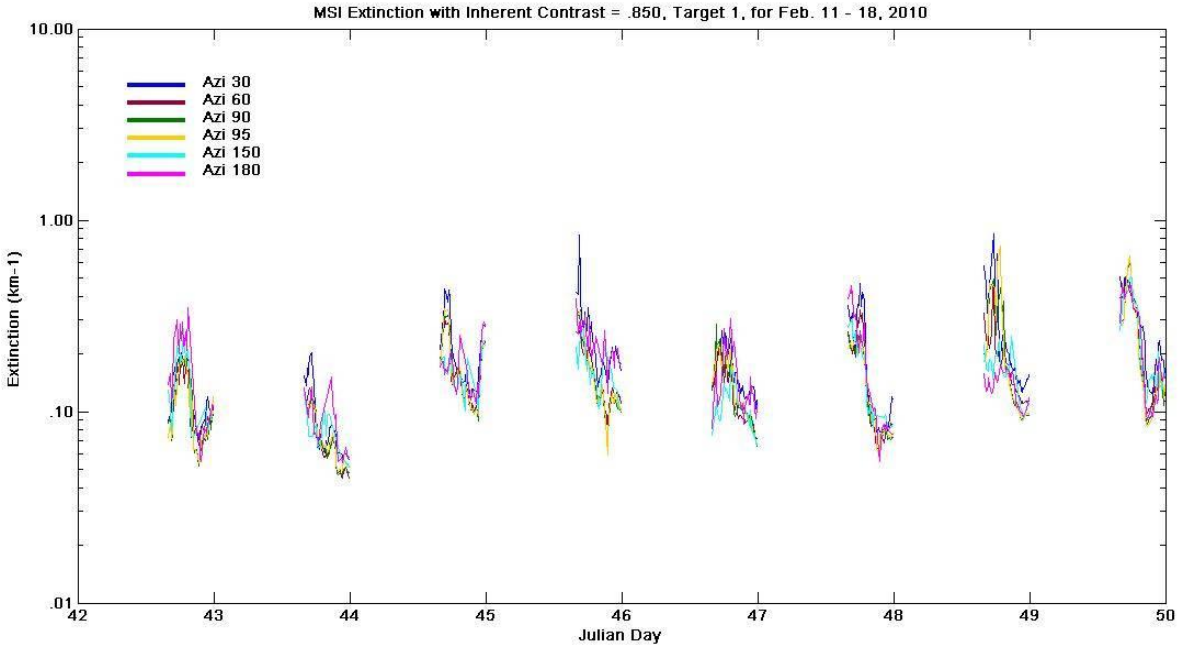

Fig. 8-8. MSI Extinction at all azimuthal angles, Target 1, inherent contrast .85, Feb 11 – 18 2010, for look angles 330° (T) (blue), 300° (T) (red), 270° (T) (green), 265° (T) (yellow), 210° (T) (turquoise), and 180° (T) (pink) (Azimuth listing in the key refers to the rotary table readout value)

As a result of the inherent contrast analysis, we determined that the optimal values are near .85 for the red filter, and .73 for the SWIR. They do not appear to vary as a function of either the solar zenith angle, or the azimuthal look angle relative to the sun. We believe these values are reasonably universal, and should not vary significantly geographically, and we found that the same values worked well for all the data we processed. More importantly, as shown in Fig. 8-7, the impact of such variations will be small except in very clear conditions with extinction coefficients less than about .1 km^{-1} and red visibilities greater than about 30 km. [Finding]

8.5. Handling of Special Conditions

There are a variety of non-optimal conditions that can affect the measurements. As part of this development work, we developed methods to detect and mitigate most of these situations.

8.5.1 White Caps, Boats, and System Noise

If there are boats or white caps in the ROI, this can affect the measured apparent contrast. To handle this situation, the extinction algorithm uses sorted averages. We select ROI's for the ocean that are large enough to include a reasonable number of pixels. As shown in Appendix B2, a ROI size of 100 x 10 pixels is typically selected. This yields 1000 measured values representative of the region. The ROI is reasonably narrow in the Y dimension, so that the range to the target is reasonably well defined. The program does a histogram of these 1000 values, and then selects those that are between the 5th percentile

point and the 35th percentile point. Thus we use roughly the darker 30% of the values, but do not use the outliers on the dark end.

In this way, any outliers caused by measurement noise or abnormal pixels not fully corrected with the uniformity correction are ignored. In addition, white caps and other bright features such as sailboats are ignored as long as they do not occupy more than 65% of the ROI. Dark objects (ships) that are darker than the ocean surface will result in a negative extinction value, and will be removed with another flag, as discussed in Section 8.5.4. Also, the Standard Deviation (STD) within the ROI is evaluated, and if it is too large, the value is flagged, as discussed in Memo AV14-001t. The analysis of the boats and white caps is discussed in Memo AV10-030t. We found the program to work quite well in eliminating these abnormalities. This feature is also included in the SRI extinction algorithm, and appears to work well with the SRI data.
[Finding/Recommendation]

8.5.2. Glitter and Gloss

For this discussion, we must first distinguish what we have called glitter and gloss. By "glitter", we mean the pattern of light on the water when looking upsun on a sunlit day. Fig. 8-9 shows an example of glitter in MSI imagery. The left image was acquired looking nearly upsun at 2000Z and has glitter; the right image, acquired an hour later, does not. At 2000Z, the sun is at an azimuth of -1° relative to the look angle on this date, and at 2100Z it is at +18° relative azimuth angle. The glitter is caused by reflections of the sun on the water. (The brighter appearance of the sky on the right hand side is an artifact of the windowing when the data are reduced from 16 bit to 8 bit for optimal display.)

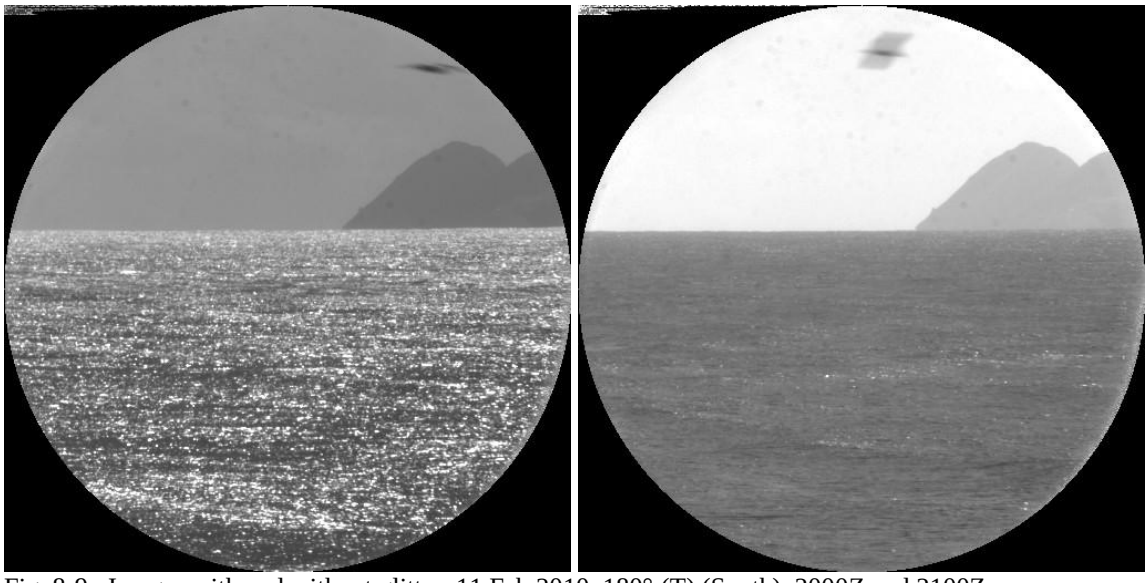

Fig. 8-9. Images with and without glitter, 11 Feb 2010, 180° (T) (South), 2000Z and 2100Z

By "gloss", we mean the enhanced radiance that occurs in any direction, generally in low wind conditions. Fig. 8-10 shows two MSI images with varying amounts of gloss. (The

white spots in the image on the right are probably gulls on the water.) The gloss appears to be a reflection of skylight, probably caused by a relative absence of small capillary waves on the water. Gloss often occurs in the off-shore kelp beds, which appears in the bright band just below the center in Fig. 8-10b.

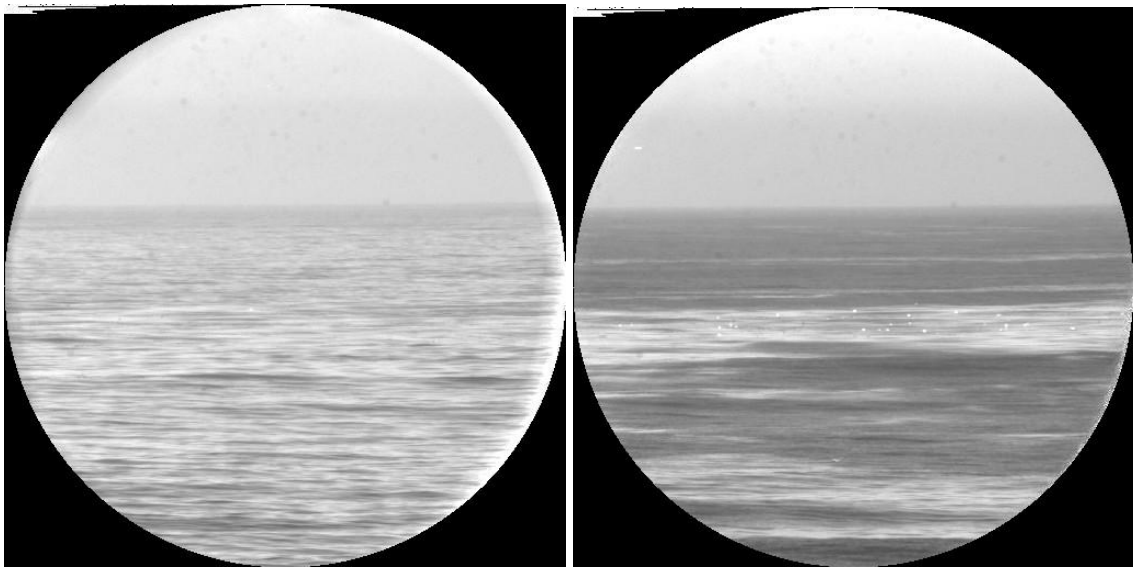

Fig. 8-10. Images with gloss and partial gloss, 13 Feb 2010, 300° (T) (West-north-west), 1700Z and 1800Z

Both glitter and gloss occur in both the visible and the SWIR. Fig. 8-11 shows SRI images. The first shows some gloss, and the second shows glitter. In the first image, the MSI was looking away from the sun. The solar azimuth was 98° (T) at 1700Z, so the MSI look angle of 270° (T) was at an azimuth relative to the sun of 270° - 98° or 172° (rel). In the second image, which was acquired at 2200Z, the solar azimuth was 252° (T) and thus the MSI look angle was at an azimuth of 19° (rel) relative to the sun. Thus there was strong glitter in the 2200Z image which was looking nearly upsun.

Fig. 8-11. SRI Images with some gloss in first image, and glitter in second. July 26 2012, 270° (T) (West), 1700Z and 2200Z

Because both of these phenomena increase the average radiance of the ocean ROI, the resulting computed extinctions can be too high, as shown in the red (upper) curve Fig. 8-

12. The glitter is reasonably easy to handle. We determined that glitter only occurs when the azimuth relative to the sun is 22.5° (rel) or less, and only when the sun is unobscured. If the relative azimuth is 22.5° (rel) or less, we evaluate the STD of the unsorted data in the ocean ROI. If this STD is less than 5%, then the sorting mechanism discussed in Section 8.5.1 will successfully extract the darker portions of the ROI and yield valid extinctions. If the STD is too high, then there are not sufficient dark pixels to overcome the glitter, and the data are flagged in our program. The results processed with the glitter feature of the extinction algorithm turned on are shown in the blue curve in Fig. 8-12.

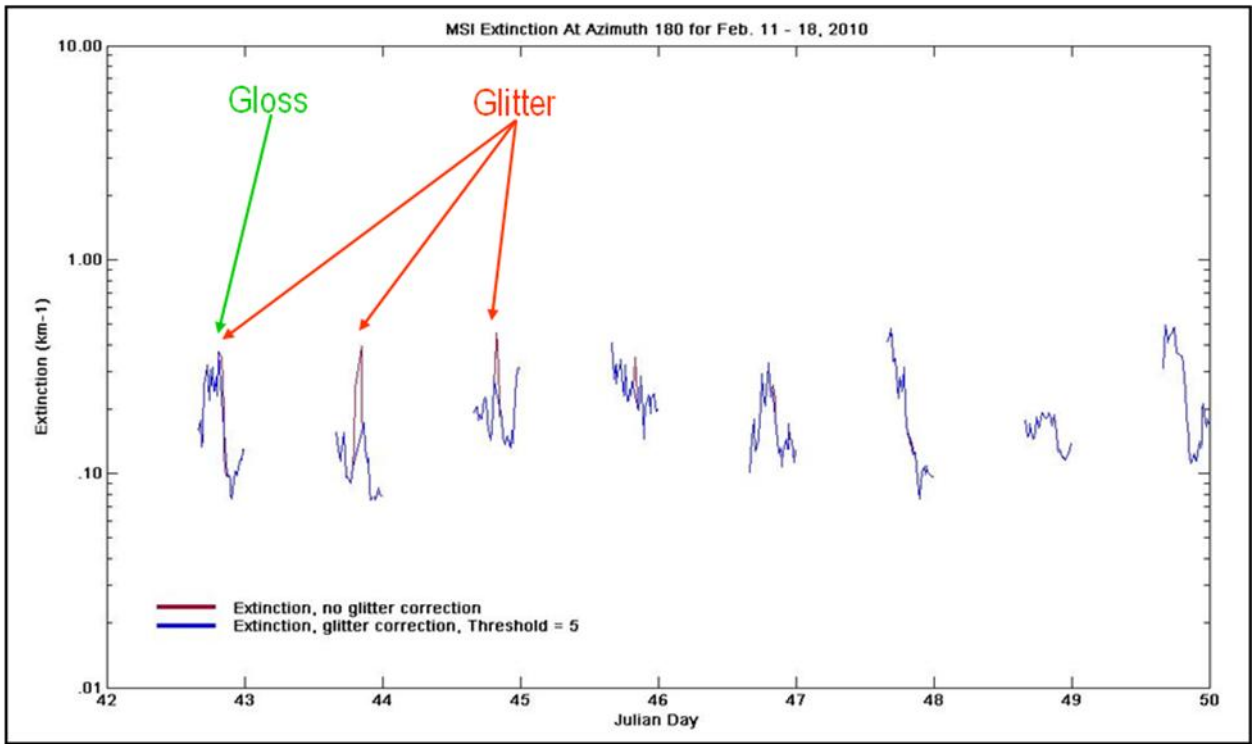

Fig. 8-12. Extinction plot for Feb 11 – 18 2010, 180° (T), with strong glitter and gloss cases marked

In an operational program, to handle glitter, we would use the same logic, and if necessary extract the extinction from a direction that is outside the ± 22.5° window. For example, if the look angle relative to the sun is 20°, the extinction could be extracted at a look angle of 25° or 30°, and still be reasonably close to the extinction for the desired line of sight. The glitter feature of the extinction algorithm and examples are discussed in Memo AV10-029t. As discussed in Memo AV13-012t, the same logic worked well for the SRI. [Finding/Recommendation]

Unfortunately, the gloss was not as straight-forward to handle. This is easiest to illustrate with SRI data, as the gloss appears to be worse in the SWIR than in the visible. Several memos discuss the gloss. The most complete is AV13-013t, which discusses ways to handle the gloss issue. Memo AV13-017t shows the comparison between the red and SWIR gloss under gloss conditions, and this is further illustrated in Section 9.3 of this report.

The impact of gloss in the SRI in a worst-case data set can be seen in Fig. 8-13, where situations that were visually determined (from the imagery) to have gloss are marked with a "G". These data were acquired looking WNW at 300^0 (T). The wind speeds measured on the buoy near the W ($270\ ^0$ T) position are shown in Fig. 8-14.

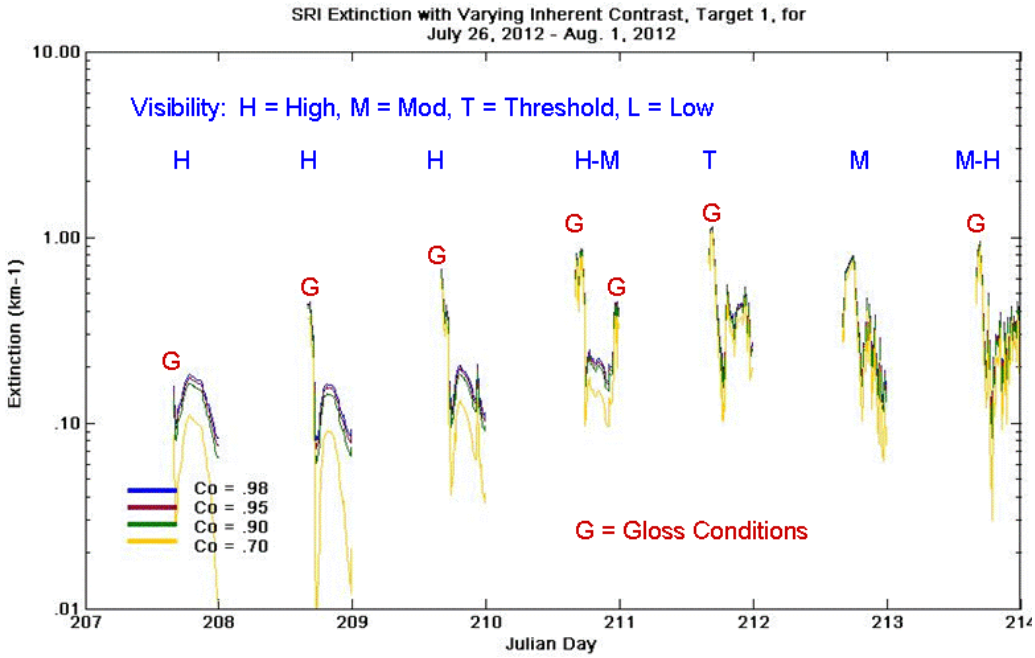

Fig. 8-13. Derived SWIR Extinction Coefficient for July 26 – Aug 1 2012 looking WNW at 300^0 (T), using varied Inherent Contrast Values

In Fig. 8-14 there is clearly a relationship between wind speed and the presence of gloss conditions. However, more detailed analysis in Memo AV13-013t showed that there does not seem to be a firm wind threshold that can be used to distinguish the gloss from the non-gloss conditions. Our sponsors told us that gloss conditions are not apt to occur much, and may not be an issue. However, this is probably the biggest uncertainty in the system, and merits further evaluation. We determined experimentally that adding a polarizer to the system should be useful in detecting the gloss. This is discussed in Section 9.3. Also, the use of a multi-spectral system may enable distinguishing gloss conditions. If, for a given application, significant times with gloss are expected, it would be important to further address this issue, and it may be important in these cases to use a system in the visible rather than SWIR, where the gloss has a greater effect. There is further discussion of gloss in Section 9. [Finding]

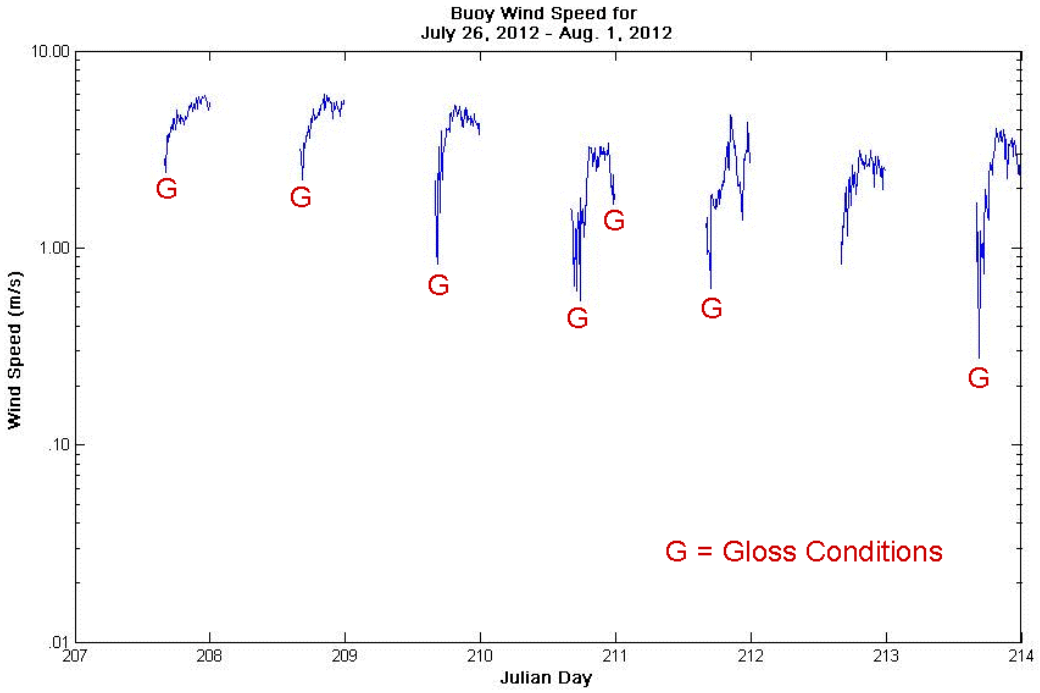

Fig. 8-14. Wind Speed from the Buoy near the West (270^0 T) Position for 26 Jul – 1 Aug 2012

8.5.3. Horizon Clouds

As discussed in Section 3, the equations for determination of extinction are only rigorous when the horizon radiance at the detector location has reached equilibrium. Equilibrium radiance, defined in Section 3.2, is not a common term, and some explanation may be useful. Equilibrium radiance is the radiance at which the incremental loss in an incremental path unit is equal to the incremental gain. The loss depends on the extinction; the gain depends on the brightness of the surround and the scattering into the path of sight. The radiance of a bright object, such as a cloud on the horizon, will exponentially approach the equilibrium radiance as range from the object is increased, and typically be within a few percent of equilibrium within a few km. (See examples in Memo AV13-007t.) The horizon will be at equilibrium when the sky is clear, or when there is a uniform overcast. If there are scattered clouds on the horizon, or if the line of sight is very non-uniform, the horizon may not be at equilibrium, especially if it is very clear.

For cases with scattered clouds on the horizon, we have two features in the extinction algorithm to deal with this. First, the same sorting step is used for the horizon ROI as for the ocean ROI. That is, the extinction algorithm uses the average of the radiances from the 5% to the 35% points on the histogram. In this way and clouds will be ignored, unless they cover more than 65% of the horizon ROI. The extinction algorithm automatically evaluates the STD within the horizon ROI, and flags the data if this value is greater than 5%. This should flag any cases in which the scene is not near equilibrium. We have found that the impact of clouds at the horizon is small. If the conditions are quite hazy, then the horizon reaches equilibrium very quickly, even if there are non-uniform clouds. If there is little haze, the target is relatively dark. This means that in Eq.

3.23, the abnormal horizon radiance has little impact on the apparent contrast. Memo AV13-015t evaluates these impacts. We found that in this 22-day data set, there were only 2 cases in which the horizon visually appeared to be not at equilibrium. In each of these cases, the extinction algorithm handled the calculations properly, and the resulting extinction was not impaired. [Finding/Recommendation]

8.5.4. Other Flagged Conditions

As discussed above, the extinction algorithm includes several flags for abnormal data. In addition to those discussed above, we check to see if either the horizon or ocean surface data are offscale bright or dark. This protects against processing invalid data. Finally we check to see whether the derived extinction is negative. This can occur rarely, for example if there is a dark ship in the field of view. The resulting flags are listed in Memo AV14-001t. [Finding/Recommendation]

8.6. Summary of the Day Extinction Algorithm

The extinction algorithm programs, ProcMSI and ProcSRI, are designed to determine the extinction coefficients from the raw imagery. Classic equations are used to determine extinction from the relative radiances of the ocean ROI and the horizon sky ROI. As part of this process, the images are calibrated so that the processed signals are proportional to the radiances. The extinction algorithm also includes several features to protect against non-ideal conditions, including boats, white caps, glitter, and clouds on the horizon. The extinction algorithms are quite similar for the MSI and the SRI, with the primary differences being due to the image format. The analysis of the resulting data is discussed in Section 9.

9. ANALYSIS OF DAYTIME EXTINCTIONS

Much of the analysis effort on the daytime MSI and SRI data was involved with development of the extinction algorithm, especially determining how to handle the special situations involved in using the ocean as a passive target. It was important to understand whether the inherent contrast was well behaved, and whether it would be possible to handle special situations such as boats in the field of view. That analysis is presented in Section 8. As discussed in Section 8, the inherent contrast was found to be well-behaved, and we were able to address all of the issues associated with the ocean target except for gloss, which we believe can be handled in other ways.

Another part of the analysis, which was done in parallel with the above, was evaluating whether the results made sense and appeared to be reliable. We evaluated the anticipated uncertainties involved in this method. This analysis is also discussed in this section.

During the previous project, discussed in Section 4, we analyzed the MSI extinctions as a function of filter, and found them to be generally well behaved except in the NIR filter, which was somewhat limited by signal level. For this project, we concentrated on just the red filter in the MSI (and the open hole in the SRI). This concentration was because an early evaluation showed that the upwelling radiance from the water is extremely low in the red and NIR, so the use of an ocean target should be most practical in these bands. Further we felt the red filter would be better than the blue or green for estimating the SWIR extinctions.

We analyzed daytime data between approximately 4 hours before and 4 hours after local apparent noon, i.e. from 1600(Z) to 2400(Z). The daytime data were at optimal flux levels during these hours. The MSI is capable of acquiring excellent data all day and night. The SRI can acquire excellent data from sunrise through sunset, as discussed in Memos AV13-002t and AV12-009t. We did not develop a flux control algorithm for the MSI or SRI that would automatically adjust the exposures to current conditions. Our other instruments [24, 27] include flux control algorithms, but we felt this was not a priority for this project.

The detailed analysis is documented in the following memos: AV09-033t, AV09-034t, AV09-035t, AV09-036t, AV09-037t, AV09-047t, AV10-003t, AV10-012t, AV10-013t, AV10-014t, AV10-023t, AV10-031t, AV11-001t, AV12-017t, AV13-007t, AV13-009t, AV13-011t, AV13-012t, AV13-013t, AV13-015t, AV13-017t, AV13-018t, and AV13-019t. In this list, we have included not only the memos directly related to the MSI and SRI analysis, but also several memos related to the analysis of the supporting instrumentation we were comparing them with, and also memos such as AV13-007t that were related to the interpretation of the data.

9.1. The September 2008 Data Set

In our early analysis of the MSI data, we found that the MSI extinctions were reasonably well related to the extinctions from the transmissometer and the Vaisala PSM. Fig. 9-1

shows a time series for extinction data acquired in September 2008. The SRI had not yet been built at that time, so SRI data were not included in this analysis.

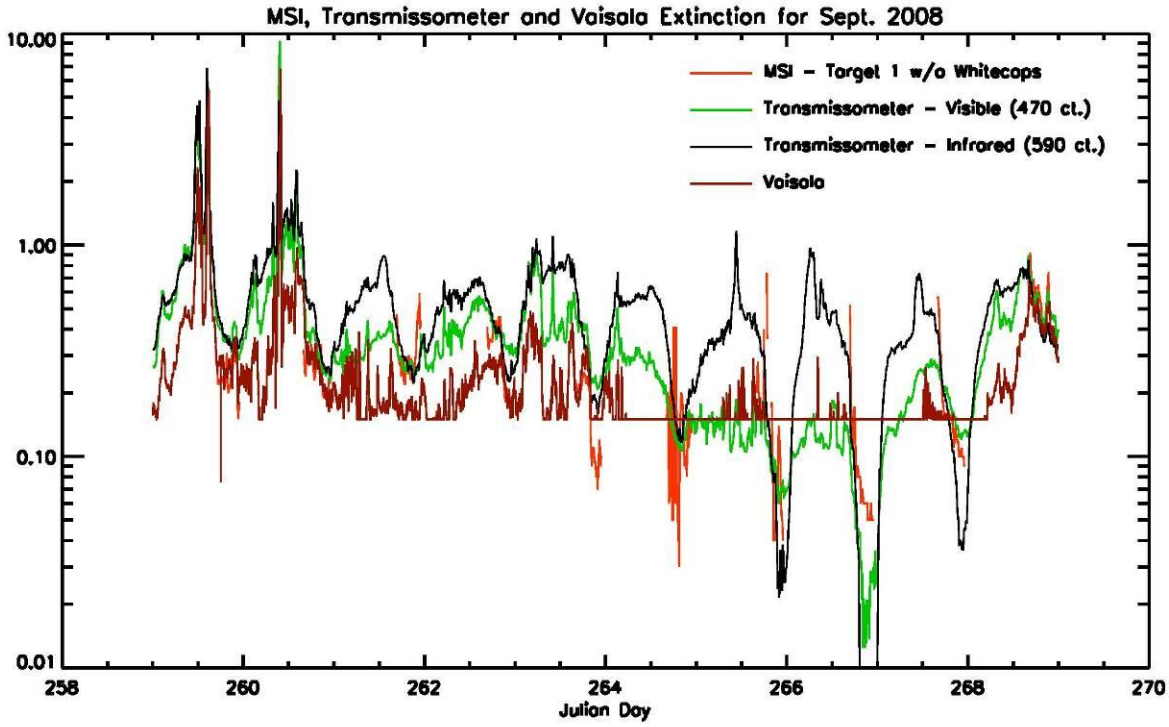

Fig. 9-1. MSI Extinctions derived from Initial Processing of September 2008 Data, days 258 – 270, looking South at 180 ^{o} (T). Color code is MSI extinction at .65 μm (red), Transmissometer extinction at .55 μm (green), Vaisala PSM scattering at .875 μm NIR (shown in deep red), and IR transmissometer extinction at 1.06 μm SWIR (shown in black)

These data had not yet been optimized for the optimal inherent contrast, but for an initial result we felt the relationship was very good. We evaluated the MSI extinctions in comparison with the imagery, making particular use of the islands in the scene at the 180º (T) position to estimate visibility and evaluate the presence of abnormal conditions. We felt that the relative changes in extinction were appropriate, based on the appearance of the images. Moreover, most of the magnitudes compare reasonably with the extinctions measured with the other instruments. There were a few cases of gloss, but gloss had little impact on this data set, as discussed in Memo AV09-037t.

We were concerned that the SWIR transmissometer extinctions seemed to be too high. Considerable analysis of the transmissometer data was done, as discussed in the memos listed above. We eventually found a problem with the transmissometer hardware which was repaired in January 2010 (Memo AV10-003t). Note also that the Vaisala PSM does not return data below values of .15 km^{-1} or "NIR visibility" of 20 km. There were some cases in which the MSI and the visible transmissometer did not relate well. Such was the case on Day 263, when the MSI data were lower than the transmissometer, and Day 266, when the MSI data were higher than the transmissometer. However, we found from the

appearance of the islands in the imagery that the MSI extinction was valid in both these cases, as shown in Memo AV09-037t.

We also found the data related well with relative humidity. Fig. 9-2 compares the MSI, transmissometer, and relative humidity data. The data analysis is discussed in more detail in the memos from 2009 listed above.

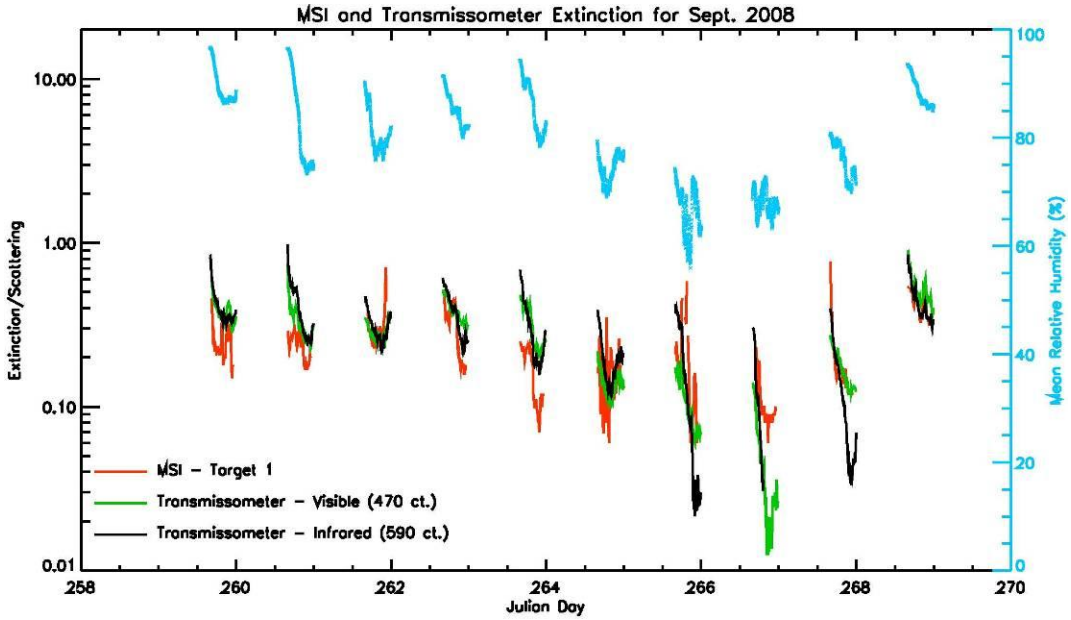

Fig. 9-2. September 2008 Extinctions looking South at 180 º (T), in comparison with measured Relative Humidity

Thus, from this September 2008 data set, our initial analysis indicated that the extinction algorithm appears to work well using the ocean surface. We found that use of a fixed inherent contrast value was surprisingly effective. We also found that in cases in which the MSI disagreed with standard instruments, the MSI data appeared to be the more accurate based on the appearance of the islands in the imagery. [Finding]

9.2. The February 2010 Data Set

Once the SRI was installed and had acquired a data set, we began detailed analysis of the Feb 2010 MSI and SRI data set, as documented in the 2010 memos listed above and in Memo AV13-018t. These data were also reprocessed in 2013 after we completed the extinction algorithm updates, as documented in Memo AV13-019t. Although much of the analysis is in the earlier memos, we will present the plots from the later analysis, when we had the correct calibrations and inherent contrast, and had developed the other extinction algorithm features discussed in Section 8. Comparisons between the MSI, SRI, and PSM extinctions (or scattering in the case of the PSM) are shown in Figs. 9-3 and 9-4.

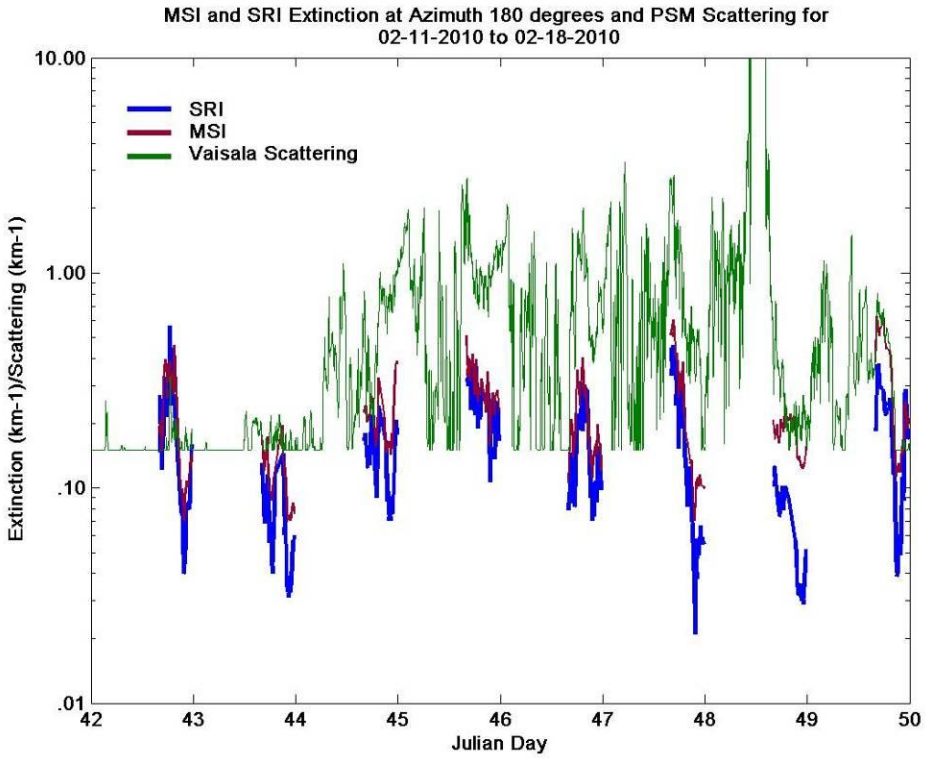

Fig. 9-3. Feb 11 – 18 2010, MSI and SRI Extinctions looking South at 180 º (T), 11 to 18 Feb 2010, with Vaisala PSM scattering

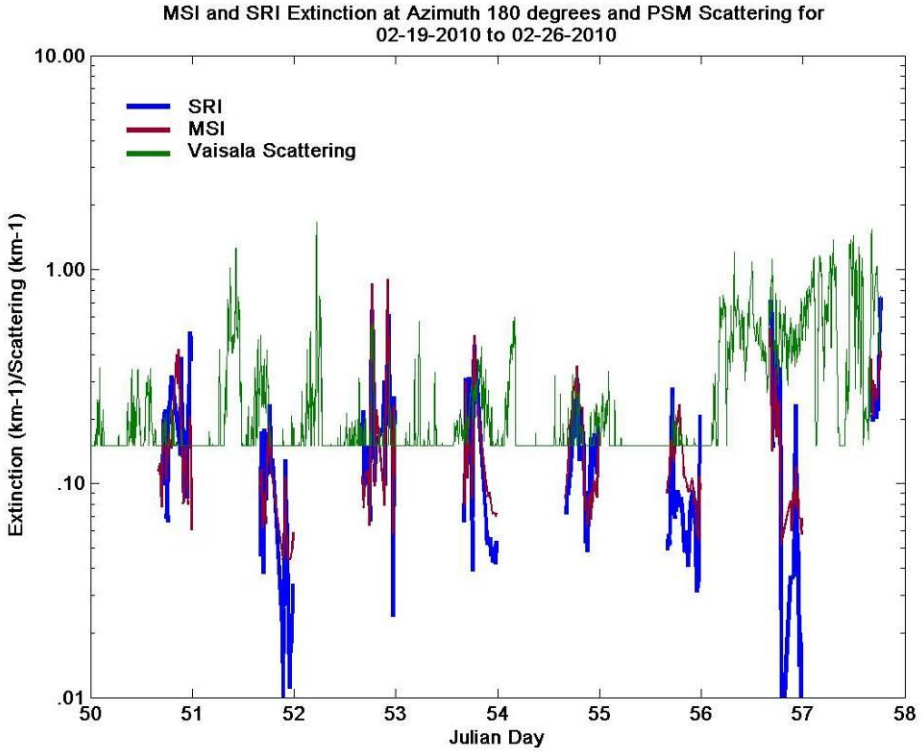

Fig. 9-4. Feb 19 – 26 2010, MSI and SRI Extinctions looking South at 180 º (T), 19 to 26 Feb 2010, with Vaisala PSM scattering

We first note in these plots that the SRI and MSI compare very well. In clear conditions, the SRI extinctions tend to be slightly lower than the MSI extinctions, as they should be. [Finding] We also note that in about 11 of the 16 days, the SRI and MSI compare well with the PSM. In the other days they do not. Figs. 9-5 and 9-6 show the same data, with the transmissometer results added to the plots. The amazing thing about these plots is that the comparison between the extinction imagers (MSI and SRI) and the PSM is better than the comparison between the PSM and the transmissometers, even though the PSM and transmissometers are considered the "gold standard" and are both on the shore. The MSI and SRI show the extended path results. We noted that the PSM and transmissometers compare well on about 7 of the 16 days.

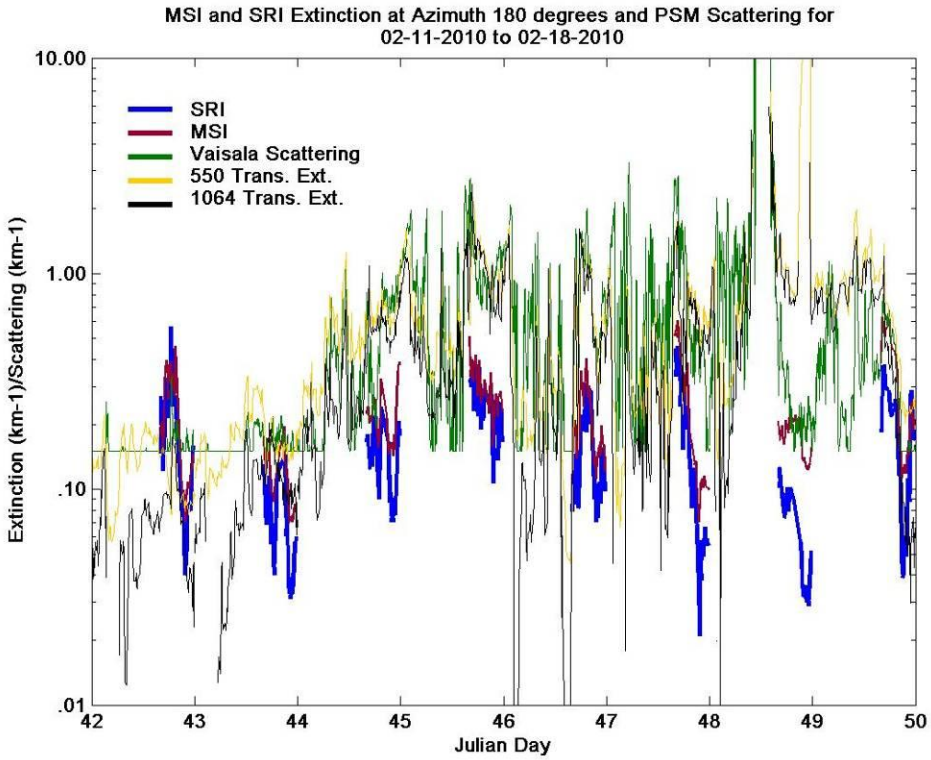

Fig. 9-5. Feb 11 – 18 2010, MSI and SRI Extinctions looking South at 180 º (T), 11 to 18 Feb 2010, with Vaisala PSM scattering and transmissometer extinctions

We evaluated all of the raw MSI images, to categorize them as clear, haze, or quite hazy, as illustrated in Fig. 9-7. As discussed in Memo AV10-031t, we found the relationship between the visual assessment and the extinction algorithm results to be quite good. [Finding]

We evaluated the February 2010 data in detail, including comparisons of MSI and SRI data, evaluation as a function of azimuth, and so on. The extinctions at the different azimuths were generally quite similar. One particularly interesting case occurred on 21 February, when we noted large changes in extinction coefficient before noon, and the data looking north-west and south differed somewhat. In Fig. 9-8, we show these images, along with the extinctions converted to "Red visibility" V'= (3/α) (see Section 3.2).

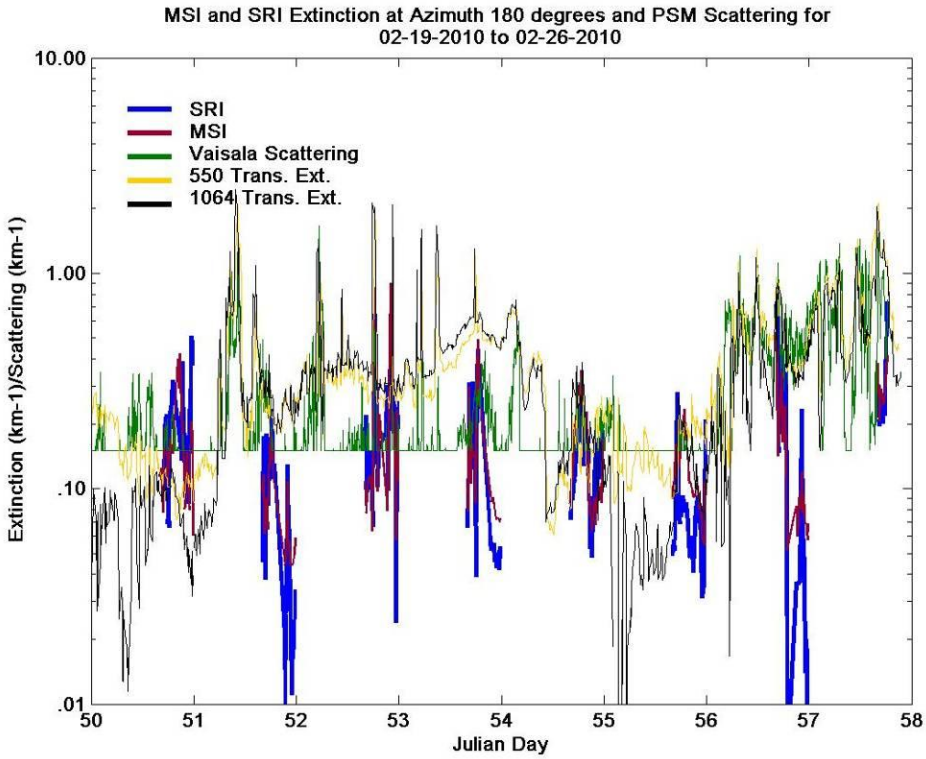

Fig. 9-6. Feb 19 – 26, MSI and SRI Extinctions looking South at 180 º (T), 11 to 18 Feb 2010, with Vaisala PSM scattering and transmissometer extinctions

Fig. 9-7. Visual Classification Examples: Category 1, clear, 12 Feb 2010 2200Z; Category 2, haze, 12 Feb 2010 1900Z; and Category 3, quite hazy, 12 Feb 2010 1600Z. All images are looking South at 180 º (T).

One can see from the imagery in Figs. 9-7 and -8 that the changes in derived extinction in Figs. 9-5 and -6 correspond to changes in the atmosphere. Note that the change occurs first in the NW and then 20 minutes later in the S. (During the two hour interval shown in Fig. 9-8, gloss occurred briefly, although not in the images shown, and it did not have a significant impact due to the fog.) The visibility from the shore also supports these changes. On this particular day there was an offset between the visibilities looking south and north-west, but this was not the case in general.

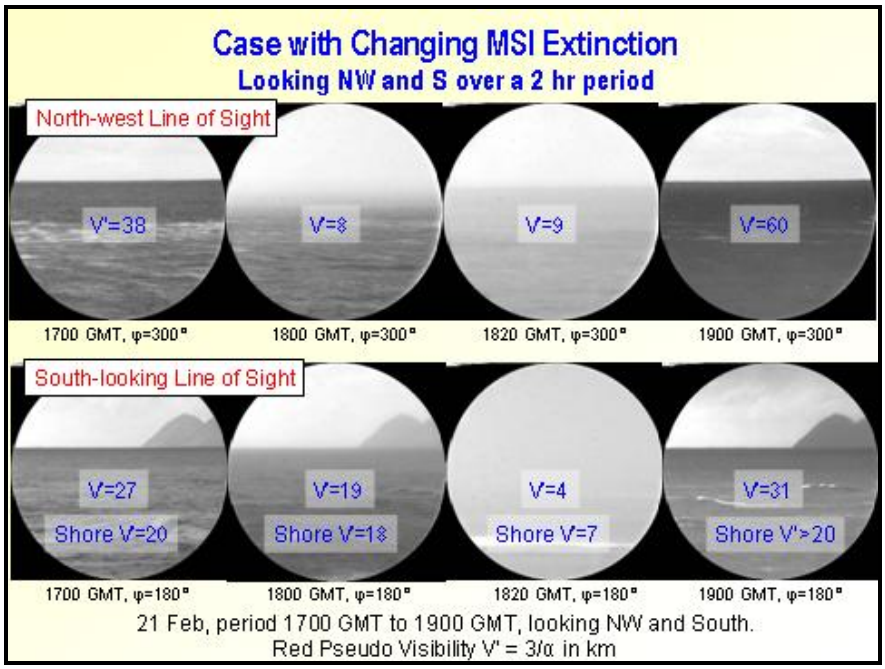

Fig. 9-8. Feb 21 2010, showing particularly dynamic conditions, looking WNW at 300 º (T) and South at 180 º (T)

As noted earlier in this section, there were several days in which the MSI and SRI did not yield extinctions consistent with the PSM. We looked into this in more detail, and selected two cases at random for further evaluation. These cases are shown in Figs. 9-9 and 9-10. In each of these examples, the PSM indicated that it was quite foggy, with visibility less than 3 km, yet both the MSI and SRI indicated that it was hazy.

In Figs. 9-9 and 9-10, we see definite signs of haze, and yet the islands can also be detected. Our interpretation of these images is that there was probably a fog at the coast, where the PSM was acquiring data, but over the extended path it was much less hazy; otherwise the island would not be detectable in the image. This is a good example of the situation in which it really helps to have an instrument like the MSI or SRI to measure the net impact of the aerosols over an extended path. The total extinction is much less over the extended path than one would guess from the measured extinction at the PSM shore location. That is, cases like these support the contention that there are times when the extended path needs to be measured with an instrument like an EI system, because instruments that measure at one end of the path cannot always accurately represent the full path. [Finding]

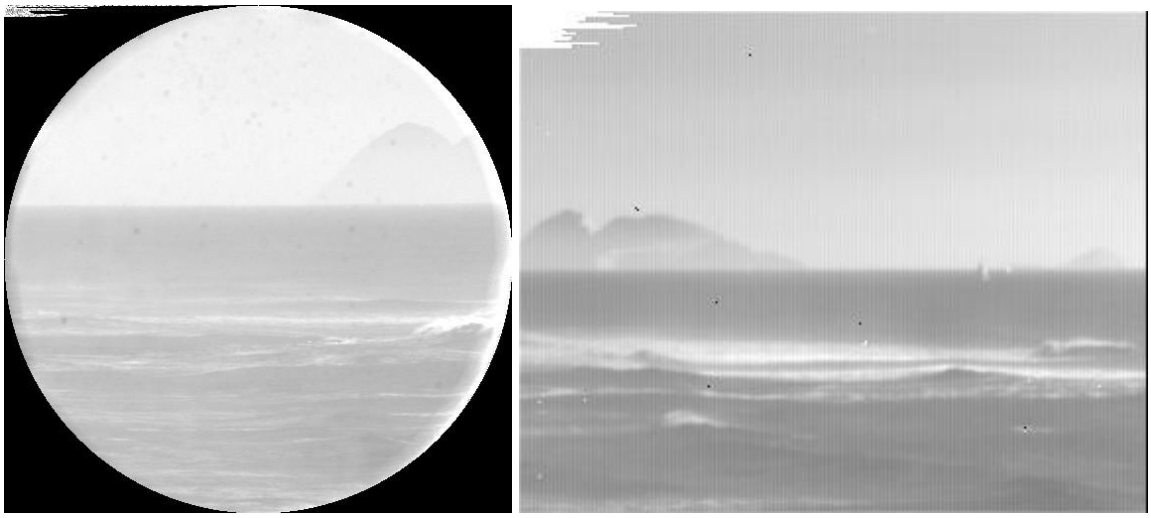

Fig. 9-9. MSI and SRI images, looking South at 180 º (T), 14 Feb 2010 2300Z (1500 PST); Ext(MSI)=.272 km^{-1}, Ext(SRI)=.168 km^{-1}; Ext(PSM)=1.12 km^{-1}; Red V=11 km, SWIR V = 18 km, PSM V = 2.7 km

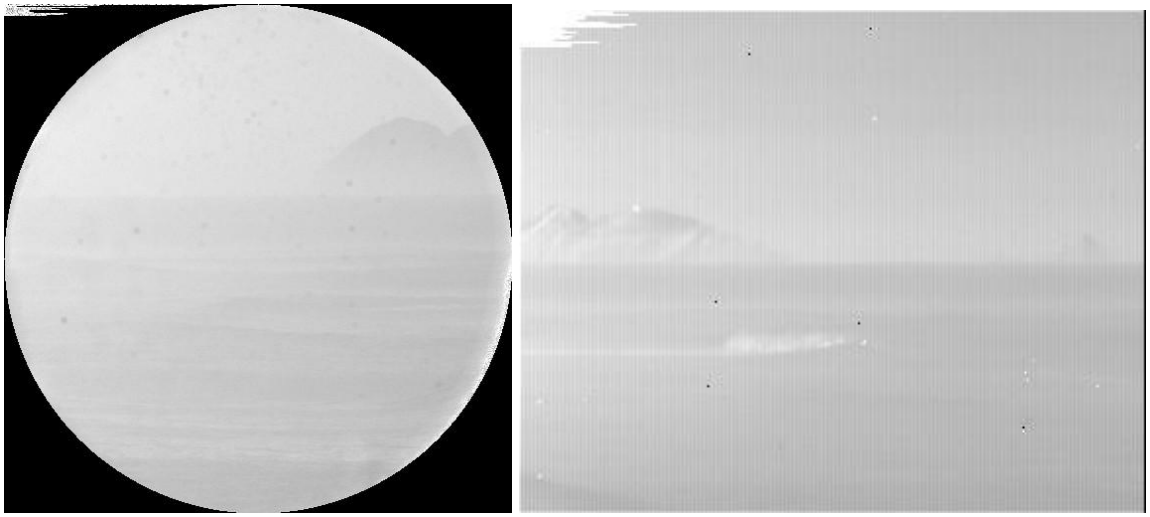

Fig. 9-10. MSI and SRI images, looking South at 180 º (T), 16 Feb 2010 1600Z (0800 PST); Ext(MSI)=.517 km^{-1}, Ext(SRI)=.447 km^{-1}; Ext(PSM)=2.81 km^{-1}; Red V=5.8 km, SWIR V = 6.78 km, PSM V = 1.1 km

Since the data during this period were also somewhat impacted by gloss, it is of interest to show the analysis of gloss vs. wind speed for this period. This is shown in Fig. 9-11. In this figure, the wind at the buoy and shore are shown in red and green respectively, and the extinctions in the direction of the buoy are shown in yellow and blue (for distant and nearby target ROI's). Cases during the 8-hour daytime analysis period that were visually determined to have gloss are marked with a red bar. The gloss cases are associated with higher extinctions, as well as low wind speeds. [Finding] Unfortunately, as noted in Section 8.5.2, the relationship between gloss conditions and wind speed does not appear tight enough to use the wind speed to predict gloss. The gloss is further discussed in Section 9.3.

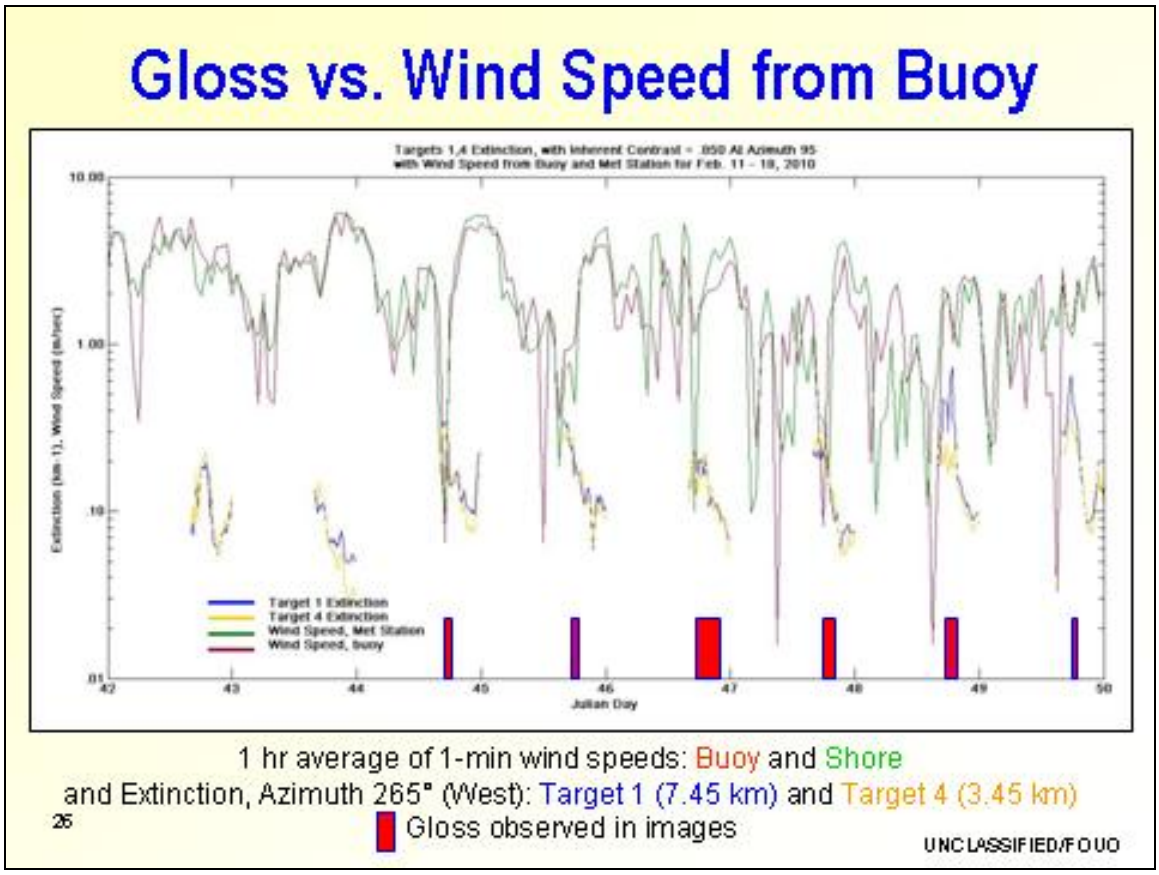

Fig. 9-11. Chart showing relationship of Wind Speed to presence of Gloss for Feb 11 – 18, 2010. MSI look angle was nearly West at 265 º (T)

9.3. The 2012 and 2013 Data Sets

SRI data from July and August 2012 were processed and presented in Memo AV13-009t. There were no useful daytime MSI data during this period, because the MSI was being used for night tests with a fisheye lens, and MSI exposures were set for night. Most of these data were used to optimize the SRI extinction algorithm, and this analysis is discussed in Memos AV13-011t, -012t, -013t, and -015t and summarized in Section 8. The analysis of the SRI data supported our earlier conclusions, that in the absence of gloss, the results were quite good, i.e. MSI and SRI are well related to each other and to the haze amount estimated from the appearance of the islands in the imagery. The extinction algorithm handled up-sun glitter, boats, white caps, horizon clouds, and other abnormalities quite well. (Also, Memo 13-009t includes a summary of developments up to that time.

One interesting case is shown in Figs. 9-12 and 9-13, and extracted from Memos AV13-009t and 13-011t. Fig. 9-12 shows part of the period plotted for several azimuthal angles. Fig. 9-13 shows images looking south toward the islands. Note the data for August 11 in Fig. 9-11 (the 6th day in the plot). The extinction indicates fog in the morning, and decreases during the day to a value indicating that it was still fairly hazy. We were interested in whether this exceptional case was valid.

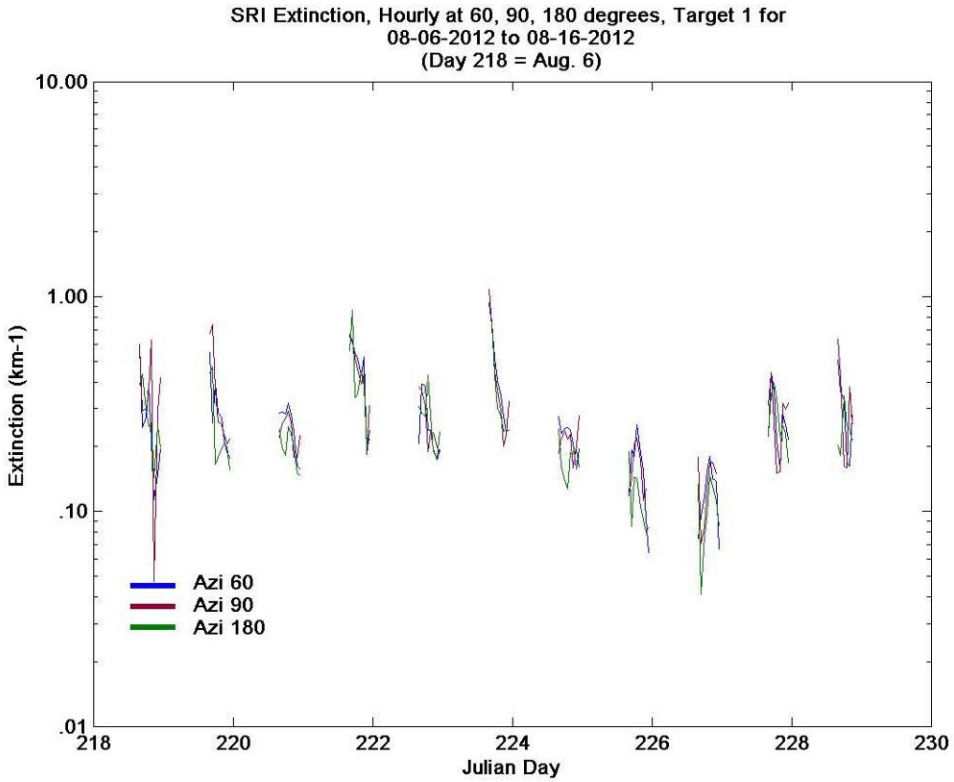

Fig. 9-12. Extinctions during Aug 6 – 16 2012, for look angles WNW at 300 º (T) (blue), W at 270 º (T) (red), and S at 180° (T) for one target, gloss cases included (Azimuth listing in the key refers to the rotary table readout value)

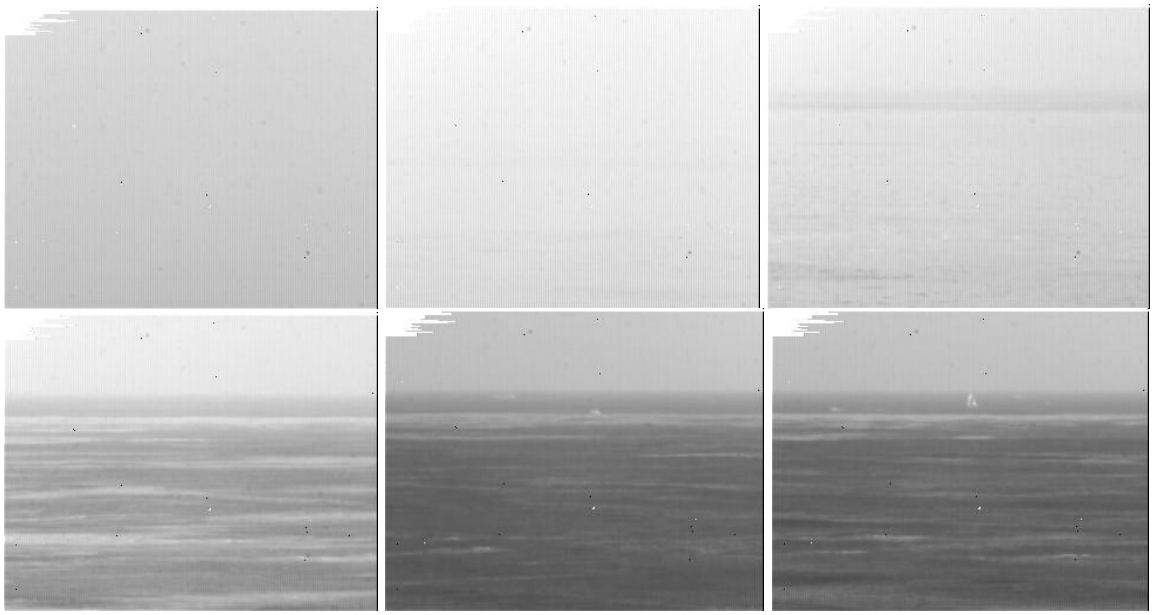

Fig. 9-13. Time series from 11 Aug 2012, in the 180° (T) direction, showing 1600Z, 1700Z, 1800Z, 1900Z, 2100Z, and 2300Z. 11 Aug is Julian Day 223 (just to the left of day 224) in Fig. 9-12. In all cases the islands are not visible, but the ocean-to-sky contrast is becoming stronger as the extinction decreases throughout the day.

In Fig. 9-13, the island is not visible throughout the period, showing that the extinction was indeed fairly high. Yet the increasing clarity of the horizon illustrates the decreasing extinction. In other words, even in this case of high extinction, the relative changes appear to be valid. It should be noted that at time 1800Z, there may be gloss on the ocean surface, but this appears to have had minimal impact on the derived extinction, because the ocean ROI was already bright due to the fog.

We also processed simultaneous MSI and SRI data from the periods March 9 – 15 2013, and May 8 – 14 2013, as documented in Memo AV13-017t. We found that the results were consistent with our earlier analysis of other data sets. [Finding] One of the interesting things to come out of this analysis was a comparison of the amount of gloss in the red MSI images and the SWIR images from the SRI. Gloss appears to be quite a bit worse in the SWIR wavelengths. Generally, if gloss is detected in the red image it also occurs in the SWIR image, but the impact is much worse in the SWIR, as illustrated in Fig. 9-14.

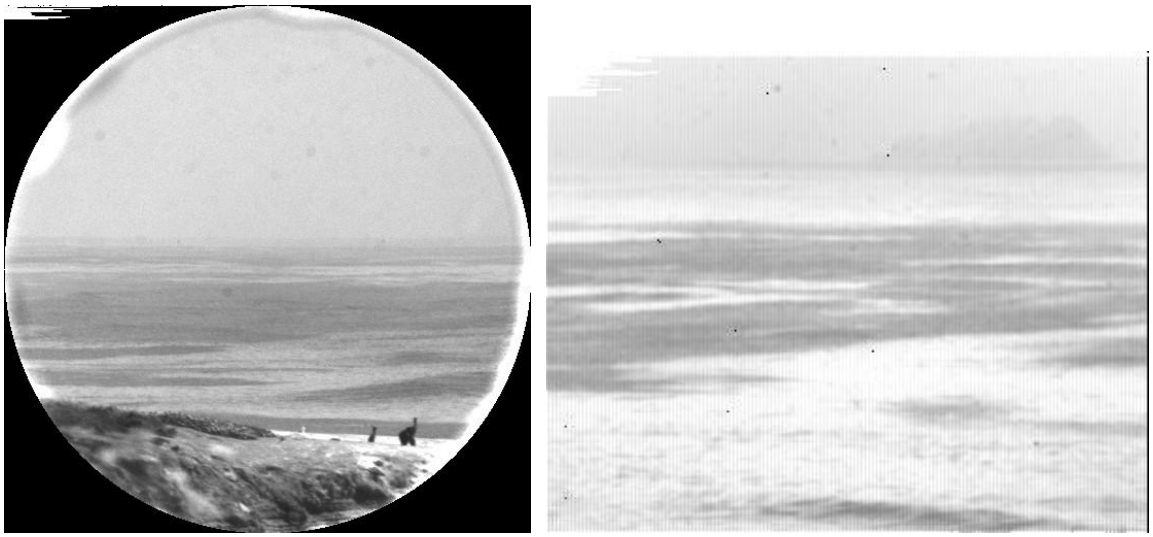

Fig. 9-14. MSI and SRI images, looking South at 180° (T), 17 Mar 2013 2200Z (1400 PST)

In Fig. 9-14, the red image is on the left. The field of view of the two lenses is different, but it is obvious that impact of the gloss is much stronger in the SWIR. [Finding] This has several implications. First, because the gloss appears to be spectrally dependent, this implies that a two-wavelength system may be useful in detecting the presence of gloss. An automated image evaluation of two images at different wavelengths should enable detection of those areas impacted by gloss (if any). Using image analysis to detect the gloss also opens the possibility for actively and automatically, in real time, selecting regions of the image that are not affected by gloss for extinction algorithm processing, and/or using the more optimal filter selection where the gloss is wide-spread. [Recommendation]

Another approach to gloss that was discussed earlier is the addition of crossed polarizers to the optical system. We found experimentally that in looking through a linear polarizer, and then turning it 90 degrees, the areas that are not gloss show a significant change,

while those with gloss do not show a significant change. Thus acquiring two images with two different polarizer orientations could enable the extinction algorithm to automatically detect gloss, and select ROI's that are not affected by gloss. If a system is developed which uses polarization to detect the presence of gloss, it may actually work best in the SWIR, where the gloss may be easiest to detect. [Recommendation]

We feel that it would also potentially be useful to further evaluate wind speed. As shown in Figs. 8-14 and 9-11, the presence of gloss is clearly related to wind speed. We were not able to determine a good wind threshold that could be used to predict gloss, but this may be because we were not using the optimal measurement integration time, or there may have been another problem with our approach. [Recommendation]

If none of the above methods can be developed to solve the gloss issue for future systems, then the remaining question is whether gloss occurs frequently in the desired test scenario. As mentioned earlier, we have been told that for some at-sea laser tests, gloss is not an issue because the tests are not allowed under gloss conditions. This is because in low/no wind–high gloss conditions, there exists a strong possibility of laser beam reflection off the mirror-like ocean surface. However, if gloss is expected to be an issue, and no changes are made to the hardware design to handle gloss, it may be best to use a visible system and extrapolate to the SWIR, so that gloss has a smaller impact. We feel that the gloss issue merits further exploration. [Recommendation]

9.4. Sensitivity Study for Uncertainty Analysis

The above analysis gives us confidence that under most conditions, the extinction imager approach provides valid results in the absence of gloss. In this section, we evaluate the anticipated precision of the Extinction Imager method. This can be done by evaluating the expected uncertainty in extinction given the uncertainty in the input and measured parameters.

Initially we anticipated that the inherent contrast estimated input value might be the largest source of uncertainty, because we do not measure it directly in the field. However, the impact of the uncertainty in inherent contrast on the extinction is very small, except in very clear (low haze) conditions. The impact of the uncertainty in inherent contrast for the MSI is shown in Section 8, Fig. 8-7.

The impact of uncertainty in the inherent contrast for the SRI is shown in Figs. 9-15 and 9-16, extracted from Memo AV13-011t. These data have been sorted to remove the cases manually detected to include gloss. Note that the impact of changes in inherent contrast on extinction is quite small, except for the very clear cases of low extinction. For the MSI, we determined that for a C_0 value of .85 ± .05, the resulting uncertainty in extinction is less than 4% for visibilities of 18 km or less, and greater than 15% for visibilities of 30 km or more. [Finding] We feel that this uncertainty is not an issue, particularly in comparison with the PSM, which truncates the extinctions for visibilities of 20 km or more. The uncertainties in the SRI extinctions are similar.

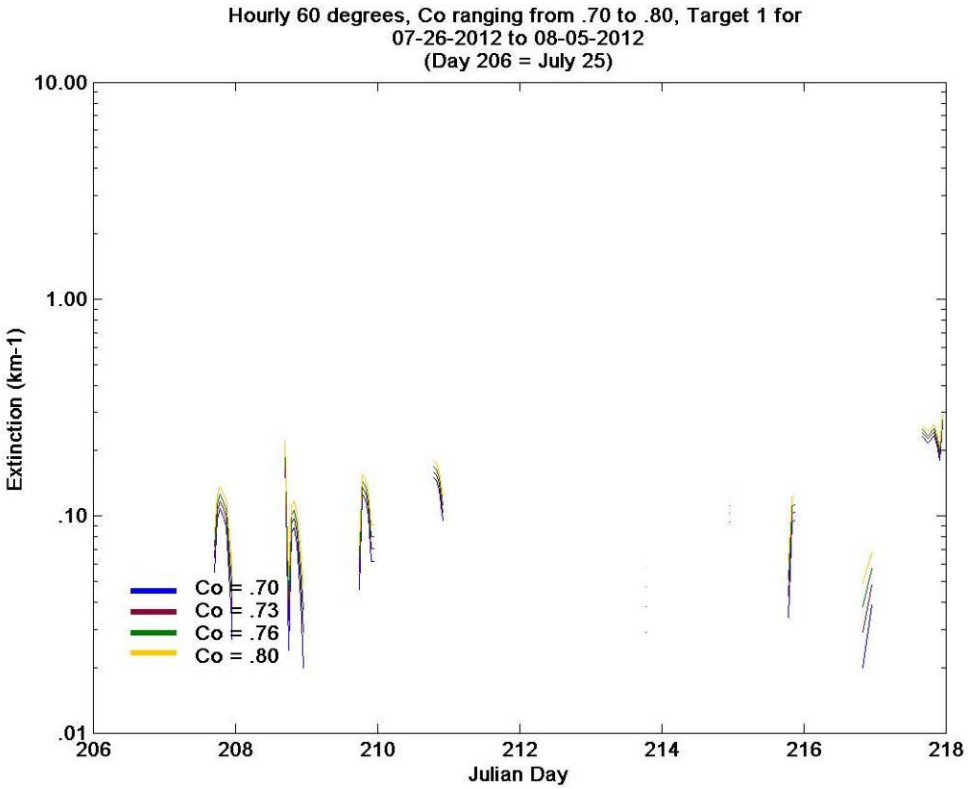

Fig. 9-15. Impact of Inherent Contrast on SRI Extinction for Jul 26 – Aug 05 2012 looking WNW at 300° (T), for one target, little or no gloss cases

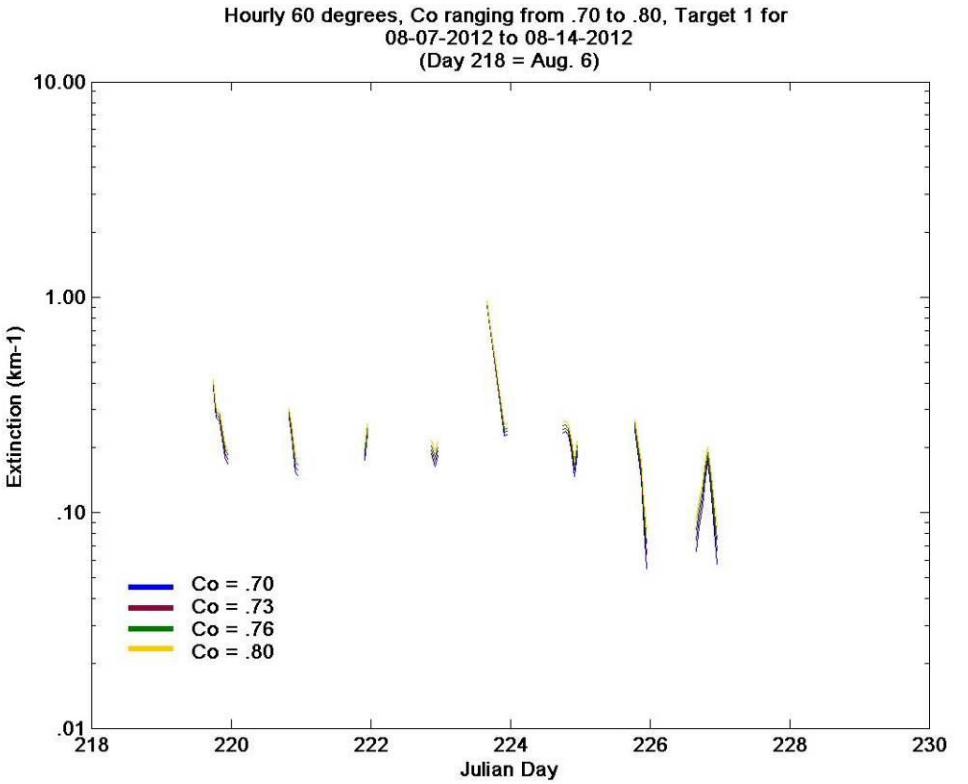

Fig. 9-16. Impact of Inherent Contrast on SRI Extinction for Aug 7 - 14 2012 looking WNW at 300° (T), for one target, little or no gloss cases

Uncertainty in the range to the ocean ROI was another source of uncertainty. The range can be determined using measurements of the angular resolution of the pixels, and thus determining the angle below the horizon for the ROI. However, it is difficult to measure the resolution accurately, particularly with the SRI. Our equations do not take into account earth curvature. However, the impact of these uncertainties on extinction is very small, for targets at our normal ranges. The impact of uncertainty in the range is shown for the MSI in Fig. 9-17. This study was done during the initial evaluation of the Feb 2010 data. In Fig. 9-17, there is a significant difference between the MSI extinctions and the PSM extinctions, but the three curves showing the uncertainty in MSI extinction as a result of range uncertainty are almost indistinguishable.

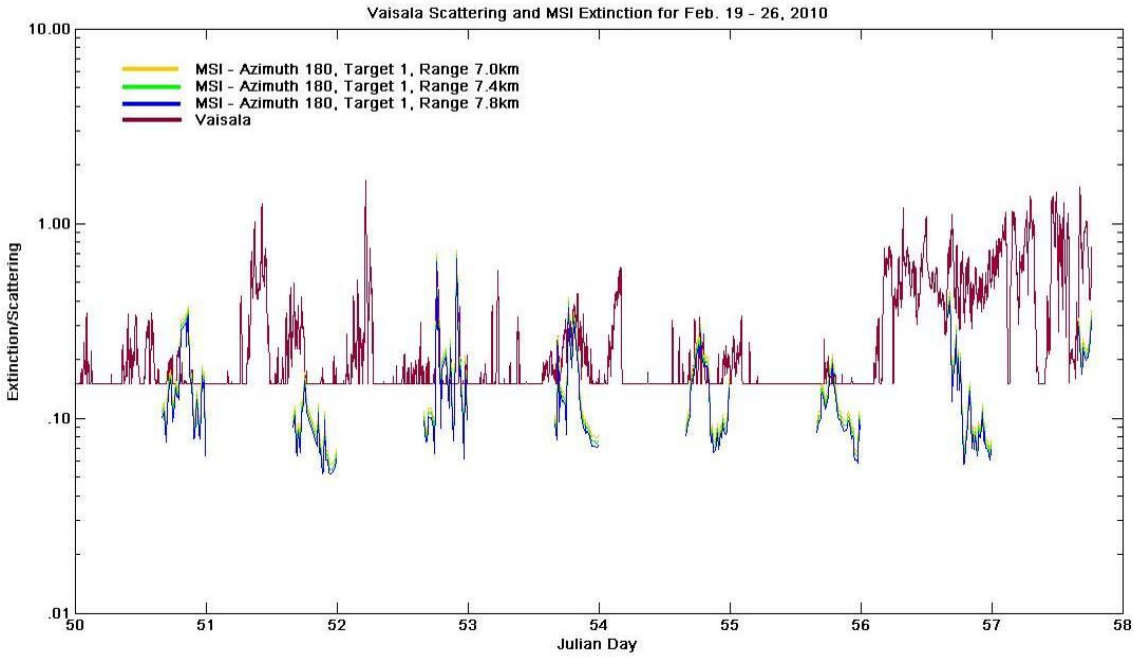

Fig. 9-17. Impact of uncertainty in range, from initial processing of Feb 2010 Data looking South at 180° (T)

For the MSI, we estimated the range uncertainty to be 7.4 ± 0.4 km. The median resulting offset extinction ratio was 5.3%. Similarly, for the SRI, the estimated range uncertainty was 6.4 ± 0.4 km, and the median resulting offset ratio was 6.3%, as discussed in Memo AV13-018t. By comparison, the median offset ratio between the two gold-standards, i.e. the transmissometer and the PSM, was 62% for this data set. [Finding] (This was after the transmissometer repair mentioned earlier.) In other words, the extinction imager technique is not perfect, but the other existing techniques appear to have much more uncertainty in comparison with each other.

We would expect that for ground-based tests using fixed targets, it should be possible to measure the range more accurately. Similarly, we would expect operational shipboard systems would have more accurate methods for determining range, or at least for calibrating the range on the EI system.

Although one might expect the impact of clouds on the horizon to cause significant error, as discussed in Memo AV13-015t, we were unable to find any cloud cases that resulted in significant error. This is partly because the extinction algorithm checks for this problem, and partly because the horizon radiance appears in both the numerator and denominator of the equation for apparent contrast. This is discussed in more detail in Section 8.5.3.

Uncertainty in camera calibration can also contribute to error. The uniformity and dark calibrations have a significant impact, but these are reasonably easy to measure and apply. The linearity calibration is somewhat more difficult to measure, and becomes significant in the SRI (but not the MSI, due to the camera selection). The impact of the SRI linearity is discussed in Memo AV11-008t. For the SRI, if no calibration is applied, the anticipated average error is about 18%. If the linearity for a different camera of the same model is applied, the anticipated average error is about 12%. If the correct linearity calibration is applied, there should be no or insignificant error. In addition to the uniformity and dark calibrations, we recommend applying linearity corrections, unless the above anticipated error is acceptable. [Finding/Recommendation] The MSI camera system is much more linear than the SRI. As discussed in Memo AV11-009t, the anticipated error for the MSI is about 1%, if either no linearity or the linearity for a different camera is applied.

Finally, there are uncertainties due to measurement error. We analyzed these early in the project, as documented in Memo AV07-046t, "Scattering Test Site Calculations". At that time, we had anticipated that we would use a ROI at a long range, but we ended up using targets at about 5 km range (ref Memo AV14-001t). The uncertainty in extinction for a target at range 4.75 km is shown in Fig. 9-18, extracted from Memo AV07-046t. The results for longer and shorter target ranges are shown in Figs. 9-19 and 9-20. The derived parameter was the uncertainty in visibility, which is $3/\alpha$.

We find that for the target range shown in Fig. 9-18, the resulting uncertainty due to measurement uncertainty is less than 2% for most visibilities, and increases significantly for very foggy conditions with visibilities less than about 3 km. [Finding] Our understanding is that conditions with visibilities less than 3 km are not of interest to our sponsors. As shown in Figs. 9-19 and 9-20, very close ocean ROI's are not good for very clear conditions, and distant ocean ROI's are not good for foggy conditions. For example, if the EI system were to use an ocean target at about 13 km range, the extinctions are only valid for visibilities higher (clearer) than about 10 km (assuming ±5 count measurement uncertainty). The target range of about 4 – 5 km should provide excellent accuracy over all anticipated conditions of interest.

These calculations were based on an uncertainty in both target and horizon count of ±5 counts, for a signal of about 1000 counts. This is unrealistic for a given pixel, but reasonable for the ROI average. We recommend that future developers measure the uncertainty in their ROI averages, which will be system-dependent. Using this uncertainty, as well as the estimated uncertainty in their range determinations, it should be possible to run calculations similar to those shown in Figs. 9-18 through 9-20, and

determine anticipated errors as well as minimum target ranges that can be used for the desired range of conditions. [Recommendation]

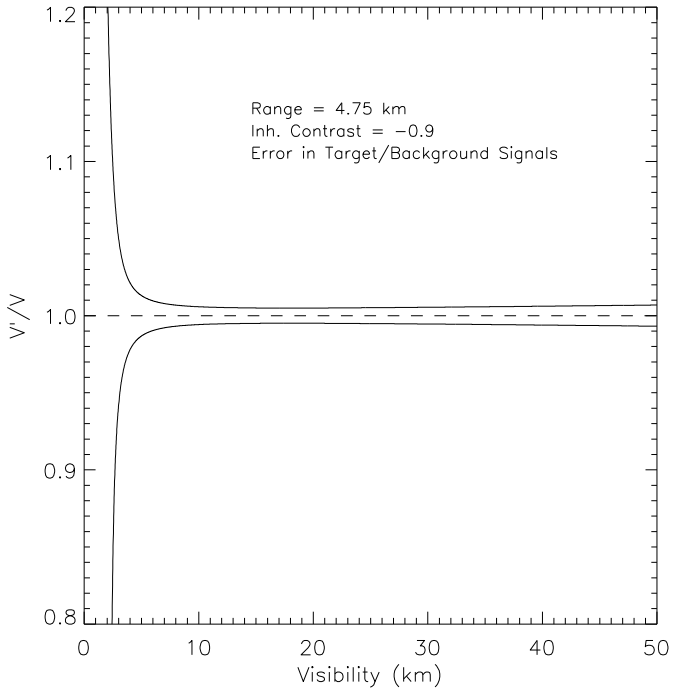

Fig. 9-18. Fractional uncertainty in visibility determinations, assuming a ± 5 count uncertainty in both target and background signals, an inherent contrast of -0.9, and a range of 4.75 km.

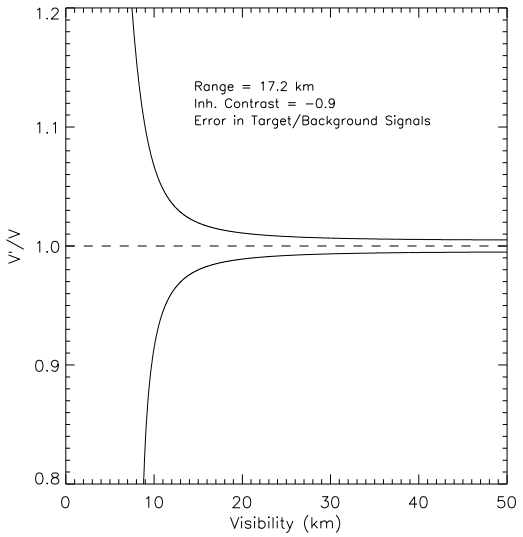

Fig. 9-19. Calculations similar to Fig. 9-18, for a range of 17.2 km (the range to the horizon from a height of 20 m)

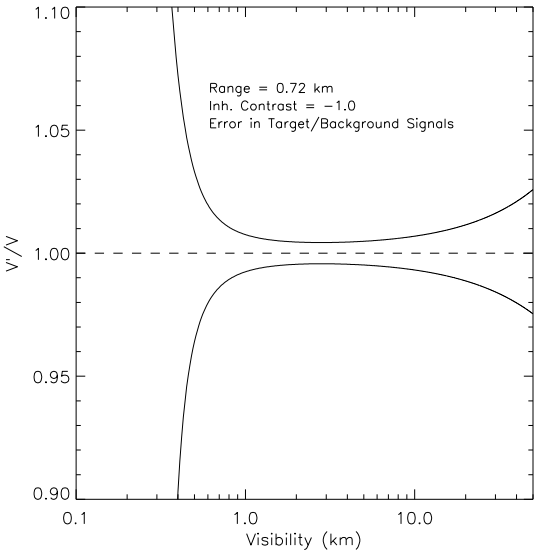

Fig. 9-20. Calculations similar to Fig. 9-18, for a range of 0.72 km (the transmissometers' path length

Additional uncertainty analysis based on the HSI system our group built in the 1990s is discussed in Shields [21].

9.5 Summary of Daytime MSI and SRI Data Analysis

Based on the error analysis in Section 9.4, we would expect the extinction imager errors to be reasonably small most of the time. The detailed analysis of field data discussed in Sections 9.1 – 9.3 demonstrates that the results are very good most of the time. In comparison with the PSM and the transmissometer results, the extinction imagers appear to be much more consistent and accurate. In addition, they bestow the important capability of providing the extinction over an extended path using a single-ended system. There are additional advantages of the extinction imagers in comparison with instruments similar to a PSM or transmissometers. The extinction imager technique should work well at any wavelength in the red, NIR, or SWIR (i.e. wavelengths for which the ocean has little upwelling irradiance little or no thermal emission). Also, the instrument can be placed on a rotary table, so that it continually documents the full surround of the ship.

The technique can be used with fixed black targets at fixed range; with reasonably black targets at variable but known range; or with passive ocean targets such as have been tested in this project. However, reasonable care prior to fielding must be taken for the method to work. For example, it is important that the data be within the instrument's valid data range (i.e. offscale bright data, above the valid range of the instrument, will not yield valid extinctions). It is similarly important to measure accurate uniformity images, and it is helpful to measure the linearity for at least a few of the cameras in the camera model. Also, gloss conditions are still an issue that may need to be resolved if the instrument will be used in scenarios with frequent gloss. With these caveats, we feel the system is much superior to either point scatter meters or transmissometers for applications in which one needs the transmittance over an extended path, but can only control one end of the path.

10. NIGHTTIME TESTS AND RESULTS

As part of our work for the optional Phase II on the JTO/ONR grant, we were asked to evaluate whether it would be feasible to acquire night data with these systems, and if so, whether the MSI method would work at night. We found that although it is possible to acquire high quality imagery at night with the MSI, the ocean does not appear to be a good target under no-moon (starlight) conditions for the extinction imager concept. However, the use of other dark targets such as drones or ships should be a good alternate approach, and there are additional approaches that can be considered. This section summarizes the work done on this task, as well as suggested future directions. Our initial plans relating to this work, as well as other work for Phase II are briefly outlined in Memo AV10-019t.

10.1. Hardware and Software Changes for Night Tests

We tested both the MSI and SRI for possible night capability. Previous tests with the cameras used in these two systems (Memo AV07-026t) led us to anticipate that the SRI was unlikely to work well at night. However, we felt it was important to test the capability for this application.

Although the MSI does not acquire data in the SWIR, which is the waveband of ultimate interest, MSI night tests are still relevant for two reasons. First, as discussed in Section 5 and in Memo AV09-038t, we analyzed the impact of measuring the extinction in the visible or NIR, and using models to extend the results to the SWIR. We feel that taking measurements in the red or NIR and using models to estimate the results in the SWIR at 1.06 or 1.6 μm should be reasonably accurate under most conditions. Second, for some applications, SWIR wavelengths between 1.0 and 1.1 μm may be of interest. The MSI cannot measure at those wavelengths due to the filter changer design, however some CCD cameras similar to that used in the MSI can measure directly at that wavelength.

The MSI camera is a 16 bit camera with very low system noise (less than one count readout noise out of 65,535 counts). (Section 10.2 includes noise figures including shot and other noise sources.) In combination with a fisheye lens, the MSI is capable of detecting very dark fields. To give the reader a sense for the capability of the camera system, we show in Figs. 10-1 and 10-2 sky images acquired under no moon, using the MSI camera system installed in a WSI [24]. Fig. 10-1 shows a typical dark environment and Fig. 10-2 shows a very dark environment. With this system, typical signal to noise ratios (including all shot noise) for the darkest part of the sky are 40:1 or better.

We ran a series of several different night tests with both the MSI and the SRI. We initially tested with the optimal daytime lenses, changing exposure times and filter selections. Later we tested the cameras with fisheye lenses, as these had better throughput and received more flux per pixel. We made some additional changes to the hardware. For example, the focus was not optimized for the fisheye lens, so we re-optimized the focus, and improved the Point Spread Function width from 2.2 pixels to less than 0.5 pixels (Gaussian half-power point). We also had to make several updates to

the software to enable the night data acquisition. These hardware and software upgrades, as well as the initial data analysis, are documented in the following memos: AV10-032t, AV11-006t, AV11-010t, AV11-011t, AV11-012t, AV11-013t, AV11-014t, AV11-015t, AV12-001t, AV12-002t, and AV12-011t.

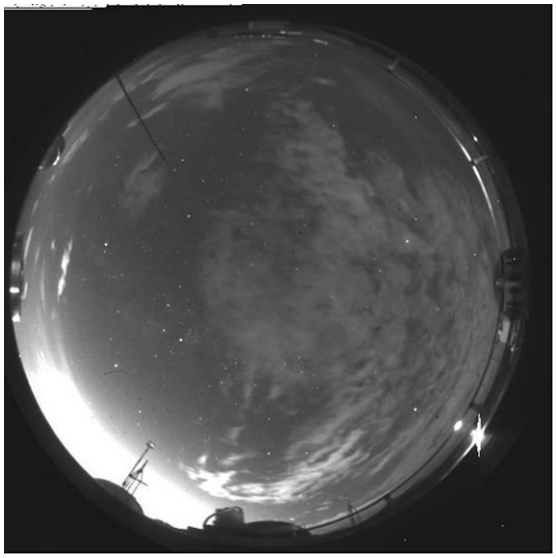

Fig. 10-1. Starlight Image from the MSI Camera at a typical sky imager site, 14 Aug 05 0902Z

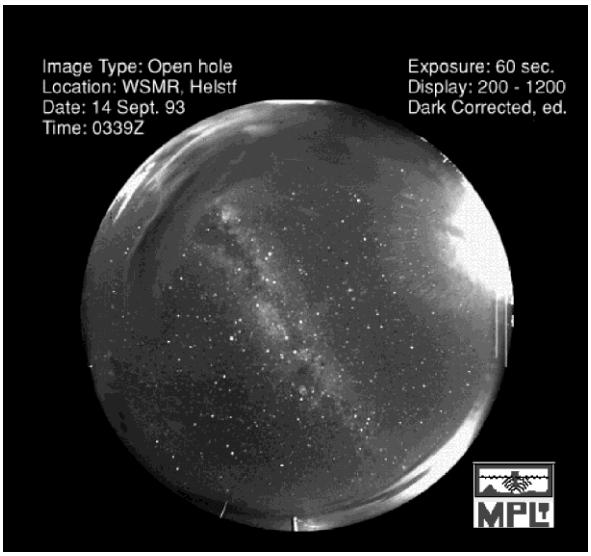

Fig. 10-2. Starlight Image at a very dark site, 14 Sep 93 0339Z. Blooming on upper right is from a city approximately 60 miles distant.

10.2. Resulting Night Imagery

We found that we were able to acquire excellent MSI imagery at night, but were not able to acquire useful SRI imagery. Memo AV12-009t "discusses the SRI data. We found that the SRI is capable of acquiring good data up to dawn and dusk, with a maximum Solar Zenith Angle of about 94° (4° below the horizon). [Finding]

For the best MSI data at night, we used a fisheye lens at f/2.8, with 10 min exposures, and an open hole (no spectral filtering) configuration, as discussed in Memo AV12-003t, "Evaluation of New MSI Night Imagery". This setup resulted in excellent images, as discussed in AV12-006t. Evaluating sample images, as well as our radiometric calibrations, we identified the following noise parameters:

Readout Noise = 3.5 e^{-1} or 1 count (full scale = 54,535 counts)
Dark Noise = 53.6 e^{-1} or 15 counts (at 10 min integration)
Shot Noise = 126 e^{-1} or 35 counts
Total Noise = 137 e^{-1} or 38 counts
Dark-corrected Signal = 15,966 e^{-1} or 4435 counts
Net S/N ≈ 116:1 for ocean surface under starlight

The raw data have a slightly higher variance, because it includes the spatial variance due to non-uniformities and spatial variance due to variations in the ocean surface radiance, as well as the temporal noise discussed above. As a result, the actual S/N within a typical

ocean ROI is about 70:1. However most of this spatial variance is either part of the scene or else removed by the flat field correction, so we feel the actual noise is close to that given in the previous paragraph. Thus the night images are excellent quality in terms of flux level and signal to noise.

Fig. 10-3 shows an image of the sky and sea acquired under nearly full moon, looking West at 270° (T). Fig. 10-4 shows and image acquired under starlight. And Fig. 10-5 shows a daytime image for comparison. In these images, the angular width from left to right is 180°, and the camera is looking west. The top and bottom of the images are blocked by the housing, and have been clipped in this display. On the horizon, the white dot to the left of center in Fig. 10-3 and 10-4 is the light from the buoy deployed for this project by NPS. (We considered extracting the beam transmittance using this light source, however the buoy does some rocking in the waves and the light is not sufficiently uniform over the angles of motion for this technique to be reliable.)

Fig. 10-3. Night Image near Full Moon: 4 Feb 2012 0600Z, Moon phase = .837, Open Hole 3 min exposure with no neutral density filter. Scene is a factor of 800,000 darker than daytime image in Fig. 10-5.

Fig. 10-4. Night Image under Starlight: 16 Feb 2012 0700Z, Moon 41° below horizon, Open Hole 10 min exposure with no neutral density filter. Scene is a factor of 4,000,000 darker than daytime image in Fig. 10-5.

Fig. 10-5. Daytime Image near noon for comparison with night images: 4 Feb 2012 2000Z, Red spectral filter, 50 msec exposure with a 2 log neutral density filter.

As documented in Memo AV12-006t, the measured flux levels were about 6.6 logs ($10^{6.6}$) darker under starlight than under daylight. [Finding] Table 10-1 shows the anticipated relative flux levels in the absence of anthropomorphic (human generated) light sources, as well as the measured relative flux levels. Column 4 shows the

anticipated open ocean relative flux changes based on measurements in open sea by Brown [36]. Column 5 shows the measured relative flux changes in our offshore San Diego environment that includes significant anthropomorphic light. Columns 2 and 3 show the sun or moon zenith angle, and the moon relative brightness derived by MPL algorithms based on moon phase and earth-to-space distance.

Table 10-1
Flux Changes for Open Ocean and Observed MSI

Condition	Source θ	Rel Moon Brightness	Brown Change Open Ocean	MSI Change San Diego
Daylight	48°	-	-	-
Near Full Moon	18°	.290	5.8 log	5.9 log
< Quarter Moon	74°	.043	7.2 log	6.4 log
Starlight	-	0	7.3 log	6.6 log

The measured relative flux changes are for the darkest part of the ocean. This kind of information will be useful if a new extinction imager is developed in the future for both day and night sensing of the ocean. For our camera, we achieved this dynamic range with a combination of neutral density filter changes and exposure changes to adjust between different images. We also made use of the cameras 16-bit dynamic range to acquire the range of radiances present within a given image. From these data, we can anticipate that if a new extinction imager is developed for Day and Night capability, it will need to be able to acquire an additional approximately 7 logs or more of extended sensitivity beyond the dynamic range in an individual image. [Recommendation]

10.3. Evaluation of the Ocean as an Optical Target at Night

The requirements for night extinction imaging are similar to those for the daytime. The extinction imager concept utilizes an image of a dark optical target and measures its contrast with respect to the horizon sky. A completely black target would have an inherent contrast of -1 at 0 range or 0 extinction, and the measured or apparent contrast approaches a contrast of 0 as range increases and/or the extinction coefficient (or haziness) increases. The MSI extinction algorithm does not require the inherent contrast to be -1, but it needs to be a constant or vary in a predictable way with parameters such as relative sun position (i.e. be well behaved). Ideally, we would like the inherent contrast to be between -0.5 and -1. This is because variations in the horizon sky radiance due to non-ideal conditions have minor impact on the measured apparent contrast if the target is dark and the contrast close to -1.

In the daytime, with red imagery, we found that the inherent contrast for the ocean at 650 nm was about -.85, and independent of angle with respect to the sun. Measured apparent contrast (which varies with haze amount and can range from the inherent value to 0) typically varied from about -.85 to -.10.

The MSI night imagery was processed so that we could evaluate the apparent contrast and its behavior at night. The processing is documented in Memo AV12-024t, and the analysis is in Memo AV13-001t. The results are summarized in Memo AV13-002t.

Table 10-2 shows sample measurements of the apparent contrast taken with the fisheye lens. These data show clear conditions (low haze), clear skies (little or no clouds), and a variety of day and night lighting conditions. Details are provided in Memo AV12-006t.

Table 10-2
Apparent Contrast between Ocean and Sky in Sample Images

Scene	Image	Contrast
Day, Red	4 Feb 2000Z	-0.64
Day, Open	4 Feb 2000Z	-0.59
Full Moon, Open	4 Feb 0600Z	-0.54
Qrt Moon, Open	16 Feb 1200Z	-0.51
No Moon, Open	16 Feb 0700Z	-0.40

In these data, we note that for similar visibility conditions, we lose some contrast by going from the red to the open hole spectral filter configuration, lose just a bit more contrast as we transition from daytime to full moon conditions, and lose more contrast as we transition to starlight (no moon) conditions. Although the apparent contrast of -0.40 under starlight is not optimal, it would still be useful if the contrast is well-behaved as a function of atmospheric conditions.

In evaluating the night imagery, we felt that the most difficult cases would be those acquired under starlight. In our earlier work with Whole Sky Imagers [24], we did considerable study of the night sky properties. We found that the spectral characteristics and the shape of the radiance distribution of the sky under full moon are nearly identical with those under sunlight, except in the presence of large cities. (Large cities add additional flux that is unique to each location, and varies with look angle and solar hour angle). This also makes sense, because the scattering mechanisms driving the sky radiance distribution are the same for day and night. For this reason, we would expect the relative radiances under full moon to behave similarly to the relative radiances under daylight, implying that the ocean surface should be a good target under full moon. An evaluation of the full moon imagery supports this conclusion.

Starlight, however, has a quite different radiance distribution over the sky than under full moon conditions. As a result, the relative radiances of the ocean and the horizon may behave somewhat differently. The equations discussed in Section 3 should work equally well under starlight if a black target is used. But it was not obvious (prior to this experiment) how black the ocean would be with respect to the horizon, or how the inherent contrast of the ocean would behave under starlight. We felt that if the system were to be useful at night, it must be useful under starlight. Thus we concentrated on this regime.

We extracted the measured contrast of the ocean surface with respect to the horizon sky for essentially all starlight cases for Feb – Sep 2012, as documented in Memo AV13-001t. We evaluated the images visually with regard to whether the horizon appeared to be clear, and the appearance of the ocean surface. We also extracted the simultaneous measurements of cloud amount, cloud height, Point Scatter Meter extinction, and Wind Speed on the shore and at the buoy. We also extracted the number of hours before sunrise (or after sunset), the number of hours from moon rise or set and the relative moon brightness. These data were tabulated and sorted and analyzed in detail.

Unfortunately, we found that under starlight, the apparent ocean contrast does not appear to be well behaved. As discussed in Memo AV13-001t, even under clear conditions and with no clouds, the apparent contrast can vary between about -.4 and near 0. The measured contrast can even become positive, meaning that the ocean is brighter than the horizon. We had hoped that the cases with positive or near-zero contrast might be related to measurable conditions such as wind speed so that we could flag them. This would have enabled the night extinction algorithm to flag conditions under which the results might not be valid. However, we did considerable analysis of the measured data, and were not able to relate the contrast under starlight to any of the meteorological parameters we measured. [Finding]

The problem is illustrated in Figs. 10-6 and 10-7, from Memo AV13-001t. Both of these images were taken under similar conditions of no clouds, low extinction, and moderate wind speeds, based on the ceilometer, PSM, and shore weather station and buoy station data. The case in Fig. 10-6 has a contrast of -0.35, while the case in Fig. 10-7 has a contrast near zero.

Fig. 10-6. A cloudless case with low extinction and contrast of -0.35, Feb 20 2012, 1200Z

Fig. 10-7. A cloudless case with low extinction and contrast of -0.04, for comparison with Fig. 10-6, Feb 23 2012, 0900Z

Similarly, Figs. 10-8 and 10-9 show cases under moderate extinction, with overcast skies and moderate wind speeds, yet the contrast values are significantly different. (In Fig. 10-

9, the nearby bushes are lit because the light was turned on outside a nearby building, but this did not affect the ocean radiances.)

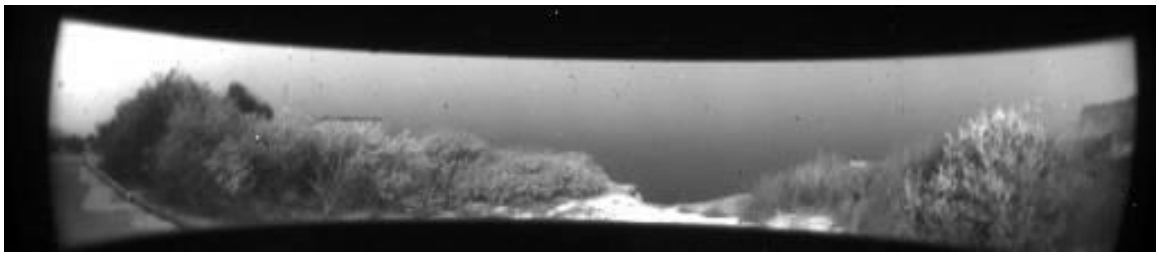

Fig. 10-8. An overcast case with moderate extinction and contrast of -0.22, Apr 21 2012, 0700Z

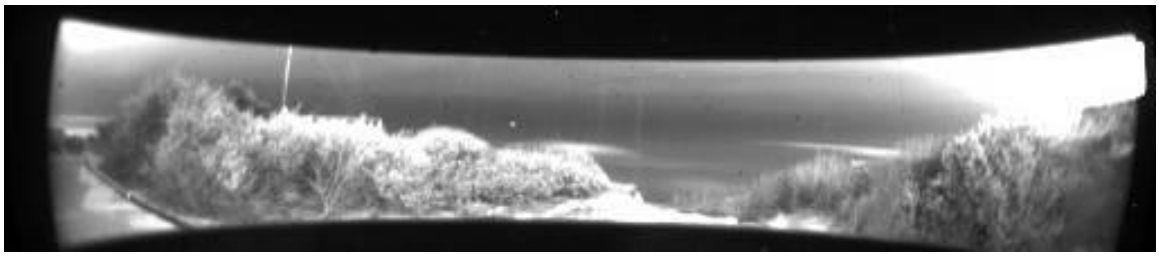

Fig. 10-9. An overcast case with moderate extinction and contrast of +0.07, for comparison with Fig. 10-8, Mar 31 2012, 1200Z

We speculate that the bright ocean radiances may be due to bioluminescence. It definitely makes sense that the bright patches in Fig. 10-9 may be due to bioluminescence, as we have also seen these bright patches under clear skies, such as in Fig. 10-6, when they could not be caused by broken cloud cover. If indeed the bright oceans are due to bioluminescence, it may be feasible to use a filter with a narrow blocking at the wavelength of bioluminescence. With a spectral blocker, it may be that the ocean surface is an adequate target for EI techniques, even under starlight. We recommend that future researchers who wish to use EI techniques at night on the ocean first evaluate whether using a spectral blocker to eliminate the bioluminescence enables use of the ocean surface as a satisfactory target at night. [Recommendation]

Interestingly, we could tell visually whether the extinction was high or low from the presence or lack of a sharp horizon. For example, in Fig. 10-10 a case is shown that looks quite hazy or foggy. We felt that developing a night extinction algorithm based on the horizon appearance was beyond the scope of this grant, but this is certainly an approach that others could consider in the future. [Recommendation]

Fig. 10-10. A case with a less distinct horizon where it appears that this is caused by haze or fog. Sep 22 2012, 0900Z

As a result of the unexplained variance in the contrast, we were not able to develop a night extinction algorithm for extracting extinction coefficient from the night imagery, even though the night measurements were of good quality.

10.4. Considerations for Future Night Development

We were not able to characterize the behavior of the ocean target well enough to use it for starlight conditions. However we feel that there are several techniques for using extinction imagers that would be worth evaluating for night capability. These are discussed in more detail in Memo AV13-002t, and briefly discussed below.

Although not mentioned in that memo, we have since realized that it's possible the bright radiances may be due to bioluminescence, as discussed in Section 10.3. We feel it would be appropriate to do additional night analysis, to determine the cause of the brighter ocean surface. If the cause can be isolated to bioluminescence, the filtering the imager to remove the bioluminescence wavelengths may enable the EI technique to work well at night.

It may be more practical to use a black target on the ship or a nearby vehicle or drone at night. Although the unfiltered ocean surface does not appear to provide an adequate black target at night, we are not aware of any reason that another black target should not work at night. The theory behind the extinction imager should work equally well day and night, whether there is a direct source such as the moon or not. This approach represents a compromise with respect to our original goals discussed in Section 2, because use of a target on the ship does not provide the extended path for night, and use of a remote black target means the system would not be single-ended for night. However, either of these approaches should be practical and still provide the benefits of being robust and cost-effective. Thus, while not ideal, we would expect use of a black target at night to be a far more practical and accurate system than other non-imaging approaches we are aware of at this time. [Recommendation]

Another potentially fruitful approach is to develop an imaging transmissometer. This system would use a radiant source at a wavelength which is not visible, and use an imager as the receiver. In concept, this approach is similar to the use of a standard transmissometer. However, by using an imager that sees the source and its surround, the method has the advantage of solving the alignment issue inherent in many transmissometers. It would be easy for the night extinction algorithm to include a feature to find the brightest source near the expected location of the source, as outlined in Section 4, so that alignment is not an issue. The details of this approach are discussed in more detail in Memo AV13-002t. [Recommendation]

In addition, there are two approaches that are potentially more complicated to develop, but that would retain the single-ended extended path advantages of the MSI. One of these possible approaches is the use of multiple filters or different filters than were used in the MSI. Cameras have continued to evolve in a number of ways since the camera

used in the MSI was developed, and even color cameras capable of documenting at least some night scenes have been developed. It would be very useful to evaluate imagery either acquired with two wavelengths, or acquired with the city lights blocked spectrally. Either of these techniques may yield imagery that could be used at night. [Recommendation]

As mentioned in Section 10.3, another possibility for developing a night extinction algorithm using the MSI or extinction imagery data is by making better use of the horizon transition and other image features. In visually assessing the images, one way that we determine whether the image appears to have low extinction is by evaluating how sharp the horizon is. At present, we are not using this information in the day extinction algorithm. If the images were sufficiently stable to enable extraction of the gradient across the horizon, this information might lead to a night extinction algorithm that can determine extinction from the starlight imagery. As discussed in Memo AV13-002t, other image characteristics such as the gradient of the radiance above and below the horizon are related to extinction. [Recommendation]

In summary, the MSI was able to acquire quality imagery at night. However we found that the ocean does not appear to provide an adequate target under starlight, at least in the wavelengths we were using. The apparent contrast of the ocean with respect to the horizon sky varied considerably, and did not appear to be related to the estimated extinction coefficient. There are several concepts that may work well for extending the extinction imager concept to night. Each of these methods has advantages and disadvantages, and each would require further development and tests. In the meantime, we feel that the extinction imagers are excellent systems for operational or test support during the daytime. We feel that further evaluation of extinction imagers for night capability is worth pursuing by future researchers. [Recommendation]

11. THE SLANT PATH TRANSMITTANCE ALGORITHM

At the end of Phase I of this grant, our sponsors asked us to evaluate slant path transmittance, and if possible to develop a method to determine this value. The MSI and SRI determine extinction near the ground (at sensor altitude) and can be used easily to determine transmittance for horizontal paths. However it would be very useful to extend the capability to lines of sight from near the ground looking to higher altitudes. This task and the night task discussed in Section 10 were given to us in lieu of other Phase II tasks in the original proposal.

As discussed in Section 5, a typical line of sight of 5 km length at an elevation angle 10º above the horizon only reaches an altitude of about 1 km. This means that the extinction coefficient at the ground, and the relative changes in the lowest altitudes, are the most critical parameters for determining the beam transmittance for many paths of interest. In fact, for very low angles, a reasonable estimate of beam transmittance can be obtained by approximating the extinction coefficient as a constant over the path. However, our sponsors wanted a more general approach that would also be appropriate for angles near the zenith and paths extending above the haze layer at higher look angles.

We developed a slant path transmittance algorithm that uses MSI or SRI extinctions at the ground, as well as ceilometer data if available. It is based in part on atmospheric physics and on an evaluation of many scattering coefficient profiles through the atmosphere measured previously by our AOG group. This section discusses the methods, program, and results, as well as alternative approaches we considered.

11.1. Theory and Methods

The beam transmittance over a path of incremental length dr is given by Eq. 11.1.

$$dT(z,\theta) = e^{-\alpha(z)dr} \qquad 11.1$$

where r is the length of the path, z_B is the initial base altitude, z_T is the final top altitude, θ is the zenith angle (0° overhead to 90° at the horizon), and α is the extinction coefficient. The θ term enters into the equation when the incremental path dr is computed. Over a full path, the beam transmittance is given by Eq. 11.2.

$$T_r(z_0, z_f, \theta) = \prod_{z_0}^{z_f} e^{-\alpha(z)dr} = e^{**}\sum_{z_0}^{z_f} -\alpha(z)dr = e^{**-\int_{z_0}^{z_f}\alpha(z)dr} \qquad 11.2$$

Although the equation is general, we limited our development to paths from a low altitude to a higher altitude. Note that if the path is horizontal, and the extinction coefficient is reasonably uniform along the path, this simplifies to

$$T_r = e^{-\alpha r} \qquad 11.3$$

The MSI or SRI measure the extinction at or near the base altitude. In order to derive the transmittance for an arbitrary line of sight, we need to know or estimate the relative change in the extinction coefficient with changing altitude. Given the measured extinction at the sensor altitude, we can determine the extinction coefficient vertical profile as a function of altitude. Given this vertical profile, the transmittance can be derived for the desired path using Eq. 11.2.

11.1.1. Pros and Cons of Simplified Methods

We would first like to discuss some simple approaches. If the desired path is quite low in angle, well within the haze layer, and below any clouds, there should be minimal error in simply applying Eq. 11.3, using the MSI or SRI extinction coefficient. As discussed in Section 12.1, this method has been used successfully [23]. A determination of extinction coefficient was made using ground-based targets, and the transmittance determined using Eq. 11.3 for applying the results to low slant-paths. However, this method is not expected to work well for paths extending above the haze layer, and for this reason we developed a more general slant path transmittance algorithm.

We had been asked whether it would be possible to simply use the MSI equations from Section 3 with a target such as a dark drone at the top of the path. The MSI equations are only rigorous for a horizontal line of sight, because in Eq. 3.14, the background radiance for a slant path is not equal to the equilibrium radiance for a non-horizontal path. However, if we had a reasonably black drone and needed the slant path transmittance for just a few degrees above the horizon, the resulting uncertainty might be reasonably small. Fig. A-9 in the Appendix shows that the error is reasonable for a path with an elevation of 1.6°. Depending on the needed accuracy and the optical characteristics of the drone, this method might be good enough for many applications. We have not done a sensitivity study for higher elevation angles, because our sponsors wanted a method that did not require a drone.

We had also been asked whether it might be possible to use the method in Section 3 using clouds as the target. We feel this method would be very error-prone, because the radiance and thus inherent contrast of clouds can vary significantly depending on the lighting conditions. As discussed in Memo AV12-008t, the error in extinction can become quite large when the target is white and the inherent contrast is not well known.

Another possibility is to use the MSI or SRI to determine the absolute value of the extinction coefficient near the ground, and a lidar to provide the relative extinction change with altitude. Although it is very difficult to develop a lidar that measures extinction directly [31], lidars that can detect relative changes in extinction are somewhat easier to develop. However, many of these are not sensitive enough to detect aerosols as opposed to clouds. In researching lidar systems capable of detecting aerosols, we determined that the cost of such an approach would be well beyond our budget. For operational use by the Navy, our sponsors felt that the cost and reliability constraints associated with lidars that we are aware of made this option undesirable. This work is

documented in Memo AV10-005t. However, ceilometers, which are quite robust and inexpensive, do provide some information on the aerosols along the vertical path. They can in some cases detect the top of the haze layer, and can routinely detect cloud layers. We developed our method so that ceilometer data can be used if available.

11.1.2. The Slant Path Transmittance Algorithm Logic

Given the constraints discussed in Section 11.1.1, we developed another method. This method uses MSI or SRI data to provide the absolute magnitude of the extinction coefficient near the ground. The slant path transmittance algorithm also estimates the relative change in the extinction coefficient as a function of altitude (vertical profile), and modifies this vertical profile based on ceilometer data if available. The MSI or SRI extinction normalizes the vertical profile at the sensor altitude, and Eq. 11.2 (first part) is used to determine the beam transmittance for the desired path.

This approach depends on several considerations. First, if the air below the top of the haze layer is well mixed, the profile can be modeled quite accurately, as will be discussed below. Second, we have found that when the haze layer is not well mixed, the variations within the layer have much less impact on transmittance for the full path than the magnitude of the extinction near the ground. Third, the exact magnitude of the extinction coefficient above the haze layer top has little impact, because it contributes so little to the overall light loss. Fourth, the exact magnitude of the extinction coefficient within clouds has little impact, because the transmittance falls below acceptable levels so quickly within the clouds.

In past years our research group completed over 200 research flights with an instrumented Air Force C-130 aircraft [e.g. 10, 11, and 12]. As part of this research, vertical profiles of measured scattering coefficient were acquired, typically in 3 filters, and typically to altitudes of about 6 km. Most of these profiles are characteristic of atmospheres with well mixed haze layers, and as a consequence well behaved, as discussed later.

In some cases, the lower layer was not well mixed, and the extinction varied in non-ideal ways. For the current study, we evaluated many of the profiles, and found that this did not appear to be a common condition. We evaluated one of the worst case profiles (in terms of variance within the haze) to determine the impact of the variance with altitude. This analysis is discussed in Memo AV10-006t. We found that for a given path geometry, there will be uncertainties if the relative extinction varies significantly within the lower haze layer, but that the magnitude of the path transmittance is driven primarily by the absolute magnitude of the extinction near the ground. That is, there will be some error if the haze layer is not well mixed, and the extinction coefficient within the haze layer does not fit the model discussed below, but this error is relatively small if we know the absolute magnitude of the extinction coefficient near the ground. [Finding]

In detailed analysis of the C-130 measured profiles, Hering[11] [37] showed that under most conditions, extinction profile within the haze layer was well behaved. He defined the optical scattering mixing ratio Q as the ratio of total scattering coefficient to Rayleigh scattering coefficient. He found that this mixing ratio was nearly constant within the haze layer. In addition, he found that in the absence of clouds, he could represent most profiles with a two-layer model, with a fixed value of Q below the haze, and a different but fixed value of Q above the haze. Sample results are shown Fig. 11-1, and discussed further in Memo AV12-015t. In Fig. 11-1, the solid lines show the modeled mixing ratio profile, and the other lines show the measured mixing ratios. [Previous Finding]

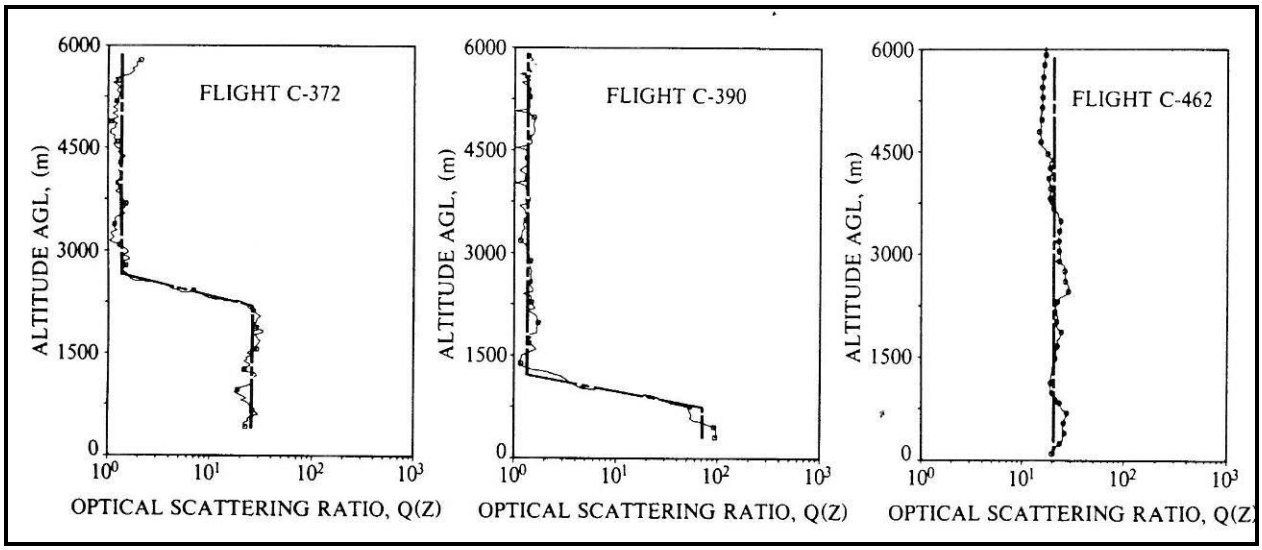

Fig. 11-1 Sample vertical profiles of Measured Mixing Ratio Q, which is measured scattering coefficients divided by the Rayleigh scattering coefficients for each altitude

In the absence of clouds, following Hering's work, our slant path transmittance algorithm models the vertical profile for relative extinction coefficient using a lower haze layer and an upper clear layer. The altitude of the top of the haze layer must either be estimated visually or from meteorological data, or measured with a ceilometer or other device. The Q value within the haze layer is determined from the extinction coefficient measured near the ground with the MSI or SRI, and the Rayleigh scattering coefficient at the sensor altitude [38]. The relative change in the Rayleigh scattering coefficient is based on the atmospheric density profile, as discussed in Memo AV11-016t. Following Hering's research, the Q value for the upper layer for the red filter was set at a value of 1.15, as discussed in the above memo.

In the slant path transmittance algorithm, cloud layers can be inserted anywhere within the vertical profile. If a ceilometer is available, the cloud altitudes are extracted from these data, and Q values are estimated from these data as discussed below. If ceilometer data are not available, the cloud base must be estimated using other methods. In that

[11] Hering was a member of the AOG for several years

case, the Q value within the clouds can also be estimated. Hering provides estimates of the Q values within the clouds, as discussed in the above memo.

The uncertainties resulting from this approach will be discussed later in this section.

11.2. Implementation of the Slant Path Transmittance Theory

The first version of the slant path transmittance algorithm was written to require only MSI or SRI data, without any ceilometer data. The important inputs are the MSI or SRI extinction at sensor altitude, the path geometry, the height of the haze layer, and the cloud base if any. The program determines the relative estimated extinction vertical profile from these inputs, and then uses Eq. 11.2 to determine the beam transmittance for the whole path. The details of the implementation of this logic are discussed in detail in Memo AV11-016t, "Logic for Slant path Transmittance Version 1". The Version 1 program is documented in Memo AV11-017t. The results of the test runs, and the analysis of these results, are presented in Memo AV11-018t, and in Section 11.3.

Sample results for three zenith angles (0°, 60°, and 85°) are shown in Fig. 11-2. (The x axis is labeled "scattering coefficient", because we were testing visible wavelengths at the time, where extinction coefficient is essentially equal to scattering coefficient.) The horizontal axis shows a range of atmospheric conditions. If these scattering values are interpreted to occur in the green, then they correspond to visibilities of 300 km at the left end to 3 km at the right end. Likewise, for other filters, these values correspond to spectral visibility V' values of 300 km to 3 km (Section 3.2). These calculations are for a path from 0 to 2 km altitude (not fixed path length) with a haze top at 1 km. "Cloud Base: 99" indicates no clouds were used in the calculations.

As expected, the beam transmittance values are lowest for the vertical line of sight, which leaves the haze layer most quickly, and in all cases the beam transmittance decreases with increasing scattering coefficient, i.e. increasing haziness.

Following the above development, we did detailed analysis of the ceilometer data acquired during this program, to determine whether we could refine the haze top altitude, cloud base altitude, and Q value within the cloud based on the ceilometer data. Fig. 11-3 shows the backscatter profiles extracted for four times (1600Z, 1800Z, 2000Z, and 2200Z) on one day from the measured ceilometer data. There is a fair amount of noise in the profile, but the clouds bases and tops are fairly obvious on visual inspection of these profiles.

As discussed in Memo AV12-012t, we found that the cloud base and top parameters automatically determined by the Vaisala software provided with the ceilometer were not adequate for our purposes. The noise in the profile sometimes resulted in cloud base or top determinations that were inconsistent with a visual evaluation of the profile (i.e. false cloud bases from noise). We developed alternative methods to evaluate the measured profiles, and extract the cloud parameters directly from these measured profiles, as

discussed in the above memo. Analysis showed that this alternative method yielded more consistent results for our application. [Finding]

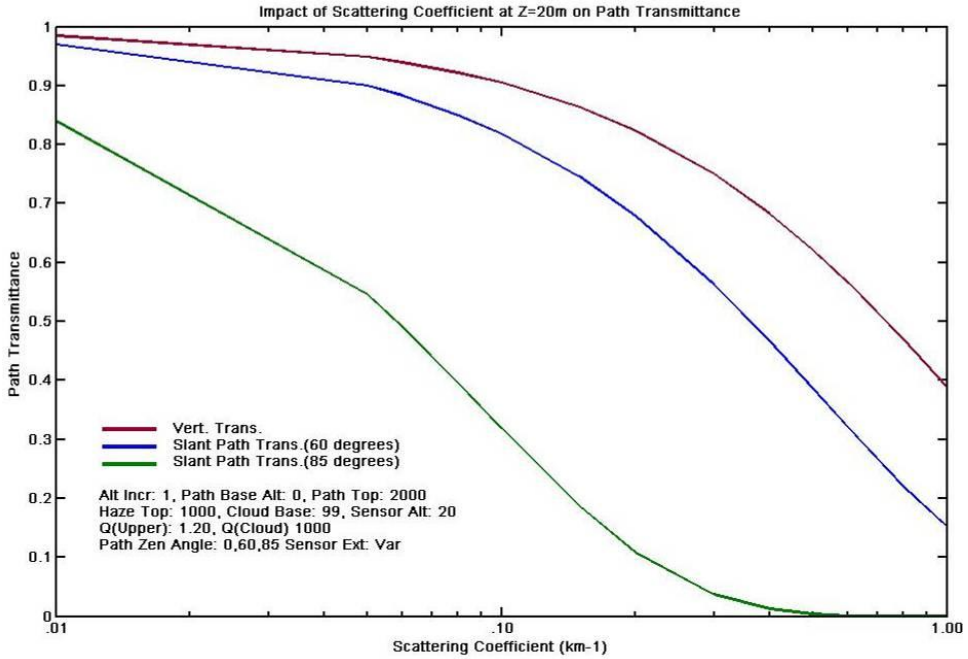

Fig. 11-2. Slant Path Transmittance as a function of extinction near the ground, for three paths, at look angles 0°, 60°, and 85°.

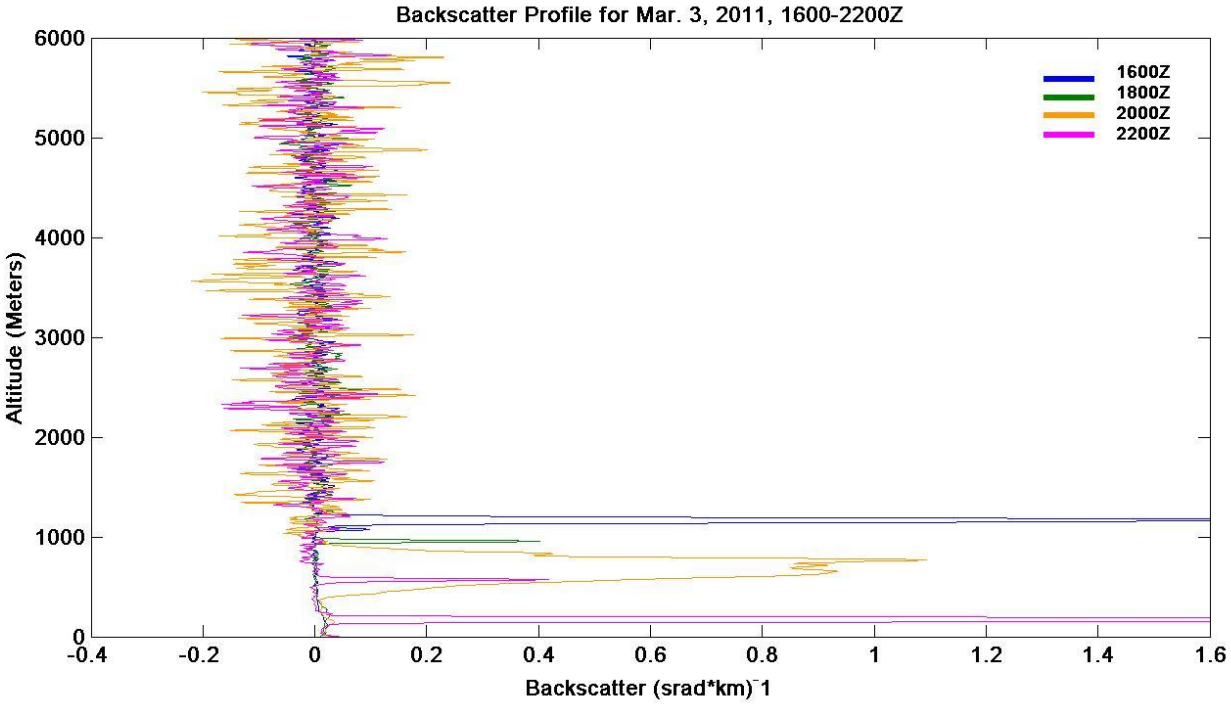

Fig. 11-3. Vertical Profile of backscatter coefficient for 3 Mar 2011 measured by ceilometer, showing a day with variable low cloud layers (on a linear scale)

The ceilometer measures backscattering coefficient, and we are interested in extinction coefficient. These two values are not always proportional, depending on the aerosol drop size distribution; however for our purposes we can treat them as being roughly proportional. The Vaisala documentation provides a typical value for estimating extinction coefficient from the backscatter coefficient. We used this value to determine the variation of Q within the clouds from the ceilometer data, and it yielded reasonable results. More importantly, as discussed in Memo AV11-018t, we found that the actual Q value within the clouds makes little difference, because the transmittance drops so quickly that the path within clouds is not expected to be useful for our sponsors' purposes.

When combined with the previously input haze layer parameters, this method resulted in the extinction coefficient profile shown in Fig. 11-4 for times 2000Z and 2200Z. In comparing Figs. 11-3 and 11-4, be aware that the horizontal axis parameters (backscatter vs. extinction) and scale (log vs. linear) changed.

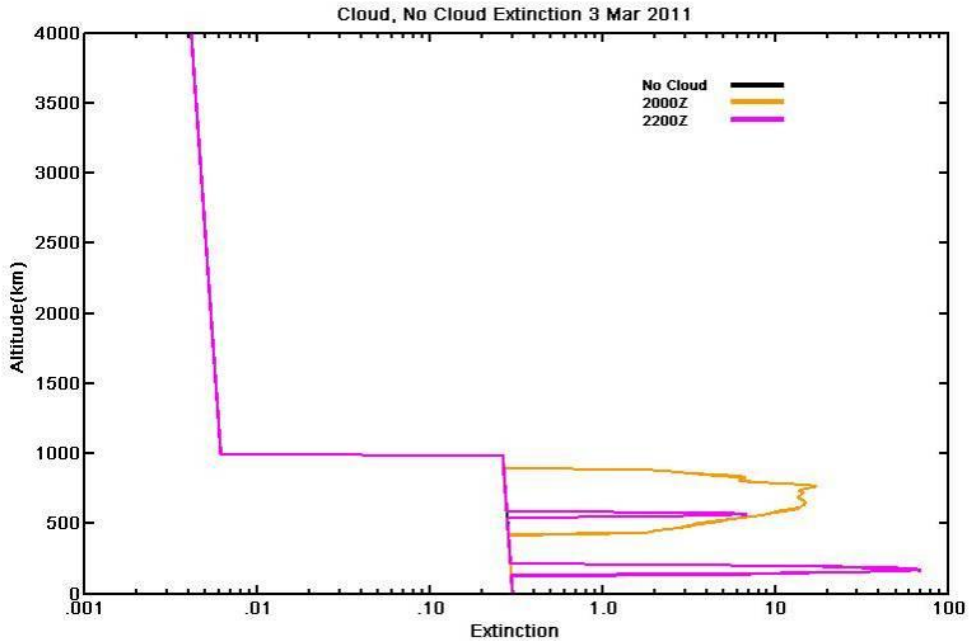

Fig. 11-4. Resulting modeled vertical profile of extinction coefficient for two times (on a log scale)

The ceilometer software can also provide an estimate of the haze top. The ceilometer is not sensitive enough to provide high resolution measurements of changes in aerosol amount at other altitudes, but the haze top often does appear in the profile, as shown in Fig. 11-5. The haze top is not obvious, but often its magnitude is significant in comparison with the noise level at that altitude. This is discussed in Memo AV12-013t.

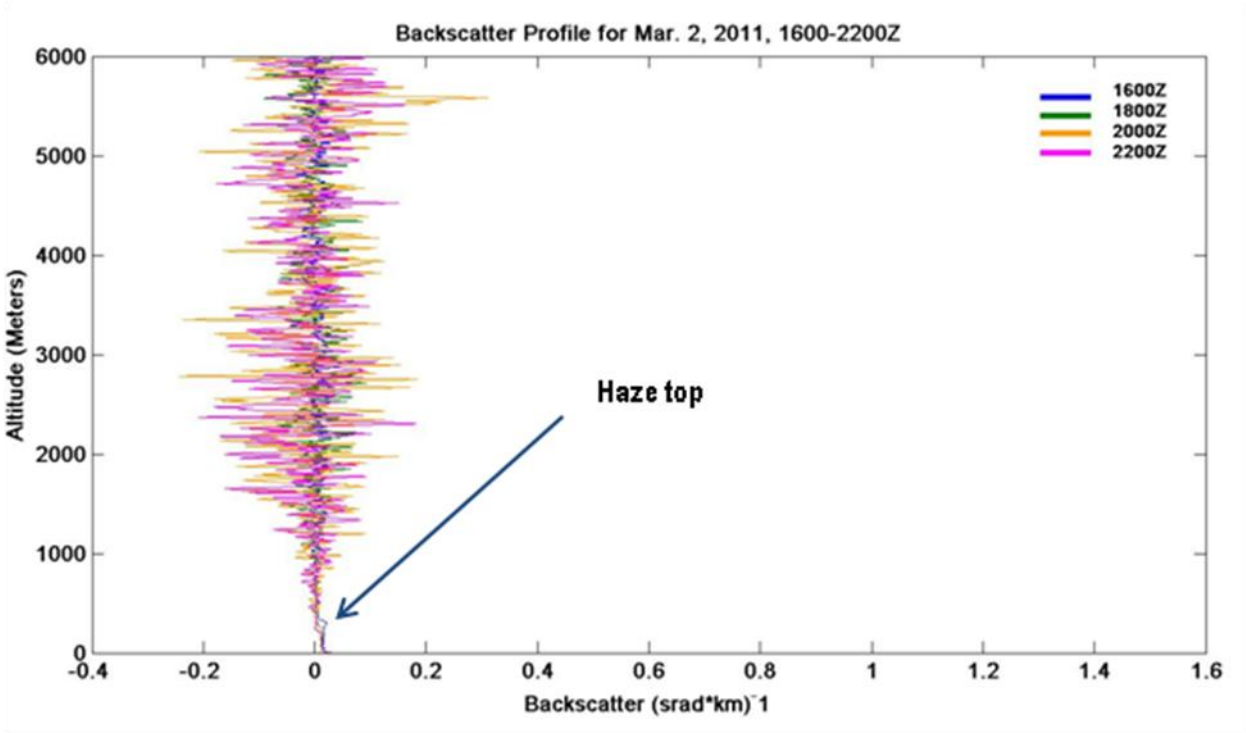

Fig. 11-5. Vertical Profile of backscatter coefficient for 2 Mar 2011 measured by ceilometer, showing a day with no clouds but a discernible haze top (on a linear scale)

We evaluated the haze top altitudes determined by the ceilometer software, and found that most of the time, the Vaisala algorithm either returned a reasonably accurate value or indicated it could not make a determination. Occasionally, the results do not appear valid. For this reason, use of the haze top algorithm from the ceilometer is an option in the slant path transmittance algorithm. We would suggest that future developers further evaluate whether the ceilometer haze top determination is accurate enough for their purposes. In the absence of a determination of haze top altitude by the ceilometer, an estimated haze top altitude must be input based on a visual or other assessment. [Finding/Recommendation]

The details of the ceilometer work are documented in several memos. Memo AV12-012t, documents the analysis of the ceilometer cloud data, discusses how the ceilometer profiles are processed to extract the cloud data, and provides sample results. Memo AV12-013t has similar discussions of the ceilometer haze data. Cloud top information, as well as horizontal transmittance, were added to the slant path transmittance algorithm soon after, and are discussed in Memo AV12-014t.

We developed the slant path transmittance algorithm as a stand-alone program. Memo AV12-016t provides details on how to run the slant path transmittance algorithm, and how to choose the input parameters. Memos AV12-018t and AV12-019t describe how to process the optional ceilometer data. Memo AV12-020t documents the program and its inputs. The program has been delivered to our sponsors, and is available on request by contacting the authors. We also anticipate mounting it on our web site listed in Section

16. The Version 2.0 software is the correct version to use whether a ceilometer is being used or not, as it includes several improvements with respect to Version 1.0 that apply even if no ceilometer data are used.

11.3. Sample Results and Error Analysis of the Slant Path Transmittance Algorithm

As documented in AV11-018t we did a sensitivity study of the input parameters. This was done in order to determine which parameters were most important, and evaluate the level of uncertainties implied in this method. The results will be discussed in this section, and are summarized below. [Findings]

a) Path Geometry is the strongest driver. This is a known parameter.
b) For a given path, measured sensor extinction (MSI or SRI) is the strongest driver in the absence of clouds. This is measured, and thus introduces no additional uncertainties beyond those discussed in Section 9.
c) Cloud base is vitally important, in the sense that it is important to know if the target is within the clouds (above the cloud base). This value is calculated from the ceilometer measurements, or provided by visual assessment, or other information sources the ships may have available.
d) Haze top altitude is also important if the line of sight penetrates the top of the haze layer without entering a cloud (i.e. the haze top is below the cloud base and below the top altitude of the line of sight). This is our biggest uncertainty in the absence of clouds within the path. It can be calculated from ceilometer measurements using the ceilometer software, or can be estimated from meteorological conditions. As lidars develop in the future, a lidar that can detect the haze top (but doesn't have to detect the extinction – which is much more difficult) could be a good complement to the MSI method. At present, the ceilometer is able to make this estimation much of the time. [Recommendation]
e) When the haze layer is not well mixed, the relative changes within the haze layer can cause uncertainties. However, these are not as important as knowing the measured sensor extinction.
f) The Q value (mixing ratio) within clouds is unimportant for this application, because the path transmittance drops below useful values quickly in clouds.
g) The Q value in the upper clear layer is unimportant for this application, because it does not contribute significantly to the losses.

In Fig. 11-6, we show the data from Fig. 11-2, with some added interpretation. Here we wish to consider the conditions under which the path transmittance will be 50% or better.

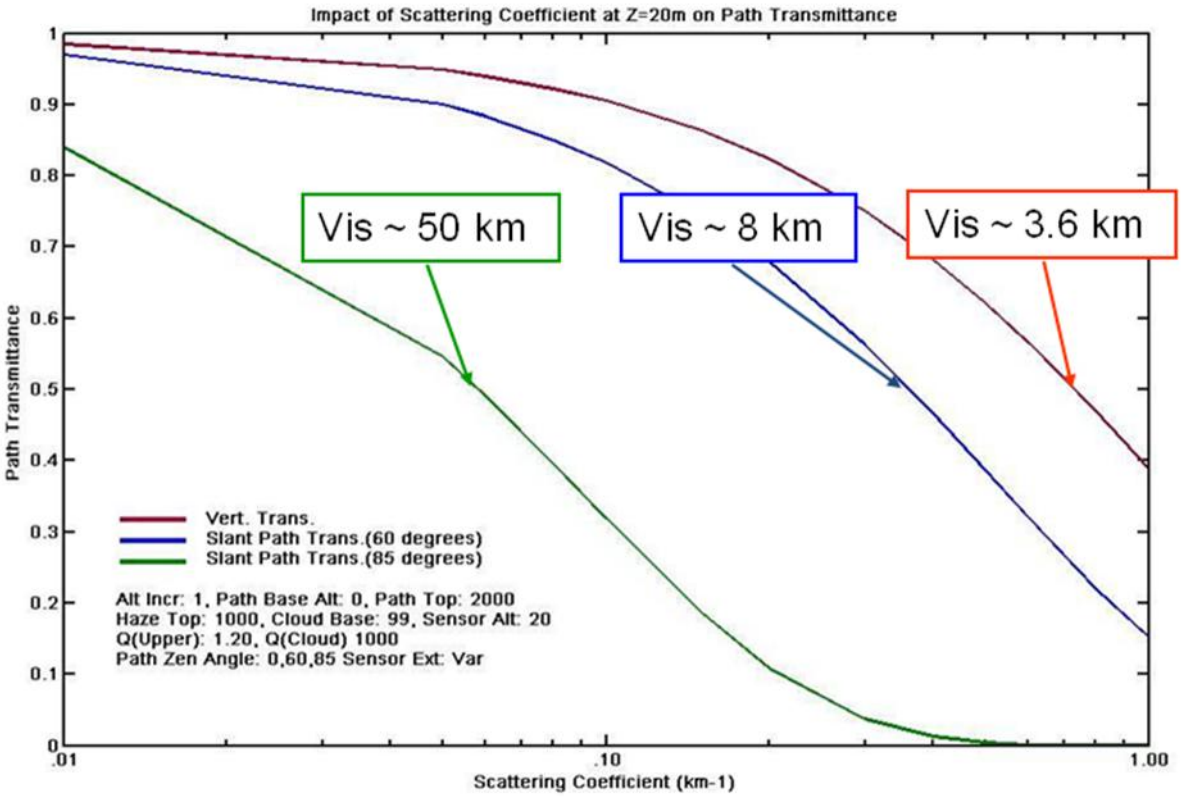

Fig. 11-6. Illustration of the impact of path geometry and MSI or SRI extinction

In Fig. 11-6, the top curve shows path transmittance as a function of the MSI or SRI extinction for a vertical path from ground to a 2 km top altitude. This curve drops to a path transmittance of 50% at an extinction value of about 0.83 km^{-1}, or a spectral visibility V'=3/α of 3.6 km. This means that for any conditions with the spectral visibility better (clearer) than about 3.6 km, the path transmittance for this vertical path will be 50% or better. Similarly, we see in Fig. 11-6 that for a path at 60° zenith angle to a 2 km top altitude, conditions must be clearer than a spectral visibility of about 8 km for the path transmittance to be 50% or better. For a path near the horizon at 85° zenith angle, the spectral visibility must be better than 50 km – a condition that does not occur often. This is partly because the extinction coefficient is higher near the ground, and partly because a path from 0 to 2 km altitude at 85° zenith angle has a path length of 34 km. Thus Fig. 11-6 illustrates how important the path geometry is, and also illustrates the importance of the extinction near the ground.

In the above plot, the path lengths were quite different for the three selected paths, varying from 3 km for the vertical path to 34 km for the 85° path. In Fig. 11-7, we show the impact of path length for a selection of look angles closer to the horizon. All of these calculations are for an extinction coefficient of .30 km^{-1}, and a haze top of 1000 m.

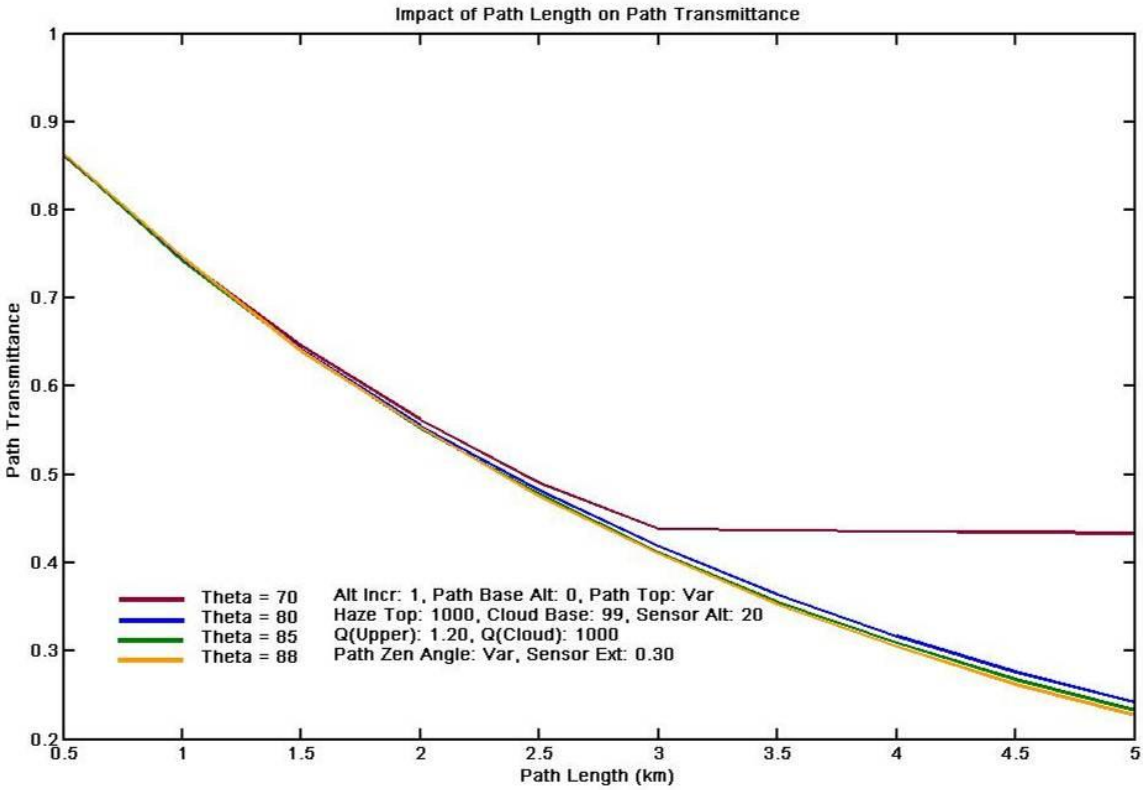

Fig. 11-7. Impact of varying Path Length for Zenith Angles 70°, 70°, 85°and 88°

As expected, even at a fixed zenith angle, path length is quite important as long as the path remains within the haze layer. Once the path extends above the top of the haze layer, as in the 70° path at a range of about 3 km, then the path transmittance is nearly invariant. This is because the Q value in the upper layer can be expected to be much lower than in the haze, based on the C-130 data. Typical upper-layer Q values were used in the calculation, and one can see that relative changes in the upper layer will have a minor impact.

Memo AV11-018t also shows the impact of varying the zenith angle, for paths to 2 km and a selection of 3 extinction coefficients. As expected, the impact increases with increasing zenith angle. We are not including this plot, as the impact can also be seen in Fig. 11-6.

To evaluate the impact of haze top altitude, in Fig. 11-8, we show curves for three zenith angles, 0°, 60°, and 80° for a path from the ground to 3 km, an extinction coefficient of .3 km^{-1}, and a variable haze top (x axis). For the vertical (0°) path, the transmittance changes from about 90% for a thin haze layer to about 50% for a haze layer of 3 km. If the haze top is any higher, it will have no impact, because the path is fully within the haze layer already. For the moderate path at 60°, the transmittance changes from about 85% to about 20% as the haze top altitude increases. The path length for this angle and geometry is 6 km. For the path closer to the horizon (10°), the transmittance drops below 50% when the haze top is about 400 m or higher. However, this path is a long path of 17 km. If one wishes to detect a target with a path length of 5 km, for example, then the path at

10° to the top of the path will be only 860 m altitude, and we only care about the height of the haze top if it is less that this 860 m. We feel, at present, that the impact of the uncertainty in the top of the haze layer is the largest uncertainty in the path transmittance, unless the path is fully within the haze layer.

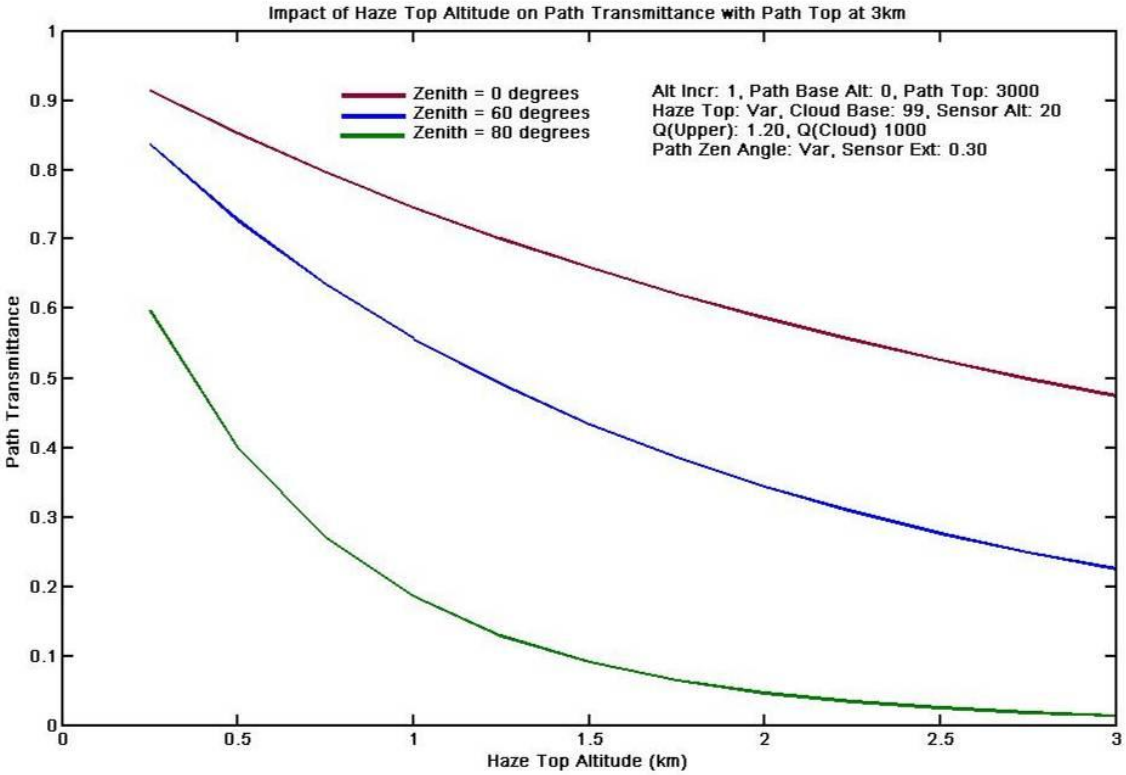

Fig. 11-8. Impact of varying Haze Top for a Path Top of 3 km and for Zenith Angles 0°, 60°, and 80°

In the presence of clouds, we would anticipate that any path that penetrates the clouds significantly would not be useful for laser applications, due to blooming within the atmosphere. However, such paths may be useful for detection of targets. Detection is not our area of expertise, but we felt it would be useful to derive the impact of clouds on the path transmittance. The details are shown in Memo AV11-018t.

As an example, we evaluated a path with a zenith angle of 60°. For thin cirrus, the path transmittance drops below 50% before it has penetrated 100 m into the cloud. For clouds of higher density, this happens much more quickly. Thus for most purposes, we believe that it will suffice to know whether the target is above or below the cloud base. We feel that the cloud base is detected reasonably accurately when a ceilometer is available. Use of a ceilometer may turn out to be quite practical on ships, as the Vaisala ceilometers (and perhaps others we did not evaluate) can be both inexpensive and robust, in our opinion. They do not provide accurate extinction coefficients, but they are a nice complement to the MSI or SRI in providing cloud base and sometimes haze top altitudes.

11.4. Application of the Slant Path Transmittance Algorithm

The slant path transmittance algorithm requires as inputs a measurement of the extinction coefficient near the ground, and an estimate or measured value for the haze top altitude, as well as the cloud base (if clouds are present), unless the path is known to be below these altitudes. Ceilometers, if available, can provide measurements of these values most of the time, and, if not, these heights must be estimated. Although it would be ideal to have a measurement of relative extinction coefficient with altitude to complement the MSI or SRI measurements of absolute extinction near the ground, this is apt to be expensive and difficult for the near future. In the absence of measured relative vertical profiles, we feel that the slant path transmittance algorithm combined with the MSI or SRI provides a quite accurate value for the beam transmittance, and is the best method we know for determining the path transmittance over slant paths.

The slant path transmittance algorithm is very useful in its present stand-alone form for parameter studies such as those discussed in Section 11.3. Using the algorithm, researchers may evaluate the impact of path length and geometry, as well as other atmospheric parameters like extinction magnitude, haze top, and cloud type for their specific applications. [Recommendation]

In addition, the program can either be used in stand-alone mode, or can be integrated into a real time program, for test support. At present, when ceilometer data are used, separate stand-alone programs process the ceilometer profiles to estimate haze top and cloud bases, as well as the Q values within the clouds. For a real-time application, these programs would need to be integrated into the slant path transmittance algorithm. [Recommendation]

Finally, if used on ship-board for defense applications, we visualize that the slant path transmittance algorithm, or some variant of it, would be integrated into a real time program for determining beam transmittances as both the aerosols and the path to the target change. Prior to any engagements, the EI system could routinely monitor extinction coefficient in all directions. During a test or engagement, the EI system would only look in the direction of the path, and update the extinction coefficient for the path. The range to target, as well as the path geometry to the target, would be continually and automatically updated from other systems on the ship. The slant path transmittance algorithm would continually update the computed transmittance as the path to the target changes. We visualize that these real time transmittances would be fed into a ship's tactical decision aid or similar software. [Recommendation]

12. TRANSFER OF THE TECHNOLOGY

As discussed in earlier sections of this report, our primary purposes for Phase I of this project were to determine whether the EI approach could be applied using the ocean surface as a dark target, and to extend the results from the visible into the SWIR. Under optional Phase II funding, we were asked to evaluate whether it would be possible to extend the capability to night-time, and to evaluate how to handle slant paths. Throughout this project, we also evaluated how the Extinction Imager technology might best be transitioned into operational use by the military.

This transition effort was helped considerably when we were given permission by our sponsors and the University of California San Diego (of which we are part) to transition the algorithms and the concepts to Pennsylvania State University's Electro-Optics Center (EOC). The EOC was funded to apply the EI method for their test applications with the Navy's Laser Weapons System (LaWS) [23]. The EOC provided funding to our AOG group to support our efforts in transitioning the technology. In this section, we will discuss this technology transfer and the results, and then discuss wider applications.

12.1. Application of the EI Technique and Algorithms for LaWS Tests

In support of the technology transition to EOC, we (the AOG) shared our methods and both the extinction and slant path transmittance algorithms with the EOC group. We advised them on initial camera selection, on data acquisition and on test interpretation. The EOC acquired an AlphaNIR camera like the one used in the SRI and used it for initial tests with dark targets such as the forest on hills. We initially sent them the SRI data acquisition program and the extinction algorithm. Our methods were partially documented in memos and earlier references [2, 3] and these were also provided to the EOC. The AOG group was developing the slant path transmittance algorithm discussed in Section 11 at the time, and later provided this to the EOC as well. However the EOC tests used sufficiently low angles above the horizon that the slant path transmittance algorithm was not needed for their application.

As part of their development effort, the EOC adapted the data acquisition and processing software for their system using the LabView environment. The AOG provided sample test data, as documented in Memo AV11-019t. We also performed extensive tests to determine the causes of differences in the results of the AOG and EOC program versions, as documented in Memo AV12-010t. With minor software modifications for consistency, we were able to obtain less than 1% variation between the extinctions determined with the AOG and the EOC software. Initial tests at EOC with the extinction imaging technique yielded reasonable results. At that point, they made further modifications to adapt the technique for their specific test application in support of the LaWS tests.

Before discussing their results, we would like to make a minor note. Although the EOC refer to the technique as "Contrast Imaging", we have preferred the term "Extinction Imaging", as we feel it is less confusing. As EOC is aware, contrast transmittance,

defined in Eq. 3.18, is different from beam transmittance, defined in Eq. 3.4. As discussed in Section 3.2 the extinction imagers measure apparent contrast as a means to determine beam transmittance. They do not determine contrast transmittance.

We were not involved with the adaptation of the EI technique to the LaWS tests, but were interested in EOC's modifications and innovations, and very pleased with their results. One of their modifications was to use the apparent contrast at two ranges (Eq. 3.25) rather than the apparent contrast at one range in conjunction with the inherent contrast (Eq. 3.24). As discussed in Section 3.4, this approach is more subject to the impact of measurement error, but it avoids the requirement to determine inherent contrast. We were delighted to hear that this approach worked well except for clear day conditions (as would be expected). We feel that the use of an input inherent contrast (Eq. 3.24) will yield more accurate results when it is practical, but the use of multiple ranges (Eq. 3.25) will be much more practical for some applications.

Secondly, although the EOC used a system similar to the SRI for the early tests, they were also able to use the sensors that are already part of the LaWS system for extinction imaging. Thus their test optics served the additional function of acting as an extinction imager. This seems especially important, as it means that for similar test scenarios it may be possible to use the modified EI extinction algorithms without the need for any additional hardware – which can be a tremendous advantage in some situations.

Finally, rather than using the horizon sky for the background, the EOC tested a grey and a white plaque as the background. We were initially concerned about this approach, because as discussed in Section 3.4, the theory is not solid when backgrounds other than the horizon sky are used. However, there was less than a 1% difference between the results with the grey background plaque and the white background plaque. In retrospect, this makes a lot of sense, because when the optical target (as opposed to the background) is black, the absolute radiance of the background has very little effect in Eq. 3.23. Also, the radiance of the plaques reaches equilibrium after a relatively short range, and that equilibrium value is the same as the horizon radiance. This result also helps demonstrate why our results obtained using the horizon were so unaffected by clouds on the horizon, as discussed in Section 8.5. Although we have not fully explored the consequences of using a plaque for the background, we are pleased that it seemed to work well.

The EOC compared the extinction results with results using measurements of laser power on the target. The two methods were consistent with variations ranging from 0 to 10% depending on range to the target. EOC provided in their report one example in which the comparison between the transmittance determined from the two methods is excellent at all ranges, as a target traveled through varying atmospheric conditions. There was one case with poor results, and it was determined that the extinction imager approach yielded good results, while measurement conditions in that case adversely affected the other method. The EOC's final recommendation was that "Because of ease of implementation and the excellent results obtained on this program, we believe the contrast imaging approach warrants further investigation for incorporation into future laser weapons" [23].

12.2 Extinction Imaging for Test Support

The EI technique may also be used for a variety of other test scenarios. Depending on the specific goals of a given test, different modifications to the EI technique may be required. For example, use of a different EI camera would dictate minor changes to the data acquisition software and the extinction algorithm. Other modifications might be as demonstrated in Section 12.1. However, several generic commonalities exist for most tests situations, and these are discussed below.

12.2.1. Wavelength Considerations: Visible or SWIR?

We tested both a visible and SWIR camera throughout this project, in order to extend the capability to the SWIR. We expect that for many applications, the extinction coefficient and/or beam transmittance in SWIR wavebands will be needed. As discussed in Section 5, one approach is to take the EI measurements in the visible wavebands, where cameras tend to have better linearity and signal to noise characteristics, and then use MODTRAN© or similar modeling to estimate the desired SWIR parameters. The other approach is to measure the extinction coefficients directly with systems operating in the SWIR band.

During this project we found that the SRI provided excellent results, and these results compared very well with the visible results. The SWIR camera we used was a 12-bit camera (as opposed to 16 bits for the visible camera), and the linearities, uniformities, and signal to noise were not as good as with the visible system. However, they were good enough! The results compared very well with the visible data. Thus for most applications, we would recommend using a system at the wavelength for which the beam transmittance values are needed. [Recommendation] For wavelengths near 1.6 µm, a SWIR or visible/SWIR camera would be required. For wavelengths near 1.0 µm, a CCD-based visible camera may have the required sensitivity to measure at the waveband of interest.

There are two exceptions we are aware of, when a visible system would be preferable to a SWIR system. One is if the application demands test results at night. Our tests indicated that the SWIR camera used in this project was not capable of acquiring adequate images at night. However, the visible CCD imager used in the MSI was able to acquire excellent images. Although the ocean surface appears not to be ideal at night (Section 10.3), a visible system could be used to determine extinction using dark targets. [Recommendation] As more sensitive cameras become more available, this will mitigate the possible need to use a non-optimal wavelength.

Another exception to the recommended use of a SWIR camera may be when the test is done at sea using the ocean surface as a target. As discussed in Sections 8.5.2 and 9.3, gloss was much more of an issue in the SRI than in the MSI. We have suggested methods to deal with the gloss, but have not developed these methods. We have been told gloss will not be an issue for testing, because laser tests are not allowed in the presence of gloss. However, if gloss is expected to occur in the test environment and

expected to be an issue, it may be preferable to use a visible system with a red filter, where the effects of gloss are much less, rather than a SWIR system. [Recommendation]

We found the difference between the red wavelength extinctions and the SWIR wavelength extinctions to be small in comparison with typical changes caused by atmospheric change. This was found both in model (Section 5) and measurement (Section 9). Thus we feel that use of the red wavelength in combination with model or empirical extrapolation should also yield good results.

Normally, to acquire atmospheric extinctions at a specific wavelength such as 1.6 μm, one would expect to filter the instrument response to the desired waveband. The SRI system measures the images with a semi-broadband response. However, as noted in Section 3.4, this results in determination of the extinction coefficient in the clearest part of the response, i.e. in the atmospheric windows. This means that the extinction coefficient for a window region can be measured using a somewhat broader response if flux levels or other considerations make it preferable to do so.

12.2.2. Other Sensor Considerations

It is not important that the sensors be calibrated for absolute radiance, but it is important that they provide a reasonable measure of relative radiance. The more accurately this is done, the more accurate the extinctions will be. This sounds trivial and obvious, but we would like to share some experience in this regard. The SWIR camera we used acquires the images at 12 bit resolution, but the most user-friendly software provided with the camera saves the images at 8 bit resolution. The commercial software, as part of the conversion from 12 to 8 bits, makes the images "look pretty", but in the process the relative signal values between pixels is not maintained. As a result for the SRI data acquisition program developed at MPL, we had to develop our acquisition software making sure we saved the original 12 bit images, which was not straight-forward. These 12 bit images were still somewhat nonlinear, but the non-linearities were consistent as a function of signal level in a given exposure, and could thus be measured and corrected. Thus some care must be used in camera and software selection and development to ensure that relative radiance levels are maintained within an image. [Recommendation]

Another implication of the need for relative radiance to be measured accurately is that calibrations can make a significant difference. We found that uniformity calibrations and dark calibrations were important for both the MSI and SRI. These are relatively easy and cost effective to acquire and implement (Section 8.3). As discussed in Section 8.3, the relative linearity calibration makes a significant difference in the SRI camera data. Acquiring a linearity calibration requires somewhat more expertise than dark and uniformity calibrations. However, we expect that if many systems were to be deployed for operational use, it would be sufficiently accurate to calibrate a few cameras and apply the average results to all the cameras. Depending on the accuracy needed, it may be reasonable to not use the linearity calibrations (Section 9.4). However, depending on required system accuracy, and the linearity characteristics of the cameras, this is something future developers should be aware of. Thus we feel that uniformity and dark

corrections are vital and quite easy, and linearity corrections will enhance the result but may not be required depending on the desired accuracy. [Recommendation]

It is important that the acquired data be in a reasonable portion of the camera's sensitive range. [Recommendation] If data are offscale dark or bright, they will not correspond to the relative radiance of the elements in the scene. We chose not to use data less than 100 counts above the dark level, as we were concerned that the results would be distorted by noise and non-linearities. Similarly, we blocked the high end of the response to avoid linearity issues.

In the operational data acquisition, it would be important to automatically adjust the exposure levels depending on the solar (and lunar) position. We did not include a flux control algorithm in either the MSI or the SRI, because we were able to acquire good onscale data for the central 8 hours of the day without it, and that was our priority for test and development. However, for a system that needs to run all day, addition of flux control logic may be important. [Recommendation] One of the features of the Whole Sky Imagers for cloud detection [24] was a flux control algorithm. Our 16-bit Day/Night WSI systems predict the flux level, based on sun position and moon position, phase, and brightness. Our 12-bit Day WSI systems [27] have a more limited dynamic range within a single image, and for this reason they assess the acquired images and adjust the exposures as necessary.

12.2.3. Extinction Algorithm considerations

Special adaptations of the extinction algorithm software may be required depending on the test environment. For example, the current extinction algorithm is optimized for using the ocean surface, and includes features such as a check to handle glitter on the ocean when looking up-sun. Clearly this is not needed if the tests are done on land with black plaques for targets. However, if a black plaque at a long range is used, in a manner similar to that discussed in Section 4, it would be important to include a feature that automatically aligns the system in the presence of refraction. This technique is discussed in Section 4. [Recommendation]

The shape of the ROI will also depend on the application. Using the ocean surface, we chose ROI's that were narrow in height so that the range uncertainty would be minimized, but wide so that many pixels would be included. In the case of distant black targets (Section 4), we only used the darkest 3 x 3 pixel region of the target. This is because there will always be some scattering of light within the optics, as well as potentially cross-talk in the electronics. We carefully measured the point spread function (a measure of the focus) for the MSI, and found it could be represented by a Gaussian curve with a FWHM width of approximately 0.4 pixels. In spite of this, we feel that pixels immediately adjacent to large radiance gradients could be distorted. For this reason, we chose to only extract the 3 x 3 darkest ROI from the distant target with the system discussed in Section 4. Similarly, if black plaques are used as the target and white plaques are used as the background, as discussed in Section 12.1, it would be important to separate the ROI's so that the selected ROI's are not contaminated by the adjacent pixels.

With these caveats, we feel that the application of the extinction imaging technique to most test scenarios should be quite straightforward.

12.3. Extinction Imaging for Operational Support

In this section, we discuss the fully automated application of shipboard support. It is our (hopefully unbiased) opinion that the EI concept is the most practical system approach for determining the beam transmittance in all directions, as discussed in Section 2.4. The MSI and SRI are single-ended passive systems that can look in any direction over an extended path. EI systems are expected to be more accurate, more robust and much less costly than any other approach we are aware of.

That being said, there are still some issues that would need to be addressed for 24-hour usage. The first issue is the night application, which is discussed in detail in Section 9, and deserves further research. The second is the case of gloss on the ocean, which is discussed in detail in Sections 8.5.2 and 9.3. Gloss may or may not be an issue depending on the application, but it probably deserves further research.

For a shipboard environment, it will be necessary to deal with the moving platform. It is important that the image include some portion of both the horizon and the ocean surface. Depending on the character of the ship, this may indicate either placement of the unit on a stable table, or other stabilization optics, perhaps combined with a slightly larger field of view to accommodate changes in the level of the table. For use on an aircraft carrier, a stable table or stabilization optics may not be required, but it may be required for smaller craft.

It is also important to be able to characterize the range to the target. In our project, we knew the location of each pixel with respect to the horizon, and could derive the range to an ROI knowing the resolution and altitude of the system. For a ship, if the position of the horizon in the image becomes variable, it would be important to be able to predict the horizon location. This would require making use of the ship's pitch and roll measurements that we understand are available on a ship. If a stable table or other image alignment is used to mount the camera, it would be necessary to either have an accurate readout of the alignment corrections made by the table, or else have a direct measure of the table position with respect to a horizontal plane. With these data, the location of the horizon could be determined in the direction of the line of sight. We verified early in the program that the Navy ships provide very accurate real-time assessment of the ship parameters.

Although we are not knowledgeable about active defense systems on Navy ships, we can make suggestions that may be useful for the application of the EI technique to a defense system for incoming hostile targets. For this application, we would anticipate that the EI system would, prior to the event, continually monitor the full surround, perhaps at 30º azimuth intervals and 10 minute intervals. The system could routinely report the average of these conditions in all directions (perhaps additionally reporting the beam

transmittance for a 5 km slightly-slanted path). The EI system could be programmed such that once a target is detected, it continually monitors the atmosphere in the direction of the target, reporting extinction coefficients. The extinction algorithm and the slant path transmittance algorithm would be integrated into the camera control software. The EI system would input the constantly changing angle and range to target provided by the ship in real time. It could then derive and report estimated beam transmittance from the ship to the target. As the target position and range are continually updated in real time, the EI system could continually update the beam transmittance to the target in real time. This information could in turn be used in a tactical decision aid or input to other programs. [Recommendation]

Although we have only addressed a few applications for the EI technique, we believe there are many programs in which the determination of extinction coefficients and/or beam transmittances over extended paths would be very useful. The EI concept is a very flexible one. Although we have only applied it with black plaques and with the ocean surface as a target, we believe that it could be extended to use many different kinds of "targets of opportunity", as long as the target is reasonably dark and well-behaved.

13. CONCLUSIONS

Section 13.1 reviews the specific findings and recommendations discussed in the text of the report, in the order they appeared in the report. There is some redundancy in this section, as some of the more important findings and recommendations are mentioned in more than one section. This is included so that one can refer back to the more detailed discussion in the sections. A more general discussion of the results and conclusions is included in Section 13.2.

13.1. Findings and Recommendations

Section 5:
Finding: Based on modeling, it appears that the use of a visible instrument acquiring data in the red or NIR filter should be able to predict the extinction near 1.06 or 1.6 μm in the SWIR with reasonable accuracy. The use of two visible or NIR filters should enhance the accuracy.

Section 8.3:
Recommendation: For systems developed in the future, we recommend that developers be aware of camera calibrations, and measure and apply calibrations is needed for the desired system accuracy. Usually uniformity and dark corrections are easy and important, and linearity correction may or may not be important. For the SWIR camera we used, applying calibrations made a significant difference.

Section 8.4:
Finding: The inherent contrast of the ocean surface with respect to the horizon on the red wavelength is very well behaved, and independent of solar angles and weather conditions. We found that the optimal values for the wavelengths we used were -.85 in the red, and -.73 for the SWIR. In addition, the residual uncertainties in the inherent contrast result in small errors, except under very clear conditions. This result implies that it is acceptable to use the ocean surface as a dark target in these wavelengths.

Section 8.5.1:
Finding/Recommendation: Algorithm features designed to deal with white caps, boats in the ROI, and some other abnormalities work very well. We recommend these features be included by future developers in their extinction algorithms.

Section 8.5.2:
Finding/Recommendation: The glitter feature in the algorithm worked very well. It was able to handle many glitter conditions, and flag other conditions that were not well handled. We recommend this feature be included by future developers. For those cases that are flagged, we recommend that the instrument be programmed to acquire additional imagery just outside the glitter region, and use these images to estimate the extinction coefficient.
Finding: We were unable to develop an algorithm feature to handle gloss conditions. See Section 9.3 for more discussion of gloss.

Section 8.5.3:
Finding/Recommendation: The algorithm features designed to deal with clouds on the horizon appear to work very well. We recommend these features be included by future developers

Section 8.5.4:
Finding/Recommendation: The other algorithm features testing for offscale data or results are also important. We recommend these features be included by future developers.

Section 9.1:
Finding: The Sep 2008 data set showed that the MSI extinctions are reasonably well related to the other instruments. An evaluation of the imagery showed that when they disagreed, the MSI results were more accurate than the shore-based instruments for these extended paths. Also the MSI extinctions were well related to relative humidity.

Section 9.2:
Finding: The Feb 2010 data set showed that the MSI and SRI data were well related, further supporting the finding from Section 5 and 9.1.
Finding: The Feb 2010 data set showed that the MSI/SRI and Vaisala PSM related much better than the PSM and the transmissometers, which are the gold standard. Furthermore, evaluation of the imagery of the islands showed that the MSI/SRI derived extinctions compared well with the estimated weather conditions based on the imagery.
Finding: Evaluation of specific cases in which the MSI/SRI and PSM disagreed showed that the disagreement was due to non-uniform haze and fog conditions along the path, and that the extended path MSI/SRI measurements were more accurate than the shore-based PSM measurements for the extended path.
Finding: Although gloss cases were clearly related to low wind speed, our data did not show a tight enough relationship to use our wind speed as a tight predictor.

Section 9.3:
Finding: The 2012 and 2013 data sets showed similar results to those related earlier, i.e. MSI and SRI are well related to each other and to the haze amount estimated from the appearance of the islands in the imagery.
Finding: The effect of gloss is much stronger in the SWIR than in the red filter.
Recommendations regarding gloss:
a) Evaluate the possibility of using two wavelengths to detect and avoid gloss.
b) Evaluate the possibility of using two crossed polarizers to detect and avoid gloss.
c) Evaluate the possibility of using wind speed to predict and avoid gloss.
d) If none of the above is effective, and gloss is expected to be an issue for the desired tests or uses of EI systems, consider using a visible system acquiring data with red filters and using modeled extrapolation to the SWIR.

Section 9.4:

Finding: Given the MSI inherent contrast values of -.85 ± .05, the resulting uncertainty in extinction is less than 4% for visibilities of 18 km or less, and greater than 15% for visibilities of 30 km or more. The uncertainties in the SRI extinctions are similar.

Finding: For the MSI, we estimated the range uncertainty to be 7.4 ± 0.4 km. The median resulting offset extinction ratio was 5.3%. Similarly, for the SRI, the estimated range uncertainty was 6.4 ± 0.4 km, and the median resulting offset ratio was 6.3%. By comparison, the median offset ratio between the two gold-standards, i.e. the transmissometer and the PSM, was 62% for this data set.

Finding/Recommendation: The impact of the linearity on the SRI extinction, if the linearity correction were not applied, would be about 18%. In addition to the uniformity and dark calibrations, we recommend applying linearity corrections unless this uncertainty is acceptable.

Finding: For a moderate target range of about 4.75 km, the resulting uncertainty due to measurement uncertainty is less than 2% for most visibilities, and increases significantly for very foggy conditions with visibilities less than about 3 km.

Recommendation: We recommend that future developers measure their measurement uncertainty for the ROI average. Using this uncertainty, as well as the estimated uncertainty in their range measurements, it should be possible to run calculations to determine anticipated errors as well as minimum target ranges that can be used for the desired range of conditions. [Recommendation]

Section 10.2:

Finding: The SRI camera we used was not sensitive enough to acquire night imagery.

Finding: The MSI was able to acquire excellent night imagery. The measured flux levels were about 6.6 logs ($10^{6.6}$) darker under starlight than under daylight.

Recommendation: In darker locations, the scene may be darker than our measurements. From the data, we anticipate that if a new extinction imager is developed for Day and Night capability, it will need to be able to acquire an additional 7 logs or more of extended sensitivity beyond the dynamic range in an individual image.

Section 10.3 and 10.4:

Finding: The measured brightness of the ocean was not well related to the meteorological conditions under starlight conditions. This would make use of the ocean surface for a dark target potentially problematic.

Recommendations regarding night determinations. There are several recommended approaches, any one of which may be effective:

a) Test to determine if the ocean surface brightness problem is caused by bioluminescence, and if so use wavelengths that avoid the bioluminescent bands (Section 10.3 & 10.4)

b) Develop an algorithm based on the gradient at the horizon (Section 10.3 & 10.4)

c) Use a dark target on the ship or on another ship or drone with the EI technique (Section 10.4)

d) Develop an imaging transmissometer at a non-visible wavelength, with self-aligning logic inherent in the system logic (Section 10.4)

e) Use multiple wavelengths to detect and avoid portions of the ocean surface that are not appropriate targets (Section 10.4)
Recommendation: We feel that further evaluation of extinction imagers for night capability is worth pursuing by future researchers

Section 11.1.2:
Finding: From a study of measured scattering coefficient profiles measured previously by AOG, we found that in the absence of clouds, the vertical profile of scattering coefficient can usually be represented by two well mixed layers, and that deviations from this model generally cause relatively small errors in the estimated path transmittance.
Previous Finding: Within well mixed layers, the scattering coefficient vertical profile can be represented using a fixed mixing ratio.

Section 11.2:
Finding: To insert clouds, we found that we were able to develop an algorithm to extract cloud base and top and approximate Q value from ceilometer data – otherwise cloud base estimates are used.
Finding/Recommendation: Haze top estimates from the ceilometer are sometimes valid. We recommend further evaluation of the ceilometer haze top data.

Section 11.3:
Findings: The error analysis in this section lists which inputs are important. The most significant input that is not well known or measured is the height of the haze top, if the path extends above the top of the haze.
Recommendation: A lidar which is strong enough to provide a good measure of the haze top altitude would be a good adjunct to the MSI. This should be much simpler than developing a simple and robust lidar that could measure extinction coefficient.

Section 11.4:
Recommendation: The slant path algorithm is very useful as a stand-alone program for parameter evaluations.
Recommendation: The slant path algorithm could be integrated into the extinction algorithm for real time processing.
Recommendation: For operational use, we recommend constantly monitoring the surround, then during an event monitoring only the direction to the target. The position of the target could be continually updated to the slant path algorithm. The slant path algorithm could then continually update the estimated transmittance to the target. These values could be used in a tactical decision aid, both for decision-making and for estimating optimal laser power.

Section 12.2.1:
Recommendation: For most applications needing extinction in the SWIR, we recommend using a SWIR camera, as opposed to using a visible camera and extrapolating into the SWIR wavelengths.
Recommendation: For night applications using black targets or the ocean target, a more sensitive camera such as the visible/NIR 16 bit camera used in the MSI is required.

Recommendation: A visible camera may also be needed for situations with high gloss, if gloss cannot be dealt with using other methods.

Section 12.2.2:
Recommendation: Care must be used in camera and software selection and development to ensure that relative radiance levels are maintained within an image.
Recommendation: Uniformity and dark corrections are vital and quite easy, and linearity corrections will enhance the result but may not be required depending on the desired accuracy.
Recommendation: It is important that the acquired data be in a reasonable portion of the camera's sensitive range.
Recommendation: For a system that needs to run all day, addition of flux control logic may be important.

Section 12.2.3:
See this section for general recommendations for adapting the EI system to an operational environment.
Recommendation: For the operational tactical environment, integrate the EI extinction and slant path algorithms into the data acquisition algorithm. Set up the program to automatically read the position and distance to incoming targets, so that the transmittance to target can be continuously updated and fed into a tactical decision aid.

13.2. General Conclusions

Extinction Imaging is a method for determining the effective extinction coefficient over an extended path from one end of the path. It uses calibrated imagers to acquire the relative radiance of a dark target at the end of the path and the horizon sky near the dark target. It is completely passive and thus covert, and the hardware is robust and relatively inexpensive. It uses rigorous equations, which determine the extinction coefficient from the measured apparent contrast of the radiance of the dark target with respect to the horizon sky. The method requires reasonably accurate measurements, as well as an estimate of the inherent contrast (contrast at zero range or with no extinction losses).

In the late 1980's our research group developed an Extinction Imaging system that used targets of opportunity such as dark building features on a distant hill. This system was somewhat limited due to the characteristics of the digital imaging systems available at that time, but it generally worked quite well and is the first use of extinction imagers we know of [18, 19, and 20]. During 2005 - 2007, we developed an Extinction Imaging system that looked across the San Diego harbor entrance and viewed a black box [1, 2, and 3]. In that project, we demonstrated that the EI concept works very well using a black box for the dark target, and provided accurate results.

Under this project, we extended the capability to use the ocean surface as a dark target instead of a black box. We extended the capability from the visible to the SWIR, and also developed the capability to extend the results from the horizontal to slanted lines of sight. We determined appropriate values of inherent contrast for the red and SWIR

wavebands, and showed that these values are well-behaved and should be reasonably universal.

The current project was funded and supported during 2007 – 2013 by the JTO and ONR. This project was a collaboration between UCSD, the MIT Lincoln Laboratory, and the Naval Postgraduate School (NPS). We fielded a research site on the West side of Point Loma, in the San Diego area, looking out over the Pacific Ocean. This site included a MSI (visible extinction imager) modified for this program, a SRI (SWIR extinction imager) developed for this program, Visible and SWIR Transmissometers, a Point Scatter Meter, a Ceilometer, a Shore Weather Station, and a Buoy Weather Station. Data were collected as needed during 2008 – 2013, and several data periods were extracted for analysis.

In our research, we found that the ocean surface serves quite well as a dark target for determining extinction in the red wavelengths and SWIR. (It should also work for wavelengths between these wavebands.) The EI technique requires knowledge of the inherent contrast between the optical target and the horizon sky. We evaluated this inherent contrast, and found that it was surprisingly invariant, even as a function of solar position. Perhaps more importantly, we found that under most atmospheric conditions, the exact value of the inherent contrast does not affect the determined extinction coefficient significantly except under very clear (no haze) conditions. As a result, we feel that the values determined in this project should be reasonably universal.

The SRI, operating in the SWIR wavelengths, was developed for this project, in order to test the possibility of measuring extinction coefficients in the SWIR bands. For applications demanding extinction coefficients and beam transmittances in the SWIR, there are two ways to provide these values. One method is to take the measurements directly in the SWIR. Although the SWIR cameras we used have more noise and other calibration issues than the visible system cameras, we found that the extinction results were still excellent. Another method is to take measurements in the visible, and use modeling to extrapolate to the SWIR. Based on our modeling and measurements, we feel that this is also a viable approach in the absence of abnormally large absorption.

For daytime use, under most conditions, we recommend that a SWIR camera be used. There are two exceptions to this recommendation. On some days, we noted what we called gloss, which is reflection of light off the ocean surface occurring under low wind conditions. The gloss has a much larger impact in the SWIR. If measurements are being acquired where gloss will be an issue, and the gloss is not addressed with other methods such as polarizers, it may be preferable to acquire data using the red filters. The SWIR camera was unable to acquire useful images at night. At night, we found that the visible imager provided excellent images. The ocean surface inherent contrast was not well behaved under starlight, but this dilemma may yield to further research, and also other dark targets can be used at night.

In our project, we developed extinction algorithms for determining the extinction coefficients for both the visible and the SWIR imagers. These algorithms apply basic

radiative transfer equations, and they include features to correct for sensor characteristics. They also include many features to deal with non-ideal measurement conditions such as upsun glitter, white caps on the ocean surface, clouds on the horizon, etc. These extinction algorithms return the effective extinction coefficient for the extended path to the dark target.

We also developed a slant path transmittance algorithm for determining the optical transmittance for an extended path, both for horizontal paths and for slant paths to higher altitudes. The slant path transmittance algorithm makes use of MSI or SRI extinction coefficients, uses ceilometer data if available, and is based on both atmospheric physics and extensive measurements of scattering coefficient profiles obtained by our group in the past [10, 11, 12].

We have also transferred the EI methodology to Penn State's EOC, in support of a Navy LaWS test program [23]. We discussed the methods, and sent documentation and the algorithms to EOC. The EOC modified the extinction algorithm and methods to their test environment with our collaboration. They used the methods to support laser tests, and the results were excellent.

Our group will not be continuing development of Extinction Imaging, due to the retirement of the primary author. As others continue development of these methods for operational and test environments, we foresee two areas that would benefit in particular from additional research. Although the visible imager acquired excellent night data, the ocean surface was not consistently dark under starlight. This may be due to bioluminescence, in which case use of a blocking filter for those wavelengths may enable use of the ocean surface as a reliable dark target. Otherwise, the extinction imager approach could still be used with other dark targets of opportunity. Various options for adapting the EI techniques to night-time are discussed in Section 10. Also, we found that under low wind conditions with the sun unobscured, gloss could be an issue, particularly in the SWIR bands. We feel this can be addressed with polarizers or other filters, as discussed in Sections 8.5.2 and 9.3.

We were very pleased that the Extinction Imager technique worked so well in the non-optimal ocean environment. We anticipate that this method should be a significant asset in the future, both for the military test and operational applications, and for other general civilian and military research applications.

14. ACKNOWLEDGEMENTS

We would like to recognize and thank the many individuals and organizations that provided support and encouragement during this project. The project was funded by the High Energy Laser – Joint Technology Office (JTO) via the Office of Naval Research. In discussions with JTO, we were advised and worked most directly with Harro Ackerman and Albert Ogloza. Our primary Navy contract monitors were John T. Schreimpf (NAVSEA), Sadegh Siahatgar (NAVSEA and ARL, Inc.). Additional individuals providing support from our sponsors included Fred Marcell (NAVSEA and Schafer Corp.), Jeff Bohn (NAVSEA), Quentin Saulter (ONR and JTO), Peter Newton (ARL, Inc.), and Susan Ecker (ARL, Inc.). Without exception the above individuals were most helpful and encouraging, providing very useful experience and advice. We especially appreciate Fred Marcell's help in editing this report.

Within the MPL technical team, we benefitted from the past work of many individuals who are indicated in the reference section. We would particularly like to acknowledge Richard W. Johnson, who was previously deeply involved in the concept and hardware development; Justin Baker, who did much of the hardware design on the first version of the MSI; Eric Slater, who designed some of the modifications to the MSI and SRI; Art Burden, and Jake Streeter who were involved in the early data analysis; and Jerry Crum and our other machine shop personnel. We are very proud of the work of these individuals. We would also like to acknowledge the patient work of the MPL administrative branch, without whose support this work would be impossible.

We would like to thank Dimitris Tsinkidis and the members of the Atmospheric Propagation Branch of the Navy's Spawar Systems Center, who were very gracious in allowing us use of their experimental platform and the other facilities, as well as providing occasional logistics support.

Part way through the program, we were pleased to have the opportunity to work with Jeff Thomas and Thomas Lehecka and their team at Pennsylvania State University's Electro-Optics Center. Our goal was to transfer an understanding of the SRI and its algorithms to their group for use in applied laser tests, and to transfer the algorithms to them. This group was a pleasure to work with, and we were very pleased with their attitude, approach, and results.

15. LIST OF ACRONYMS

AOG	Atmospheric Optics Group
CCD	Charge-coupled device
CFLOS	Cloud Free Line of Sight
CMOS	Complementary Metal Oxide Semiconductor
EI	Extinction Imager or Extinction Imaging
EOC	Pennsylvania State University's Electro-Optics Center (or PSU)
FWHM	Full Width Half Max (used to describe filter passbands)
HSI	Horizon Scanning Imager
IR	Infrared
JTO	The High Energy Laser – Joint Technology Office
LaWS	Navy's Laser Weapons System
MIT	Massachusetts Institute of Technology
MODTRAN	Moderate resolution atmospheric transmission model
MPL	Marine Physical Lab at SIO
MSI	Multispectral Scattering Imager
NIR	Near Infrared (used here to mean bands within the 750 nm to 1 μm region)
NPS	Naval Postgraduate School
ONR	Office of Naval Research
PSM	Point Scatter Meter (Vaisala Present Weather Detector PWD22)
ROI	Region of Interest
SIO	Scripps Institution of Oceanography at UCSD
SPAWAR	Space and Naval Warfare Systems Command
SRI	Shortwave IR Extinction Imager
SSC	SPAWAR Systems Center
STD	Standard Deviation (usually as a percent in this report)
SWIR	Shortwave IR (used here to mean bands within the 1 - 3 μm region)
UCSD	University of California, San Diego
WSI	Whole Sky Imager

16. REFERENCES

Many of the details documented during the project are beyond the scope of the report, and yet may be very useful to others who wish to develop extinction imagers in the future. For this reason, we have referenced many of our technical memoranda (memos) in this report. These are listed in Section 16.1. These are somewhat less formal than reports, as they were primarily intended for in-house documentation, but we have decided that they are sufficiently useful that they should be made available to readers of this report. For the short term, we are transferring these memos and the software to a Box site at: https://app.box.com/s/npjgtxrpz83lh9u1xgu8. This site does not require membership. Going to that side should give the reader the ability to download the documents. We are currently working to upload the report, memos and software to this site.

In the longer term, we hope to have a web site at http://escholarship.org/uc/sio and/or a different site within UCSD or SIO, but this will take longer to accomplish. In addition, we will also provide CD's of these memos to our sponsors and to others on request.

Published references that are available to users are listed in Section 16.2.

16.1. Technical Memoranda available on Web or CD

AV07-014t, "MSI Software" 8 Mar 2007
AV07-015t, "MSI Data Results, Aug and Nov 05 Data" 12 Mar 2007
AV07-016t, "MSI Data Results, Nov – Dec 06 Data" 16 Mar 2007
AV07-026t, "Wavelength Options in Whole Sky Imaging", 3 May 2007
AV07-046t, "Scattering Test Site Calculations", 25 October 2007
AV08-003t, "3 Mar 08 MSI Installation Trip Report", 13 March 2008
AV08-015t, "MSI Window", 13 May 2008
AV08-016t, "MSI Thoughts", 13 May 2008
AV09-003t, "IR Camera Evaluation for the Visibility Project", 29 January 2009
AV09-013t, "Method to pull contrast from MSI data using AutoProcMSI program", 10 February 2009
AV09-014t, "Test to see evidence of MSI image pixel shifting over extended time periods", 10 March 2009
AV09-020t, "RunMSI Version 1.1", 23 February 2009
AV09-031t, "MSI camera re-installation 2 – 5 Mar 2009 and subsequent work", 2 April 2009, revised 23 April 2009
AV09-032t, "MSI Horizon Data Further Analysis and impact on ProcMSI", 3 April 2009
AV09-033t, "Initial Analysis of Transmissometer Data from MSI Site", 10 April 2009
AV09-034t, "Initial Analysis of Vaisala Point Scatter Meter Data from MSI Site", 10 April 2009
AV09-035t, "Initial Analysis of MSI Data", 16 April 2009
AV09-036t, "New Analysis of Transmissometer and Vaisala Data", 16 April 2009
AV09-037t, "New Analysis of MSI Data", 16 April 2009
AV09-038t, "SWIR Extinctions, Modeling and First Images", 16 April 2009
AV09-047t, "Transmissometer Stray Light Test April, May 2009", 3 June 2009

AV09-067t, “MSI Field Calibration Results and Non-Linearity Correction”, 22 July 2009
AV09-073t, “MSI Field Calibration Results and Non-Linearity Correction (reissue of memo AV09-067t with April 2009 calibration data)”, 6 August 2009
AV09-102t, “MSI Uniformity Calibration Result”, 02 December 2009
AV10-002t, “SRI Design and Deployment”, 25 February 2010
AV10-003t, “Transmissometer Diagnosis and Repair”, 25 February 2010
AV10-004t, “Modeling Study of SRI Filtering Requirements”, 11 March 2010
AV10-005t, “Comments on Lidar Costs and Availability”, 17 March 2010
AV10-006t, “Slant Path Transmittance Modeling and Comments”, 25 March 2010
AV10-007t, “MSI Site Data Record”, 31 March 2010
AV10-008t, “MSI Instrument Maintenance Checklist”, 18 May 2010
AV10-010t, “MSI/SRI March Site Repairs”, 25 May 2010
AV10-011t, “Format of the MSI Archival Drives”, 27 May 2010
AV10-012t, “Transmissometer and Vaisala Data for Feb 11 – 26 2010”, 27 May 2010
AV10-013t, “Initial Evaluation of Raw SRI Data for Feb 11 – 26 2010”, 27 May 2010
AV10-014t, “Processing and Evaluation for SRI Data for Feb 11 – 26 2010”, 27 May 2010
AV10-015t, “Resolution and Range Calculations for MSI and SRI”, 22 June 2010 [replaced by method in AV12-022t]
AV10-017t, “SRI Noise Behavior”, 12 July 2010
AV10-018t, “Theory of Operations for the MSI and Results of the Previous Contract”, 12 August 2010
AV10-019t, “Plans for MSI Project, Years 4 and 5”, 5 August 2010
AV10-020t, “The Current MSI and SRI Algorithm Logic and Inputs”, 18 August 2010
AV10-021t, “AutoProcMSI revision history”, 19 August 2010
AV10-022t, “AutoProcSRI revision history”, 23 August 2010
AV10-023t, “Processing and Evaluation of MSI Data for Feb 11 – 26 2010”, 19 August 2010
AV10-028t, “Program AutoProcMSI New Flags”, 22 November 2010
AV10-029t, “The New Glitter Feature in the MSI Extinction Algorithm”, 23 November2010
AV10-030t, “Evaluation of Boats and White Caps in MSI Extinction Algorithms”, 23 November 2010
AV10-031t, “Evaluation of MSI Extinction Magnitudes in the absence of Gloss”, 2 December 2010
AV10-032t, “Changes to MSI Site, Site Status, and Initial Night Tests”, 15 December 2010
AV11-001t, “Vaisala Stray Light Test”, 28 February 2011
AV11-002t, “SRI Camera Calibration Overview”, 2011
AV11-003t, “SRI Camera Linearity vs. Radiance Calibrations”, 3 March 2011
AV11-004t, “SRI Camera Linearity vs. Exposure Calibrations”, 3 March 2011
AV11-005t, “Optimization of Inherent Contrast in the MSI Algorithm”, 09 March 2011
AV11-006t, “RunSRI revision history”, 10 March 2011
AV11-007t, “Additional MSI Uniformity Correction in the MSI Algorithm”, 15 March 2011
AV11-008t, “Impact of SRI Calibrations on Extinction Calculations”, 29 March 2011

AV11-009t, “Impact of Linearity on MSI Extinctions, and Look-up Table Differences”, 5 April 2011
AV11-010t, “MSI Fieldwork and Updated Part Numbers”, 18 May 2011
AV11-011t, “SRI Fieldwork and Updated Part Numbers List”, 18 May 2011
AV11-012t, “MSI Night Tests Interim Results”, 20 June 2011
AV11-013t, “SRI Night Tests Interim Results”, 20 June 2011
AV11-014t, “SRI Fieldwork and Updated Parts List”, 9 August 2011
AV11-015t, “MSI Noise Tests and Analysis”, 9 August 2011
AV11-016t, “Logic for Slant path Transmittance Version 1”, 16 August 2011, Rev. 14 September 2011
AV11-017t, “Program TrAlg Version 1, Slant Path Transmittance Algorithm”, 18 August 2011
AV11-018t, “Transmittance Results from Slant Path Transmittance Algorithm Version 1”, 23 August 2011
AV11-019t, “MPL Test Set for Penn State”, 20 November 2011
AV12-001t, “MSI Camera Housing changes for Night Tests”, 12 January 2012
AV12-002t, “MSI Field Work and Updated Part Numbers and Other Field Work”, 25 January 2012
AV12-003t, “Evaluation of New MSI Night Imagery”, 22 March 2012
AV12-004t, “Spectral Response of the MSI System”, 25 April 2012
AV12-005t, “Spectral Response of the SRI System”, 10 May 2012
AV12-006t, “Further Evaluation of Night Imagery”, 24 April 2012
AV12-007t, “Comparison of MSI Algorithm with S.Q. Duntley’s Developments”, 25 April 2012
AV12-008t, “Sensitivity Study for Use of White Targets”, 26 April 2012
AV12-009t, “Conclusion of SRI Night Tests”, 16 May 2012
AV12-010t, “PSU vs. MPL AutoProcSRI differences”, 17 May 2012

AV12-011t, “MSI and SRI control program revision history”, 7 August 2012
AV12-012t, “Adding Ceilometer Cloud Data to the Slant path Transmittance Algorithm”, 7 August 2012
AV12-013t, “Adding Ceilometer Haze Top Data to the Slant path Transmittance Algorithm”, 8 August 2012
AV12-014t, “Adding Cloud Tops and Horizontal Transmittance to the Slant path Transmittance Algorithm”, 8 August 2012
AV12-015t, “Work by W. Hering Used in Slant Path Algorithm”, 14 August 2012
AV12-016t, “Running the Slant Path Algorithm, TrAlg”, 17 September 2012
AV12-017t, “Impact of Absorption on the MSI/SRI Equations”, 20 September 2012
AV12-018t, “Extracting ceilometer backscatter profile using CL-View”, 09 October 2012
AV12-019t, “Extracting ceilometer haze top using BL-View”, 09 October 2012
AV12-020t, “Slant Path Transmittance Program TrAlg.exe, Version 2.0”, 09 October 2012
AV12-021t, “SRI and MSI Uniformity Calibrations July 2012”, 16 October 2012
AV12-022t, “Range Calculations for SRI and MSI”, 18 October 2012
AV12-023t, “SRI Angular Resolution Check and Resulting Range Calculations”, 29 November 2012

AV12-024t, “MSI Night Measured Contrast under Starlight - Processing”, 19 December 2012
AV13-001t, “MSI Night Measured Contrast under Starlight - Analysis”, 16 January 2013
AV13-002t, “Summary of the Night Extinction Imager Experiments and Suggested Future Directions”, 30 January 2013
AV13-003t, “AutoProcMSI update, Version 2.0”, 5 February 2013
AV13-004t, “MSI processed image headers”, 5 February 2013
AV13-005t, “AutoProcSRI Update Version 2.2”, 6 February 2013
AV13-006t, “SRI processed image headers”, 6 February 2013
AV13-007t, “Impact of Semi-Broadband Data Acquisition on the SRI Extinctions”, 23 April 2013
AV13-009t, “Initial Analysis of Jul – Aug 2012 SRI Data Set”, 20 May 2013
AV13-011t, “Determination of Inherent Contrast for SRI Data using Jul – Aug 2012 SRI Data Set”, 29 July 2013
AV13-012t, “Analysis of Glitter Algorithm for the SRI Jul – Aug 2012 SRI Data Set”, 30 July 2013
AV13-013t, “Analysis and Handling of Gloss for the SRI Jul – Aug 2012 Data Set”, 31 July 2013
AV13-015t, “Horizon Cloud Impacts for the SRI Jul – Aug 2012 SRI Data Set”, 26 August 2013
AV13-016t, “MSI Site Hardware Updates”, 17 October 2013
AV13-017t, “Simultaneous MSI and SRI Data from 2013”, 28 October 2013
AV13-018t, “Simultaneous MSI and SRI Data from 2010 – Additional Results of 2011”, 04 December 2013
AV13-019t, “Reprocessing and Analysis of Simultaneous MSI and SRI Data from 2010”, 05 December 2013
AV13-020t, “AutoProcSRI Software Update Version 2.4”, 18 December 2013
AV14-001t, “The Final MSI and SRI Algorithm Logic and Inputs”, 9 April 2014

16.2. Published References

References with an ADA number are available on STINET, http://www.dtic.mil/dtic/search/gtips.html by entering the ADA number.

1. Berger, P. J., S. M. Hammel, P. A. Frederickson, J. E. Shields, S. Siahatgar, D. Tsintikidis, S. Di Cecca, M. E. Karr, D. Merritt, L. Farrar, D. Kichura, K. Gutekunst, R. W. Johnson, A. R. Burden, J. G. Baker, J. H. Glover, and K. Jones, *Navy Atmospheric Measurements at Zuniga Shoal: February 2005 – December 2006*, MIT Lincoln Laboratory Report. This report is “For Official Use Only”, but can be requested by qualified individuals from the MIT Lincoln Laboratory.
2. Shields, J. E., J. G. Baker, M. E. Karr, R. W. Johnson, and A. R. Burden, *Visibility measurements along extended paths over the ocean surface*, International Symposium on Optical Science and Technology, SPIE the International Society for Optical Engineering, August 2005
3. Shields, J. E., J. G. Baker, M. E. Karr, R. W. Johnson, and A. R. Burden, *Multispectral scattering measurements along extended paths using an imaging system,* International

Symposium on Optical Science and Technology, SPIE the International Society for Optical Engineering, August 2006
4. Koschmeider, H., *Theorie der horizontalen Sichtweite*, Beitr. Phys. frein Atmos. **12**, 33-53 (1924)
5. S. Q. Duntley, A. R. Boileau, and R. W. Preisendorfer, *Image Transmission by the Troposphere I**, Journal of the Optical Society of America, Vol. 47 No. 6 499-506 (1957)
6. Boyd, R. W., *Radiometry and the Detection of Optical Radiation*, a volume in the Wiley Series in Pure and Applied Optics, S. S. Ballard Founder, J. W. Goodman Advisory Editor, John Wiley & Sons, New York/Chichester/Brisbane/Toronto/Singapore (1983)
7. McCluney, R., *Introduction to Radiometry and Photometry*, Artech House, Boston, London (1994)
8. McCartney, E. J., *Optics of the Atmosphere*, a volume in the Wiley Series in Pure and Applied Optics, S. S. Ballard Advisory Editor, John Wiley & Sons, New York/London/Sydney/Toronto (1976)
9. Liou, K. N., *An Introduction to Atmospheric Radiation*, International Geophysics Series Volume 26, Academic Press, New York, London, Toronto, Sydney, San Francisco (1980)
10. Duntley, S. Q., R. W. Johnson, J. I. Gordon, and A. R. Boileau, 1970, *Airborne Measurements of Optical Atmospheric Properties at Nigh*", University of California, San Diego, Scripps Institution of Oceanography, Visibility Laboratory, SIO Ref. 70-7, AFCRL-70-0137, NTIS No. AD 870 734.
11. Duntley, S. Q., R. W. Johnson, and J. I. Gordon, 1975, *Airborne Measurements of Optical Atmospheric Properties in Western Washington*, University of California, San Diego, Scripps Institution of Oceanography, Visibility Laboratory, SIO Ref. 75-24, AFCRL-TR-53-0414, NTIS No. ADA 026 036.
12. Duntley, S. Q., R. W. Johnson, and J. I. Gordon, 1977, *Airborne Measurements of Atmospheric Volume Scattering Coefficients in Northern Europe, Spring 1976*, University of California, San Diego, Scripps Institution of Oceanography, Visibility Laboratory, SIO Ref. 77-8, AFGL-TR-77-0078, NTIS No. ADA 046 290.
13. Gordon, J. I., and R. W. Johnson, 1985, *Integrating Nephelometer: Theory and Implications*, Applied Optics 24, page 2721, August 15 1985.
14. Curcio, J. A. and K. A. Durbin, *Atmospheric Transmission in the Visible Region*, Report 5368, Naval Research Laboratory, Washington, DC (1959)
15. Hood, J. H., 1964, *A Two-Cavity Long-Base Mode Meteorological Range Meter*, Applied Optics Vol 3, Page 603, May 1964.
16. Malm, W. C., G. Persha, R. tree, R. Stocker, I. Tombach, and H. Iyer, *Comparison of Atmospheric Extinction Measurements made by a Transmissometer, Integrating Nephelometer, and Teleradiometer with Natural and Artificial Black Target*, Air Pollution Control Association Specialty Conference, Grand Teton National Park, Wyoming, 7 – 10 September 1986
17. Malm, W. C., *Considerations in the Accuracy of a long-path transmissometer*, Aerosol Science & Technology, 14:459-471, 1991.
18. Johnson, R. W., W. S. Hering, and J. E. Shields, *Automated Visibility and Cloud Cover Measurements with a Solid State Imaging System*, University of California, San

Diego, Scripps Institution of Oceanography, Marine Physical Laboratory, SIO 89-7, GL-TR-89-0061, NTIS No. ADA216906, 1989.
19. Shields, J. E., R. W. Johnson, and M. E. Karr, *An Automated Observing System for Passive Evaluation of Cloud Cover and Visibility*, University of California, San Diego, Scripps Institution of Oceanography, Marine Physical Laboratory, SIO 92-22, PL-TR-92-2202, 1992.
20. Johnson, R. W., T. L. Koehler, and J. E. Shields, *A Multi-Station Set of Whole Sky Imagers and A Preliminary Assessment of the Emerging Data Base*, Proceedings of the Cloud Impacts on DOD Operations and Systems, 1988 Workshop, pp. 159 – 162 1988.
21. Shields, J. E., R. W. Johnson, and M. E. Karr, *A Sensitivity Study of Daytime Visibility Determination with a Horizon Scanning Imagery*, University of California, San Diego, Scripps Institution of Oceanography, Marine Physical Laboratory, SIO 91-15, PL-TR-91-2189, 1991
22. Janeiro, F. M., F. Wagner, P. M. Ramos, A. M. Silva, *Automated Atmospheric Visibility Measurements using a digital camera and image restoration*, Proceedings of the First IMEKO TC19 International Symposium on Measurements and Instrumentation for Environmental Monitoring, Iasi, Romania, 2007.
23. Lehecka, T., K. Jones, P. Kazunas, and J. Thomas, Final Report: *Atmospheric Extinction Imaging System for LaWS, Contract # N00024-02-D-6604, Delivery Order 0754*, December 2012. This report is "For Official Use Only", but can be requested by qualified individuals from the Penn State Electro-Optics Center.
24. Shields, J. E., M. E. Karr, R. W. Johnson, and A. R. Burden, *Day/Night Whole Sky Imagers for 24-h cloud and sky assessment: history and overview*, Applied Optics Vol. 52 No. 8 pg. 1605-1616, Mar 10 2013
25. Shields, J. E., R. W. Johnson, and T. L. Koehler, *Automated Whole Sky Imaging Systems for Cloud Field Assessment*, Fourth Symposium on Global Change Studies, American Meteorological Society, 1993.
26. Shields, J. E., R. W. Johnson, M. E. Karr, and J. L. Wertz, *Automated Day/Night Whole Sky Imagers for Field Assessment of Cloud Cover Distributions and Radiance Distributions*, Tenth Symposium on Meteorological Observations and Instrumentation, American Meteorological Society, 1998
27. Shields, J. E., R. W. Johnson, M. E. Karr, A. R. Burden, and J. G. Baker, *Daylight Visible/NIR Whole Sky Imagers for Cloud and Radiance Monitoring in Support of UV Research Programs*, International Symposium on Optical Science and Technology, SPIE the International Society for Optical Engineering, 2003
28. Shields, J. E., 1981, *An Analysis of Infrared and Visible Atmospheric Extinction Measurements in Europe*, University of California, San Diego, Scripps Institution of Oceanography, Visibility Laboratory, SIO Ref. 82-4, AFGL- TR-81-0251, NTIS No. ADA-123-999.
29. Shields, J. E., 1983, *An Analysis of Infrared and Visible Atmospheric Extinction Coefficients Measured at One-Minute Intervals*, University of California, San Diego, Scripps Institution of Oceanography, Visibility Laboratory, SIO Ref. 84-1, AFGL- TR-83-0210, no NTIS No., available on the AOG web site.
30. *Optec, Inc., Model LPV-3 and Model LPV-4 Long Path Visibility Transmissometer, Technical Manual for Theory of Operation and Operating Procedures*, 199 Smith St, Lowell, MI, 49331, November 2011, available at web site:

http://www.optecinc.com/visibility/pdf/lpv_3&4_technical_manual_rev4.pdf
31. Vaisala, *Present Weather Detector PWD22, User's Guide, M210543EN-C, March 2004*; a Jan 2004 version is available at web site:
ftp://ftp.cmdl.noaa.gov/aerosol/doc/manuals/PWD22_Manual.pdf
32. Eloranta, E. W., *High Spectral Resolution Lidar* in *Lidar: Range-Resolved Optical Remote Sensing of the Atmosphere*, Klaus Weitkamp editor, Springer Series in Optical Sciences, Springer-Verlag, New York, 2005.
33. Huschke, R. E., editor, *Glossary of Meteorology*, American Meteorological Society, Boston, (1959, reprinted 1998)
34. Berk, A., G.P. Anderson, P.K. Acharya, L.S. Bernstein, L. Muratov, J. Lee, M. Fox, S.M. Adler-Golden, J.H. Chetwynd, M.L. Hoke, R.B Lockwood, J.A. Gardner, T.W. Cooley, C.C. Borel, P.E. Lewis and E.P. Shettle, *MODTRAN5: 2006 Update*, Proc. SPIE, Vol. 6233, 62331F, 2006.
35. Vaisala, *Ceilometer CL31 User's Guide, M210482EN-B October 2004* available at web site:
http://www.iag.co.at/uploads/tx_iagproducts/pdf_handbuch/CL31.de.pdf
36. Brown, D. R. E., *Natural Illumination Charts*, Report No. 374-1 on Project NS 714-100, Department of the Navy, Bureau of Ships, Washington D.C. (1952)
38. Hering, W. (1983), *Analytic Techniques for Estimating Visible Image Transmission Properties of the Atmosphere*, University of California, San Diego, Scripps Institution of Oceanography, Visibility Laboratory, SIO 84-6, AFG:-TR-83-0236
39. Bucholtz, A. (1995), *Rayleigh-scattering calculations for the terrestrial atmosphere*, Applied Optics Vol. 34 No. 15 20 May 1995.

Appendix A: MSI Chapter from the Zuniga Shoals Report

As discussed in Ref. 20, much of the development of the MSI occurred under the Zuniga Shoals project. Under this project, we developed the MSI hardware, and tested it looking across the entrance to the harbor at a black box target. The report for the Zuniga Shoals project is restricted to "For Official Use Only". However we have received permission from my sponsors for that project the MSI chapter to include the MSI chapter in this report, which is not restricted.

This chapter is a shortened version of the chapter that we originally submitted, and it also uses symbols for the parameters that are different from the ones we usually use. The more detailed discussion of the theory and results is included in Memo AV10-018t. We recommend that users who are interested in the details of the theory refer to this memo. However, we also wish to include the chapter from the report as it was published, as it is a more concise version. This is included below, in this appendix. In order to hopefully avoid confusion with the main body of the current report, we have changed section, figure, and equation numbers from the 8- that was used in the original, to A-.

Chapter A (8). Multispectral Scattering Imager

Janet E. Shields, Richard W. Johnson, Monette E. Karr, Justin G. Baker, and Art R. Burden
Marine Physical Laboratory, University of California San Diego
and
Paul J. Berger
MIT Lincoln Laboratory

Visibility measurements are often made in atmospheric measurement programs. Commercially available visibility sensors provide point measurements of the scatter. Visibility over long paths can be made from visual range estimates,; however, their utility is often limited by the subjectivity of the observer. The Multispectral Scattering Imager (MSI) was developed under this program to provide instrumented visibility-based measurements over long paths. The MSI was installed at the Zuniga field site along a parallel path to the transmissometers. The extinction measurements derived from the MSI were in good agreement with the extinction measurements derived from the 0.55-μm transmissometer.

A.1 Introduction

The objective of this part of the program was to develop an instrumented version of a visibility sensor and determine whether the instrument can provide reliable integrated-path measurements of the extinction coefficient. A visibility measurement (more properly a contrast-based measurement) requires a sensor at one end of the path and a passive reference target at the other end of the path. This singled-ended measurement is much easier to implement than a transmission measurement, which requires attention to instruments at both ends of the path.

Visibility measurements are often made in atmospheric measurement programs. In its most simple form, an observer looks for objects at known distances and selects an object which is just discernible. The extinction coefficient in the photopic band is determined from this visual range by Koschmeider's formula, $\alpha = 3.912/VR$ [A-1]. In practice, many ranges do not have an adequate number of objects at known distances and selecting the barely discernible object depends is somewhat subjective. Various instruments have been built to overcome these limitations, for instance, the optical pyrometer used in the NRL experiments [A-2] and teleradiometers [A-3] used in the air quality monitoring programs in the national parks. Measurements with these instruments require skilled operators and are not suitable for long-term unattended operation.

The University of California San Diego (UCSD) Marine Physical Laboratory (MPL) developed a new instrument for this program, with the goals of providing accurate measurements with an instrument capable of unattended operation. This instrument, called a Multispectral Scattering Imager (MSI), was based on UCSD's extensive

experience in building and operating a Horizon Scan Imager (HSI) for extended path visibility measurements and Whole Sky Imagers (WSI) for cloud cover measurements [A-4 – A-10]. The MSI was designed to acquire calibrated radiance images in four wavelength bands over extended paths. From measurements of the horizon radiance and the radiance of dark targets, combined with measurements of the inherent properties of the dark targets, visibility and effective scattering coefficient over the integrated path can be determined.

A.2 Theory of Operation

A rigorous set of equations describing the operation of the MSI is given by Shields [A-11]. In this report, we use a simpler formulation given in Houghton [A-12] to present the basic concepts. Figure A-1 illustrates a camera viewing a black object at a distance L against a horizontal sky. The black object does not radiate any light into the camera, however, light scattered by the air between the black object and the camera radiates light in a pixel viewing the black object, making the object appear lighter. An elementary volume at a distance z from the observer has an area $A = (\text{ifov } z)^2$ where ifov is the field-of-view subtended by a pixel in the imaging camera and a length dz. This volume is illuminated by the sun and light scattered into the volume by the environment. A fraction of this incident illumination is scattered back to the observer and attenuated on the way back by atmospheric extinction. The scattered light received by a single pixel in the camera from this elementary volume is

$$dB_O = c\,k_s\,E_o\,(ifov\,z)^2\,dz \exp\{-\alpha_{Ext}\,z\}\left(\frac{A_{Cam}}{z^2}\right) = c'\,k_s\,E_o\,dz \exp\{-\alpha_{Ext}\,z\} \qquad \text{(A-1)}$$

where E_o is the illumination from the sun, A_{Cam} is the collecting area of the camera system, k_s is the scattering coefficient, α_{Ext} is the extinction coefficient, and c and c′ are scale factors. The total light received by a pixel viewing the black object is obtained by integrating this expression from 0 to L. Assuming that the sun illumination and atmospheric parameters are independent of z, we have

$$B_O = c'\,E_O \frac{k_s}{\alpha_{Ext}} [1 - \exp\{-\alpha_{Ext}\,L\}] \qquad \text{(A-2)}$$

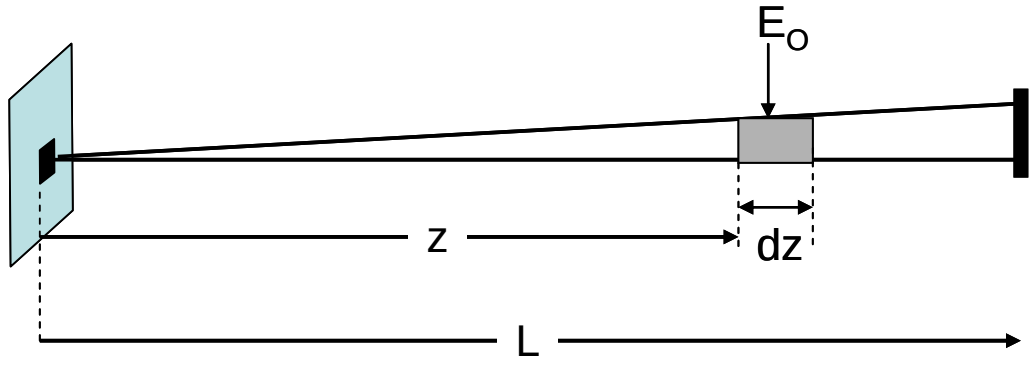

Figure A-1. Light scattering into camera viewing black object

The scattered light received by an adjacent pixel in the camera that views the horizon is obtained by integrating Equation (A-1) from 0 to infinity, giving

$$B_H = c' E_O \frac{k_s}{\alpha_{Ext}} \tag{A-3}$$

The contrast between the black object and the horizon is defined by $C = (B_H - B_O)/B_H$. From Equations (A-2) and (A-3), we have

$$C = \frac{B_H - B_O}{B_H} = \exp\{-\alpha_{Ext} L\} \tag{A-4}$$

and

$$\alpha_{Ext} = \frac{1}{L} \ln(1/C) \tag{A-5}$$

The visual range of a black object viewed against the horizon sky is given by

$$VR = \frac{\ln(1/\varepsilon)}{\alpha_{Ext}} \tag{A-6}$$

where ε is the minimum contrast detectable by the human eye. Visibility is generally measured in the photopic band, matched to the spectral response of the human eye. In the photopic band, ε is usually taken as 0.02, but can range from 0.01 to 0.05 depending on target size, observing conditions, and the observer's acuity and motivation. With ε = 0.02, ln(1/ε) = 3.912, we have Koschmeider's formula α = 3.91/VR. Note that, although scattering is the mechanism that gives rise to contrast changes, the measurement actually returns the extinction coefficient.

A.3 MSI Description

The system, shown in Figure A-2, includes a 512 × 512 16-bit digital CCD camera, a filter changer, and a Sigma 170 – 500 mm zoom lens with a doubler. The filter changer has two filter wheels. One wheel contains four spectral filters: blue (450 nm), green (550 nm), red (650 nm), and NIR (800 nm). Each of the filters has a FWHM bandwidth of approximately 40 nm, although 70 nm filters were used in the initial experiments. The spectral width of the green filter is similar to the photopic band and we will refer to data acquired with the green filter as the photopic band data. A second filter wheel contains neutral density filters that may be used to adjust the flux levels. Unlike the more common 24-bit color camera with 8-bit resolution in each color, this system has 16-bit (65,536 grey levels) in each spectral filter, as well as additional neutral density filters and exposure control for a useful dynamic range of over 10 logs or 10^{10}. The experiments reported in this document were taken at f# 350 with a doubler, and the resulting image has a 2.25° field of view.

Figure A-2. MSI sensor head, with zoom lens and 16-bit digital CCD camera

The measurements were made over a 7.07-km path across Zuniga Shoal, just outside San Diego bay. The shed containing the MSI sensor head and controller and the black target are shown in Figure A-3. The black target consists of a hollow black box 8' on a side and 12' deep.

Figure A-3. MSI installation at Zuniga Shoal: (right) shed containing sensor head at Ballast Point, and (left) black target at Naval Amphibious Base

The measured reflectance of the paint used for the target varied from 3.1% to 3.3% in the blue through the NIR wavelengths. The inherent contrast of the target with respect to the horizon was measured throughout two days at the angle of the line of sight of the experiment. The results are shown in Table A-1. The results are quite close to –1,

and relatively invariant as a function of time and spectral filter. The average values for each filter shown in Table A-1 were used in the processing.

Table A-1. Measured Inherent Contrast of the Target

Local Time	Blue	Green	Red	NIR
0900 – 1030	- 0.981	- 0.979	- 0.982	- 0.988
1030 – 1145	- 0.990	- 0.987	- 0.990	- 0.993
1300 – 1430	- 0.990	- 0.988	- 0.989	- 0.992
1440 – 1535	- 0.992	- 0.991	- 0.993	- 0.994
Average	- 0.988	- 0.986	- 0.988	- 0.992

Figure A-4(a) shows an image for a very clear day, often associated with Santa Ana wind conditions. Figure A-4(b), extracted from Figure A-4(a), shows the dark target (the black square above the sand.) The black target occupies approximately 5 × 5 pixels, of which we extract a 3 × 3 region for the visibility determination.

Figure A-4(a). Image on 4 Dec 2005
V = 74 km, S = 0.04 km^{-1}

Figure A-4(b). Zoomed image showing black target (tip of arrow) at 7.07-km range

Figures A-5 – A-6 show sample imagery acquired with the green filter along with the extracted scattering coefficients and visibility results. Figure A-5 shows an image for light haze. On this day, the Los Coronados Islands in Mexico were clearly visible at 40-km range from Point Loma. Figures A-6 and A-7 show images for moderate haze and fog. It should also be noted that we have not shown the full dynamic range of the system

in the images. The sensor has 65,535 grey levels, with a readout noise of 1 count (and a shot noise that depends on signal level). This high radiometric-resolution data is available for data processing and results in reasonable determinations even under fog conditions, when the target is not easily discerned in the image, as shown in Figure A-7.

Figure A-5. 30 Nov 2005 V = 46 km, S = 0.066 km^{-1}

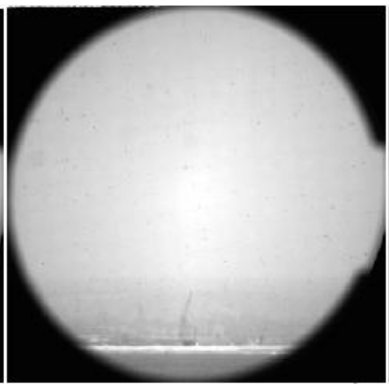

Figure A-6. 17 Nov 2005 V = 29 km, S = 0.10 km^{-1}

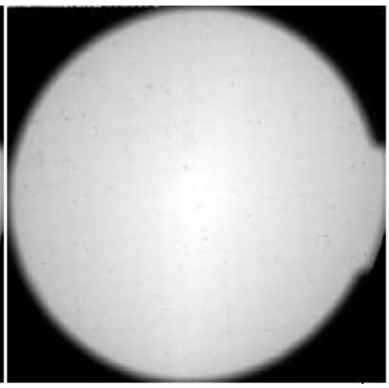

Figure A-7. 30 Aug 2005 V = 10 km, S = 0.30 km^{-1}

We now discuss three factors that can influence the accuracy of the extinction measurements determined wit h the MSI. First, the inherent target contrast with respect to the horizon is an important input. We carefully measured this contrast in the direction of the path of sight from a range of a few feet prior to the deployment. We found that the contrast was quite close to an ideal black target, with contrasts ranging from – 0.986 to – 0.992. The average value for the day was used for each filter, and the variation over the day was about 0.004. Although a perfect black target is not necessary for use with the MSI, earlier sensitivity studies showed that results are most accurate when the target contrast is reasonably dark.

Second, as shown in Figures A-4, the line of sight to the "horizon" is somewhat higher than the line of sight to the target. We did not have a horizontal line-of-sight to the sky due to the presence of mountains. Although the difference appears extreme in the imagery, the difference in angle is actually only 1.6 degrees. In Figure A-8 we illustrate the geometry and show how the terms used in calculating the light received by the camera vary between a horizontal path and a slant path. We see a competition between the different terms: at each range slice, the scattering will be lower at ΔH, but the illumination from the sun and sky will be higher at Δh and the transmission to the camera will be higher due to the reduced extinction at Δh. We have evaluated the Equation (A-1) for the horizontal and slant paths to determine two values of B_H to use in calculating the contrast ratio. If there more light is received from the slant path, the contrast ratio will be higher and the calculated extinction coefficient will be lower than a measurement made to a level horizon. Figure A-9 shows the results of a calculation using the simple assumptions shown Figure A-8 with an e-folding height of 2000 m. This figure compares the extinction coefficients calculated using the B'_H from the slant path versus B_H from the horizontal path. This scatter plot shows an S-shape – the measured extinction coefficient

is too high at the low end and too low at the high end. This figure suggests that the elevated horizon might pose a problem – more detailed calculations are needed to quantify this effect.

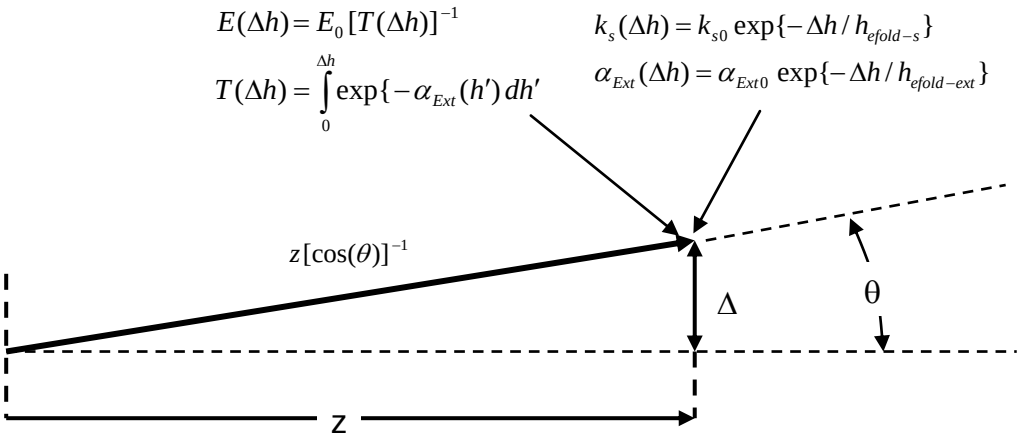

Figure A-8. Terms involved in calculating the received scattered light from a slant path and a horizontal path

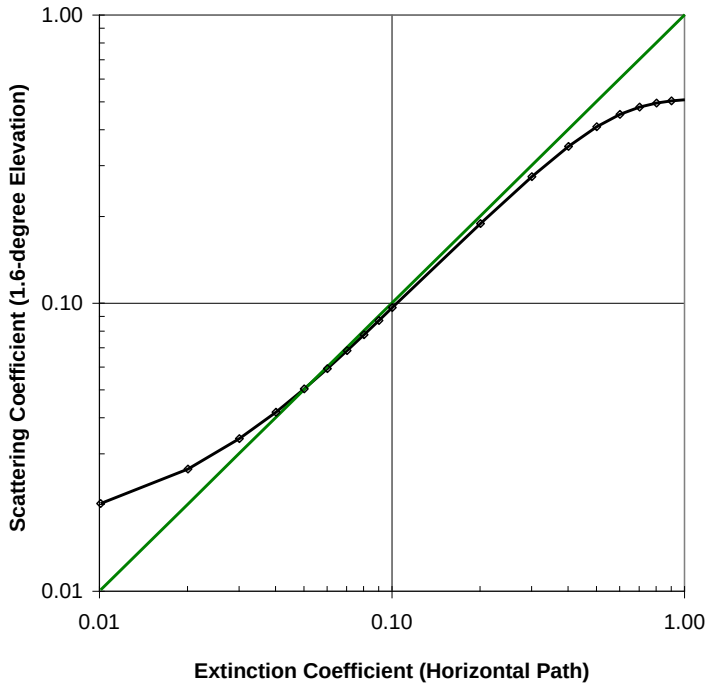

Figure A-9. Comparison of extinction coefficients determined with B'_H from slant path and B_H from horizontal path.

Third, image quality is important. The acquired images are corrected for the camera bias and dark levels. The system is carefully calibrated, and non-linearity corrections are

made. The linearity calibration is defined as a correction to the relative signal change as a function of radiance change. At signals of 100 near the low end, the correction is about 2% with respect to a signal of 10,000, and at signals over 40,000 the correction is about 4% in the other direction, with the correction varying smoothly over the full measured range. We made a uniformity correction for the target and horizon extracted Region of Interest (ROI). The uniformity calibration is defined as a correction for pixel-to-pixel sensitivity differences in the image caused by lens, filter and CCD effects. Figure A-10 shows an enlarged image of the target and regions around the target for a high extinction case ($\alpha_{Ext} \sim 0.3$ km^{-1}). The specks in the imagery are due to the non-uniformity of the fiber optic taper used in this system. These are corrected for with the non-uniformity correction. Figure A-11 shows an example of a partial uniformity correction. (The normal flat field is done at full resolution in floating point; this figure was a partial correction done with integers.) There is still some residual granularity in the image, showing that pixel-to-pixel non-uniformity correction is needed for accurate contrast measurements at high extinction. The sensor has 65,000 grey levels and a readout noise of about 1 count, so features are available to the algorithm that cannot be seen in the imagery. This is why the algorithm returns a non-zero visibility for these very foggy cases. The algorithm is taking advantage of the small, but significant, features in the numerical data, to return a reasonable number even when the features are difficult to see in the imagery.

We also investigated the effect of crosstalk on the light received from the target region. The target is right next to the highly reflective beach sand, and there may be an impact due to scattering of light (optical cross-talk) within the system. We measured cross talk, and experimented with corrections, but found that corrections did not appear to be necessary.

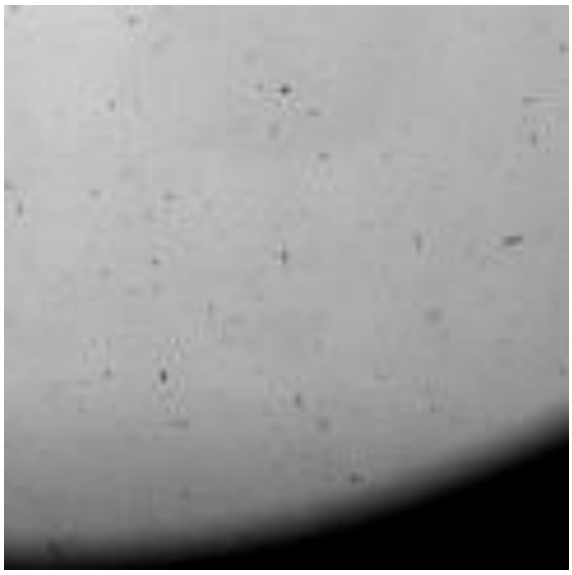

Figure A-10. Enlarged image of region around target, showing dark pixels due to fiber-optic taper

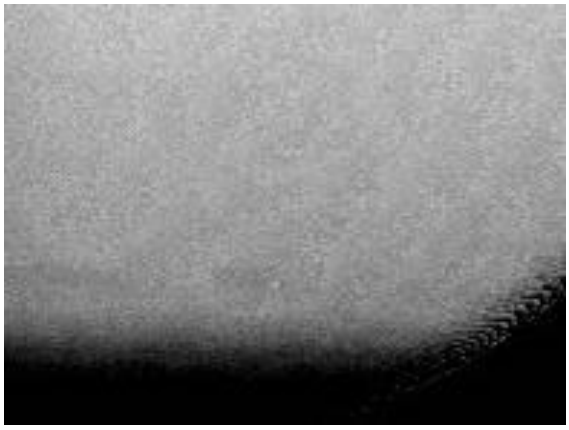

Figure A-11. Enlarged image after application of integer non-uniformity correction

A.4 Measurements

Data sets were acquired in the original hardware configuration from 3 February 2005 to 20 July 2005. Reference [A-11] describes the initial results from the winter and spring of 2005. Improvements were made to the system in July 2005. Measurements were made with the improved system from 1 August 2005 to 10 April 2006 and from 20 October 2006 to 10 December 2006. The data acquired during August 2005 and in the fall of 2006 will be presented below.

Figure A-12 shows a plot of the scattering coefficient at noon for every day in August. The variation from day to day is quite reasonable. An evaluation of data shows a very good relation-ship between the appearance of the imagery and the extracted data. For example, in the August set, the fog incidents can be seen in the imagery on days 241 and 242. The spectral behavior is well behaved in the blue, photopic, and red, however the scattering coefficients appear to be slightly high in the NIR.

We believe that the NIR data are slightly offset, because the lens coating for this lens is not optimized for the NIR. With 11 lenses in the zoom lens, the throughput of the lens is very sensitive to the coating properties. Although a zoom lens was necessary for this developmental instrument, a better design for a field device would be a fixed lens with coatings optimized for the wavelengths in use.

We also evaluated the results as a function of time of day, in order to evaluate whether there might be biases due to solar angle or other factors. Figure A-13 shows the variation during a period of 6 days in October 2005. Day 295 shows a strong change during the day, as the atmosphere cleared.

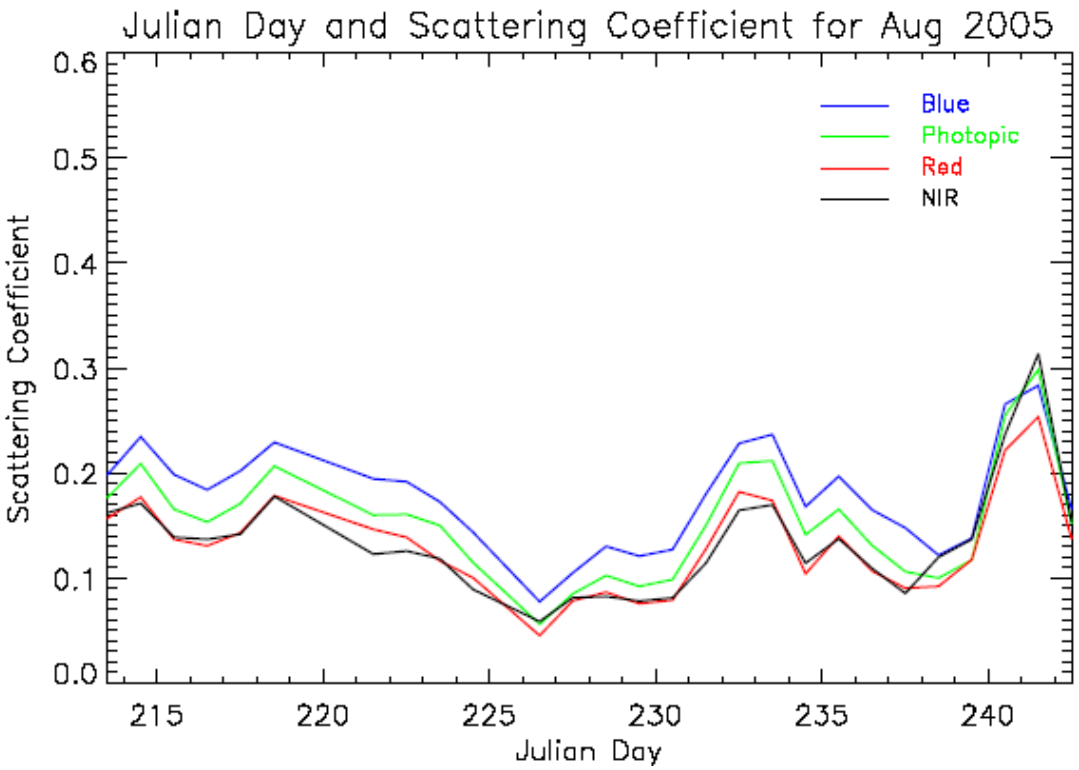

Figure A-12. Scattering coefficients measured at noon in August 2005

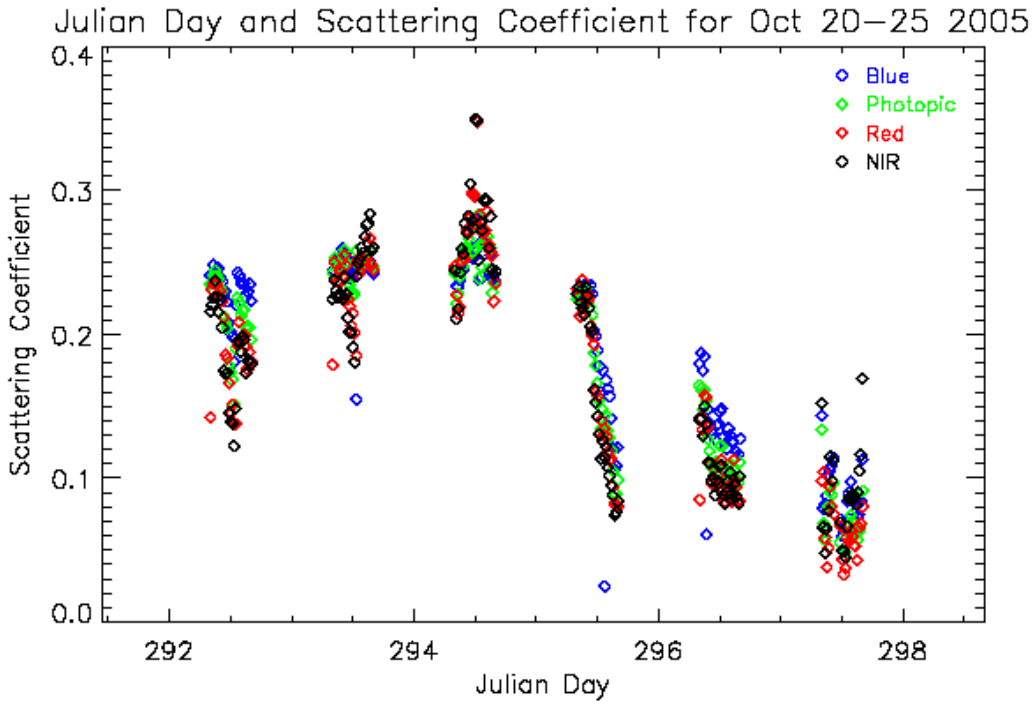

Figure A-13. Variation in scattering coefficient during the day (20 – 25 October 2005)

Although general trends were reasonable, we had not yet handled some specific problem areas in the processing of the data set. These problems that are discussed below were addressed and the August data was reprocessed. Out of the 5248 images from the August period, 56 had boats or ships in the line of sight to the target. These cases were detected visually and flagged and removed from the data set. Logic was added to the algorithm to automatically remove cases where either the target or the horizon region of interest (ROI) were off-scale, dark or bright.

Occasionally the horizon was not at equilibrium radiance due to the presence of clouds. These cases were automatically detected and removed by evaluating the standard deviation of the corrected signals within the horizon ROI. Occasionally the program was not successful in its attempt to find the target, and these cases were automatically detected and removed by evaluating the STD within the target ROI. A total of 294 cases (5.6% of the data set) were detected and removed for one of the above reasons. The remaining plots show the reprocessed August data.

A comparison of the results in the different filters with those in the photopic filter is shown in Figure A-14. In all cases, the spectral results correlate quite reasonably with the photopic results. We also note that general magnitudes are reasonable in all cases. All three filters have similar results to the photopic at high extinctions, where larger droplets should prevail and the results should be less spectrally dependent. At the low scattering coefficient end, with relatively clear air, and the scattering is higher in the blue and lower in the red and NIR, as expected.

It is also interesting that the correlation between the spectral results and the photopic results is somewhat poorer in the NIR than in the other filters. We speculate that this may have to do with variations in the drop size distribution under different conditions. The path of sight is approximately 9 - 10 m above sea level, and is subject to droplets kicked up by the surf zone. Even on relatively clear days, this path of sight may be more populated with large droplets than a typical maritime or continental air mass. Depending on the populations of these large droplets, we would anticipate potentially different scattering results in the NIR, in relation to the photopic.

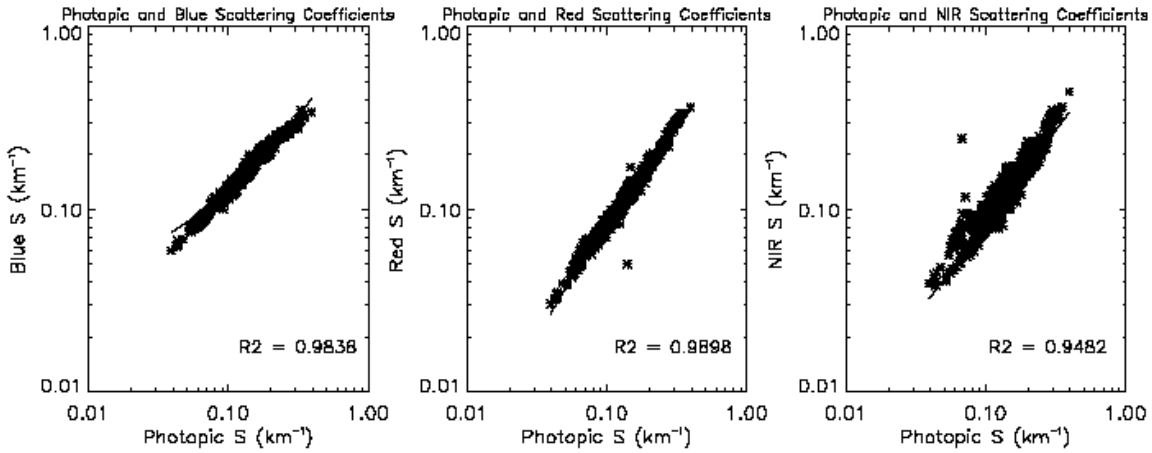

Figure A-14. Correlation of scattering coefficients at different wavelengths

A.5 Comparison with Transmissometer

In addition to the MSI, the site was instrumented with several other instrument systems, including transmissometers operating at 0.55 μm (nearly photopic) and at 1.06 μm and a nephelometer operating in the photopic band. The transmissometers were operating over the same path of sight as the MSI, and the nephelometer was located near the MSI target box.

Figures A-13 and A-14 show records of the extinction and scattering coefficients measured with the transmissometer and MSI for two 7-day periods in the fall of 2006. Since the MSI is limited to daylight operation, only the daytime values from the transmissometer are shown in these charts. The agreement between the two measurements is extremely good. Figure A-12 shows a scatter plot comparing the two measurements for this time period. This plot confirms the agreement seen in the 7-day records – the correlation coefficient is 0.84 and most of the data fall near a line with unity slope. At times of high extinction (extinction coefficient ≥ 0.4 km^{-1}), the transmissometer tends to report higher values than the MSI. There are two possible reasons for this behavior. First, at these high extinction levels, the transmission over the 7.07-km path is less than 6 % and small changes in the measured transmission (due to variations in the back-ground level) result in large errors in the calculated extinction coefficient. Second, at high extinction, measuring the contrast of the black box in the MSI image is affected by imperfections in the non-uniformity correction used in the image processing. In the current version of the MSI, a value of ~ 0.5 km^{-1} may be the upper limit on the capability of the instrument to accurately measure scattering coefficients.

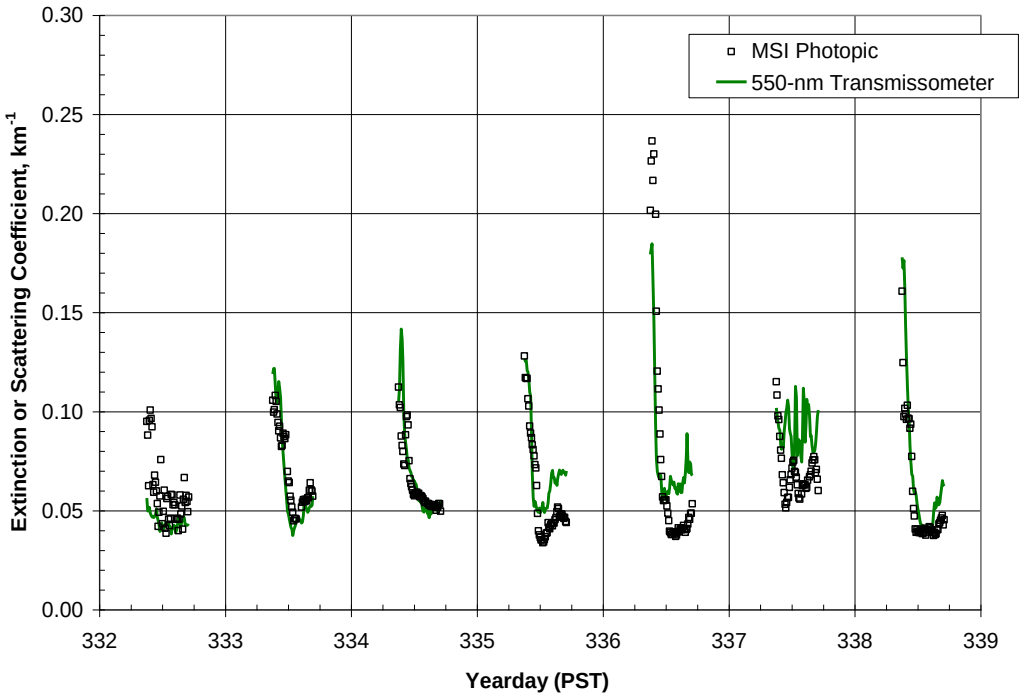

Figure A-10. Record of MSI and 0.55-µm transmissometer measurements (28 November 2006 – 4 December 2006)

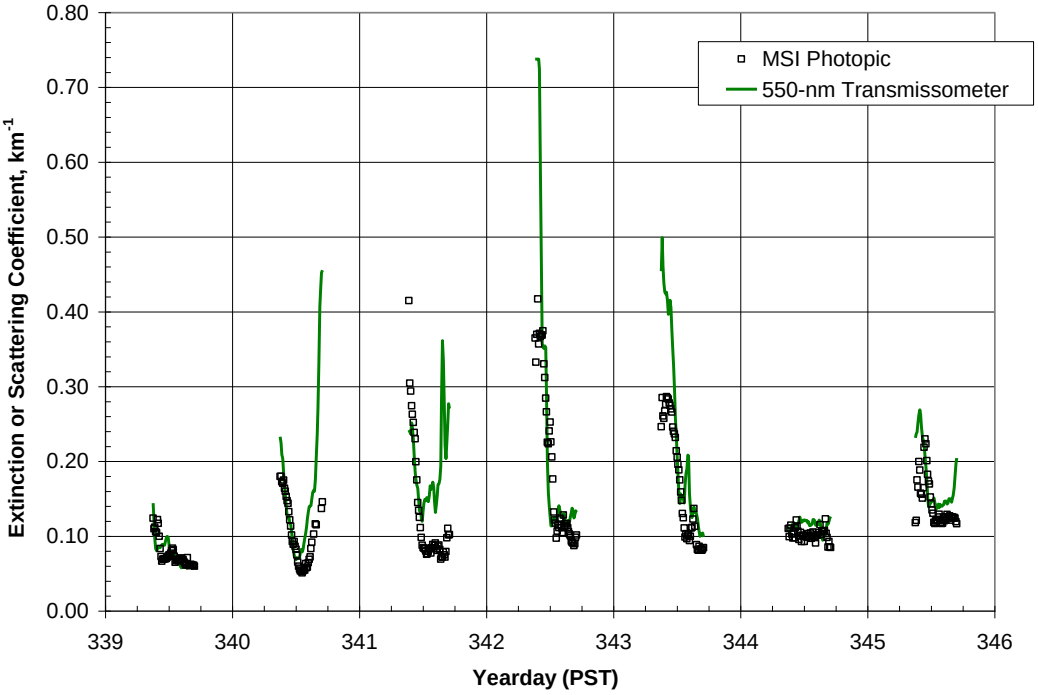

Figure A-11. Record of MSI and 0.55-µm transmissometer measurements (5 December 2006 – 11 December 2006)

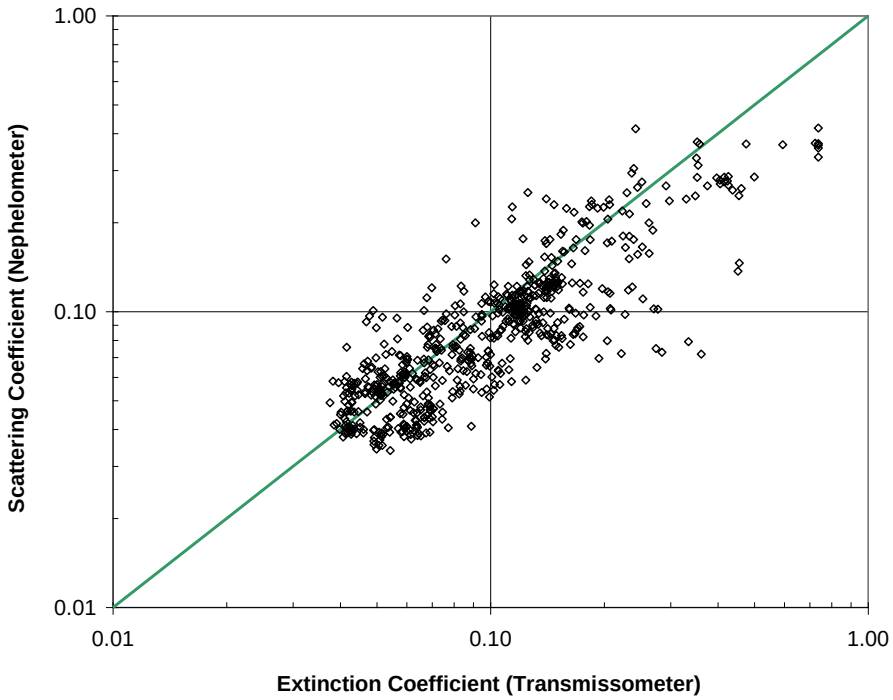

Figure A-12. Scatter plot comparing MSI and 0.55-μm transmissometer data for two-week period from 28 November to 11 December 2006

A.6 Potential for Future Development

For some applications, it would be useful to either measure or estimate the scattering coefficient along paths of sight in Short Wave IR (SWIR) wavelengths between 1 and 3 μm. One approach to this goal would be to design a SWIR MSI. We have not fully investigated this approach, but feel it may be a very fruitful approach. A second method would be to use a visible MSI, and use the multi-spectral nature of the measurements to provide an estimate of the SWIR scattering, either empirically or using modeling. Although extensive modeling of this approach is beyond the scope of this work, we have evaluated the SWIR extinction measurements in relation to the MSI data. Figure A-13 shows a scatter plot of SWIR extinction, derived from the SSC transmis-someter, as a function of the photopic MSI scattering coefficient. We see from this figure that the photopic scattering coefficient measured by the MSI is a reasonable predictor of the SWIR extinction coefficient, particularly when the NIR/photopic ratio from the MSI is taken into account. There is surprisingly little scatter in this plot, and a simple curve fit, as a function of NIR/photopic ratio, would enable one to predict the approximate range of anticipated SWIR extinction from the visible data. This plot represents a very limited data set. Clearly more study would be required to determine whether, for applications requiring an estimate of the SWIR extinction, it is more productive to design a SWIR MSI or use a visible MSI and an empirical extrapolation to the SWIR. SWIR sensors tend to have higher noise and non-uniformity; however they may be sufficiently accurate for some MSI applications.

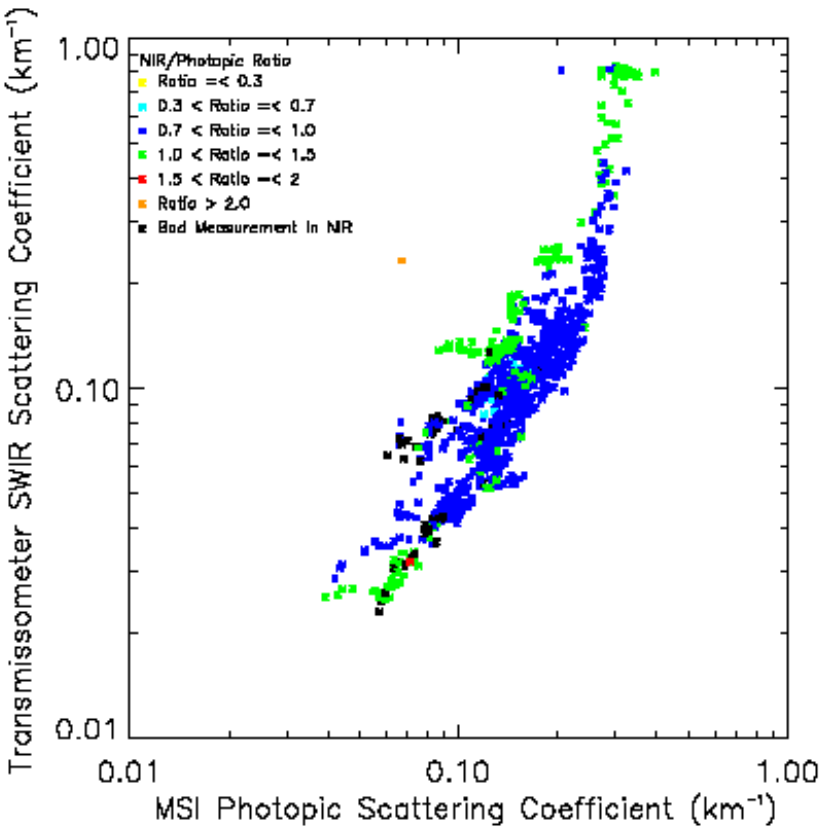

Figure A-13. Extinction coefficient at 1.06 μm, from SSC transmissometer, versus MSI photopic scattering coefficient, color-coded by NIR/photopic ratio

We recommend beginning development of systems for use in field operations. For this application, we would no longer use the black target used in this experimental setup. Potential optical targets of opportunity include dark landscape features, open doors and other dark objects in an urban environment, and the air/sea interface as well as ocean radiant characteristics in ocean environments. The MSI technique depends in large part on the accuracy of the measure-ments and algorithm, but it also depends on having a reasonably well-known optical target. Clearly studies of the natural variations in targets of opportunity (as a function of wavelength) would be important in isolating the most useful targets of opportunity. For example, we would anticipate that some directions and wavelengths will have higher air/sea interface contrast than others; those with inherent contrast closest to negative one will yield the most accurate extinction results. The impacts of using these less optimal targets on the overall system accuracy can be derived using system sensitivity studies [A-14], such as were done with the HSI. We feel that development of a SWIR or IR system, in conjunction with further hardening of the visible MSI system, should enable development of field systems for operational use in the future. Although a field hardened system may be slightly less accurate than the current system, it should be far more accurate than any other approach of we are aware for determining the scattering over an extended path from a single location.

A.7 Conclusions

A new system, the Multispectral Scattering Imager or MSI, has been developed to measure scattering coefficients over extended paths. This system makes measurements of visibility and scattering coefficient in the blue, green, red, and NIR wavelengths, and can be adapted to other wavelengths. The MSI results correlated very well with simultaneous transmissometer data, achieving a correlation constant of 0.84. The data appear to vary reasonably as a function of spectral band. The images also provide a convenient means to visually verify the conditions that were occurring at the time of the measurements. The results compare very well with scene weather as evaluated from visual inspection of the imagery.

Although we have developed the theory for extracting visibility at night from data such as that acquired by the MSI, we did not develop the programs and specific methodology to process nighttime data for this project.

The MSI has a number of attractive features for supporting extended atmospheric measurement campaigns or in future use as a decision aid for military systems. First, it provides an integrated-path measurement, but only requires an active element at one end of the path. It is a passive system appropriate for covert use. Second, the system alignment is robust – the image processing algorithm can find the darkest pixels corresponding to the reference target and compensate for alignment errors due to mechanical disturbances or atmospheric refraction. Third, the system was extremely reliable. Data sets were acquired every 10 minutes, except for periodic maintenance and occasional data loss due to power failures. We are pleased with how far the MSI has come in this relatively short development time, and feel it has exceptional potential for the future.

A.8 References

A-1. H. Koschmeider, "Theorie der horizontalen Sichtweite", Beitr. Phys. frein Atmos. **12**, 33-53 (1924)

A-2. J. A. Curcio and K. A. Durbin, "Atmospheric Transmission in the Visible Region", Report 5368, Naval Research Laboratory, Washington, DC (1959)

A-3. W. C. Malm, G. Persha, R. tree, R. Stocker, I. Tombach, and H. Iyer, "Comparison of Atmospheric Extinction Measurements made by a Transmissometer, Integrating Nephelometer, and Teleradiometer with Natural and Artificial Black Target", Air Pollution Control Association Specialty Conference, Grand Teton National Park, Wyoming, 7 – 10 September 1986

A-4. R. W. Johnson, W. S. Hering, and J. E. Shields, *Automated Visibility and Cloud Cover Measurements with a Solid State Imaging System*, University of California, San Diego, Scripps Institution of Oceanography, Marine Physical Laboratory, SIO 89-7, GL-TR-89-0061, NTIS No. ADA216906, 1989.

A-5. J. E. Shields, R. W. Johnson, and M. E. Karr, *An Automated Observing System for Passive Evaluation of Cloud Cover and Visibility*, University of California, San Diego,

Scripps Institution of Oceanography, Marine Physical Laboratory, SIO 92-22, PL-TR-92-2202, 1992.

A-6. R. W. Johnson, T. L. Koehler, and J. E. Shields, *A Multi-Station Set of Whole Sky Imagers and A Preliminary Assessment of the Emerging Data Base*, Proceedings of the Cloud Impacts on DOD Operations and Systems, 1988 Workshop, pp. 159 – 162 1988.

A-7. J. E. Shields, R. W. Johnson, and T. L. Koehler, *Automated Whole Sky Imaging Systems for Cloud Field Assessment*, Fourth Symposium on Global Change Studies, American Meteorological Society, 1993.

A-8. J. E. Shields, R. W. Johnson, M. E. Karr, and J. L. Wertz, *Automated Day/Night Whole Sky Imagers for Field Assessment of Cloud Cover Distributions and Radiance Distributions*, Tenth Symposium on Meteorological Observations and Instrumentation, American Meteorological Society, 1998

A-9. J. E. Shields, R. W. Johnson, M. E. Karr, A. R. Burden, and J. G. Baker, *Whole Sky Imagers for Real-time Cloud Assessment, Cloud Free Line of Sight Determinations and Potential Tactical Applications*, The Battlespace Atmospheric and Cloud Impacts on Military Operations (BACIMO) Conference, Monterey, CA, 2003

A-10. J. E. Shields, R. W. Johnson, M. E. Karr, A. R. Burden, and J. G. Baker, *Daylight Visible/NIR Whole Sky Imagers for Cloud and Radiance Monitoring in Support of UV Research Programs*, International Symposium on Optical Science and Technology, SPIE the International Society for Optical Engineering, 2003

A-11. J. E. Shields, J. G. Baker, M. E. Karr, R. W. Johnson, and A. R. Burden, *Visibility measurements along extended paths over the ocean surface*, International Symposium on Optical Science and Technology, SPIE the International Society for Optical Engineering, August 2005

A-12. H. G. Houghton, *Physical Meteorology*, MIT Press, Cambridge, Massachusetts, 353 -356 (1985)

A-13. J. E. Shields, R. W. Johnson, and M. E. Karr, A Sensitivity Study of Daytime Visibility Determination with a Horizon Scanning Imagery, University of California, San Diego, Scripps Institution of Oceanography, Marine Physical Laboratory, SIO 91-15, PL-TR-91-2189, 1991

Appendix B: Sample Input Files for Program ProcMSI

B1: File AutoProcMSI.inp

[Note, this file was used for the final re-processing of the 2010 data set]

```
    AutoProcMSI Input File

Pathname for Inherent Contrast Input File -----------------------
D:\MSIVis13\Programs\ProcMSI\InherentContrast.txt
Pathname for Target ROI Coordinates Input File ------------------
D:\MSIVis13\Programs\ProcMSI\Target ROI 60 and 180 2010.Txt
Pathname for Linearity Correction File --------------------------
D:\MSIVis13\Programs\ProcMSI\MSICamNonLinFeb09.txt
Pathname for NIR Uniformity Correction File ---------------------
D:\MSIVis13\Programs\ProcMSI\nirDRKCORUNIF.DAT
Pathname for Photopic Uniformity Correction File ----------------
D:\MSIVis13\Programs\ProcMSI\phtdrkcorunif.dat
Pathname for Red Uniformity Correction File ---------------------
D:\MSIVis13\Programs\ProcMSI\reddrkcorunif.dat
Pathname for Open Uniformity Correction File --------------------
D:\MSIVis13\Programs\ProcMSI\bludrkcorunif.dat
Path to Input Image Data ----------------------------------------
D:\MSIVis13\MSI 2010 Data Reprocess\MSI Raw\
Path to Output Tables -------------------------------------------
D:\MSIVis13\MSI 2010 Data Reprocess\MSI Proc Test 2\
Human Contrast Threshold ----------------------------------------- 0.05
NIR Filter Normalization Constant for Uniformity Correction ------ 3816
Photopic Filter Normalization Constant for Uniformity Correction - 3956
Red Filter Normalization Constant for Uniformity Correction ------ 7217
Open Filter Normalization Constant for Uniformity Correction ----- 1261
Process sub directories? ----------------------------------------- 0
Time correction (in Minutes) ------------------------------------- 0
Offscale bright for drk corr sig (Flag 91) (count)----------------
64000
Offscale dark for drk corr sig (Flag 91) (count)------------------ 100
Target Glitter ROI STD Threshold (Flag 92) (%)-------------------- 5.0
Glitter Azimuth Threshold (Flag 92) (deg) ------------------------ 22.5
Target ROI STD Threshold for sorting case (Flag 93)--------------- 5.0
Target ROI STD Threshold for not sorting case (Flag 93)----------- 7.0
Horizon ROI STD Threshold (Flag 94) (%) -------------------------- 5.0
Image Dwell Time (seconds) --------------------------------------- 0
Start time of data to be processed in corrected time space ------- 1600
End time of data to be processed in corrected time space --------- 2400
Set flag if scattering coefficient S < 0? (Flag 95) -------------- 1
Do Uniformity Correction? ---------------------------------------- 1
Save U2 corrected image (targets with 2nd unif corr)? ------------ 0
Get darker pixels within target ROIs? (i.e. sort data?)----------- 1
Process NIR images? ---------------------------------------------- 0
Process Photopic images? ----------------------------------------- 0
Process Red images? ---------------------------------------------- 1
Process Open images? --------------------------------------------- 0
Do Linearity Correction? ----------------------------------------- 1
Path base altitude in meters ------------------------------------- 0
Path zenith angle ------------------------------------------------ 85.0
Use path top altitude? - if 0, path length will be used ---------- 1
```

```
Path top altitude in meters---------------------------------------- 2000
Path length in meters ---------------------------------------------- 99
Sensor altitude in meters ------------------------------------------ 1000
Use ceilometer input? ---------------------------------------------- 0
Pathname for ceilometer input file --------------------------------- C:\
Haze layer top in meters ------------------------------------------- 1000
Cloud layer base in meters ----------------------------------------- 99
Use constant for Raleigh Scattering? ------------------------------- 0
Constant for Raleigh Scattering ------------------------------------ 0.0
```

B2: File TargetROI 60 and 180 2010.txt

[Note, in this run we were only processing data at 60 and 180 degrees, as indicated in the top line. We did not update the target information for the other angles. We were only processing data for one target, so we did not update the ranges or uniformity corrections for ROI 2 – 4.]

```
Horizon and Target information file
From positions defined below, enter table position(s) to process:
60,180

NumberofROIs: 5 for images at Rotary Table Position: 30
ROI 0 : XLeft: 200 YLeft: 148 XRight: 300 YRight: 158
ROI 1 : XLeft: 200 YLeft: 194 XRight: 300 YRight: 204  Range in miles: 7.45   Unif corr:
1.00
ROI 2 : XLeft: 200 YLeft: 209 XRight: 300 YRight: 219  Range in miles: 5.38   Unif corr:
0.92
ROI 3 : XLeft: 200 YLeft: 224 XRight: 300 YRight: 234  Range in miles: 4.20   Unif corr:
0.84
ROI 4 : XLeft: 200 YLeft: 239 XRight: 300 YRight: 249  Range in miles: 3.45   Unif corr:
0.75

NumberofROIs: 2 for images at Rotary Table Position: 60
ROI 0 : XLeft: 200 YLeft: 159 XRight: 300 YRight: 169
ROI 1 : XLeft: 200 YLeft: 205 XRight: 300 YRight: 215  Range in miles: 5.59   Unif corr:
1.00
ROI 2 : XLeft: 200 YLeft: 230 XRight: 300 YRight: 240  Range in miles: 5.38   Unif corr:
0.92
ROI 3 : XLeft: 200 YLeft: 235 XRight: 300 YRight: 245  Range in miles: 4.20   Unif corr:
0.84
ROI 4 : XLeft: 200 YLeft: 250 XRight: 300 YRight: 260  Range in miles: 3.45   Unif corr:
0.75

NumberofROIs: 5 for images at Rotary Table Position: 90
ROI 0 : XLeft: 200 YLeft: 170 XRight: 300 YRight: 180
ROI 1 : XLeft: 200 YLeft: 216 XRight: 300 YRight: 226  Range in miles: 7.45   Unif corr:
1.00
ROI 2 : XLeft: 200 YLeft: 231 XRight: 300 YRight: 241  Range in miles: 5.38   Unif corr:
0.92
ROI 3 : XLeft: 200 YLeft: 246 XRight: 300 YRight: 256  Range in miles: 4.20   Unif corr:
0.84
ROI 4 : XLeft: 200 YLeft: 261 XRight: 300 YRight: 271  Range in miles: 3.45   Unif corr:
0.75

NumberofROIs: 5 for images at Rotary Table Position: 95
ROI 0 : XLeft: 200 YLeft: 171 XRight: 300 YRight: 181
ROI 1 : XLeft: 200 YLeft: 217 XRight: 300 YRight: 227  Range in miles: 7.45   Unif corr:
1.00
ROI 2 : XLeft: 200 YLeft: 232 XRight: 300 YRight: 242  Range in miles: 5.38   Unif corr:
0.92
ROI 3 : XLeft: 200 YLeft: 247 XRight: 300 YRight: 257  Range in miles: 4.20   Unif corr:
0.84
```

```
ROI 4 : XLeft: 200 YLeft: 262 XRight: 300 YRight: 272  Range in miles: 3.45   Unif corr:
0.75
NumberofROIs: 5 for images at Rotary Table Position: 150
ROI 0 : XLeft: 200 YLeft: 179 XRight: 300 YRight: 189
ROI 1 : XLeft: 200 YLeft: 225 XRight: 300 YRight: 235  Range in miles: 7.45   Unif corr:
1.00
ROI 2 : XLeft: 200 YLeft: 240 XRight: 300 YRight: 250  Range in miles: 5.38   Unif corr:
0.92
ROI 3 : XLeft: 200 YLeft: 255 XRight: 300 YRight: 265  Range in miles: 4.20   Unif corr:
0.84
ROI 4 : XLeft: 200 YLeft: 270 XRight: 300 YRight: 280  Range in miles: 3.45   Unif corr:
0.75

NumberofROIs: 2 for images at Rotary Table Position: 180
ROI 0 : XLeft: 200 YLeft: 176 XRight: 300 YRight: 186
ROI 1 : XLeft: 200 YLeft: 222 XRight: 300 YRight: 232  Range in miles: 5.59   Unif corr:
1.00
ROI 2 : XLeft: 200 YLeft: 258 XRight: 300 YRight: 268  Range in miles: 5.38   Unif corr:
0.92
ROI 3 : XLeft: 200 YLeft: 252 XRight: 300 YRight: 262  Range in miles: 4.20   Unif corr:
0.84
ROI 4 : XLeft: 200 YLeft: 267 XRight: 300 YRight: 277  Range in miles: 3.45   Unif corr:
0.75
```

B3: File Inherent Contrast.txt

[Note, for this run we were only using one target, so we did not update the inherent contrast for targets 2 – 10.]

```
Inherent Contrast
Number of water targets to read: 1

Tar#  NIR   Pht   Red   Opn
1  0.850 0.850 0.850 0.850
2  1.000 0.80  0.850 1.000
3  1.000 0.95  0.850 1.000
4  1.000 0.89  0.850 1.000
5  1.000 0.950 0.630 1.000
6  1.000 0.950 0.630 1.000
7  1.000 0.850 0.630 1.000
8  1.000 1.000 0.630 1.000
9  1.000 1.000 0.630 1.000
10 1.000 1.000 0.630 1.000
```